THE QUARTERLY JOURNAL OF

MECHANICS AND APPLIED MATHEMATICS

VOLUME X PART 4

NOVEMBER 1957

OXFORD

AT THE CLARENDON PRESS

1957

Price 18*s. net*

PRINTED IN GREAT BRITAIN BY CHARLES BATEY AT THE UNIVERSITY PRESS, OXFORD

THE QUARTERLY JOURNAL OF MECHANICS AND APPLIED MATHEMATICS

THE QUARTERLY JOURNAL OF MECHANICS AND APPLIED MATHEMATICS is published at 18*s.* net for a single number with an annual subscription (for four numbers) of 60*s.* post free.

NOTICE TO CONTRIBUTORS

1. *Communication.* Papers should be communicated to Dr. D. M. A. Leggett, Department of Mathematics, King's College, Strand, London, W.C. 2.

If possible, to expedite publication, papers should be submitted in duplicate.

2. *Presentation.* Papers should be typewritten (double spacing) and should be preceded by a summary not exceeding 300 words in length. References to literature should be given in standard order, *author, title of journal, volume number, date, page.* These should be placed at the end of the paper and arranged according to the order of reference in the paper.

3. *Diagrams.* The number of diagrams should be kept to the minimum consistent with clarity. The lines of the figures should be drawn in ink either on draughtsman's paper or on good quality white paper. Each individual line in the figure should bear reducing to one-half of the size of the original, and great care should be exercised to see that the lines are regular in thickness, especially where they meet. Lettering of the figure should be in pencil and should be sufficient to define clearly the lines and curves in it. The writing of formulae or of explanations on the diagram itself should be avoided. All explanations of symbols, etc., should be given in underline. Contributors should indicate on their manuscripts where figures should be inserted.

4. *Tables.* Tables should preferably be arranged so that they can be printed with the columns parallel to the longer edge of the page.

5. *Notation.* All single letters used to denote vectors in the manuscript should be marked by underlining with a wavy line. Scalar and vector products should be denoted by $\underset{\sim}{a}.\underset{\sim}{b}$ and $\underset{\sim}{a} \wedge \underset{\sim}{b}$ respectively. Real and imaginary parts of complex quantities should be denoted by re and im respectively.

6. *Offprints.* Authors of papers will be entitled to 25 free offprints. This number is available for sharing between authors of joint papers.

7. All correspondence other than that dealing with contributions should be addressed to the publishers:

OXFORD UNIVERSITY PRESS
AMEN HOUSE, LONDON, E.C. 4

TWO-DIMENSIONAL PROBLEMS OF THE DECAY OF MAGNETIC FIELDS IN MAGNETOHYDRODYNAMICS

By T. G. COWLING *and* A. HARE (*The University, Leeds*)

[Received 24 January 1957]

SUMMARY

The normal modes of decay of a magnetic field in the presence of steady motions in a fluid conductor are studied in the two-dimensional case. Slow motions are considered by perturbation methods, which show that to a first approximation the motion always increases the rate of decay in the lowest mode. For fast motion, there exists a limited class of modes little affected by the motion, in which the lines of force and streamlines nearly coincide. In the general class of modes the motion profoundly affects the decay; these are studied in two special cases, those of streaming in a fluid slab between parallel walls and of non-uniform rotation in a circular cylinder. The motion is found to transport and distort the field, and to increase the rate of decay in the lower modes, roughly proportional to the $\frac{2}{3}$ power of the velocity. For the slab problem, velocities of intermediate magnitude are studied by numerical methods. The extension of the results to more general classes of two-dimensional motion is briefly considered.

1. Statement of the problem

Recently Bullard and Gellman (**1**) have established, by numerical methods, that a steady magnetic field can be maintained by dynamo interaction with a steady motion of suitable size and type in a conducting fluid. The details of the mechanism are, however, somewhat obscure. For this reason it appears desirable to study the normal modes of decay of magnetic fields in the presence of general classes of steady motions in conducting fluids. By this is meant modes in which the field $\mathbf{H}$ after time t is connected with the initial field $\mathbf{H}_0$ by an equation

$$\mathbf{H} = \mathbf{H}_0 e^{-\sigma t}, \tag{1}$$

where σ may be either real or complex. Dynamo maintenance of a steady field corresponds to $\sigma = 0$; more generally, whenever the real part of σ passes from positive to negative values as the velocity is varied, the field passes from a decreasing mode to an amplifying mode.

The simplest problem to discuss is a two-dimensional one, in which currents flow parallel to Oz in a cylinder of uniform liquid with generators parallel to Oz; the velocity $\mathbf{v}$ and the magnetic field $\mathbf{H}$ are perpendicular to Oz. In this case dynamo maintenance is known to be impossible (**2**), so that the results have only an indirect bearing on the dynamo problem.

Nevertheless, because of that indirect bearing, and because illustrative results are easier to obtain than in the three-dimensional case, the two-dimensional problem will be considered here. Chandrasekhar has recently considered the three-dimensional problem with axial symmetry (**3**); the topological similarity of this with the two-dimensional problem should lead to similar results in the two cases. However, Chandrasekhar found that a sufficiently fast motion might slow down the decay almost indefinitely. The present work gives no support to such a view; it indicates that a rapid motion always leads to rapid decay. The discrepancy between the results appears to be due to the inadequacy of certain approximations made by Chandrasekhar. It can in fact be shown by general methods that no motion whatsoever can, either in the two-dimensional or the axisymmetric case, increase the time of decay beyond a definite upper limit.

In the two-dimensional case, to avoid having an infinite total magnetic energy per unit length in the z-direction (which would make any decay problem meaningless) it is necessary to suppose that zero total electric current flows across any section $z =$ constant of the conducting cylinder. Appropriate methods of approximation to the fields are available when the motion is either slow or fast. These do not apply to intermediate values of the velocity; to link up the results for slow and fast motions, a special problem of intermediate motions has been considered numerically.

2. Basic equations

Let $\mathbf{E}$, $\mathbf{H}$, and $\mathbf{j}$ denote the electric and magnetic field-strengths and the current-density, all measured in e.m.u. In the two-dimensional case, $\mathbf{E}$ and $\mathbf{H}$ are derivable from a vector-potential $\mathbf{A}$, parallel to Oz, by the relations†

$$\mathbf{H} = \operatorname{curl} \mathbf{A}, \qquad \mathbf{E} = -\partial \mathbf{A}/\partial t. \tag{2}$$

Also if κ is the electrical conductivity,

$$\operatorname{curl} \mathbf{H} = 4\pi \mathbf{j} = 4\pi\kappa(\mathbf{E} + \mathbf{v} \wedge \mathbf{H}). \tag{3}$$

Substituting (2) into (3), the magnitude of $\mathbf{A}$ is found to satisfy the equation

$$\nabla^2 A = 4\pi\kappa\left\{\frac{\partial A}{\partial t} + (\mathbf{v}.\operatorname{grad})A\right\}. \tag{4}$$

This is the equation valid inside the conducting cylinder; outside it A satisfies

$$\nabla^2 A = 0. \tag{5}$$

On the surface of the cylinder, A and its derivatives have to be continuous.

† In three dimensions it is necessary to include a term $-\operatorname{grad} V$ in the relation giving $\mathbf{E}$. In the two-dimensional case, however, $\mathbf{E}$ is a vector parallel to Oz but independent of z; thus grad V can only be a vector parallel to Oz, independent of all the spatial coordinates. The contribution from grad V can accordingly be included in the $-\partial \mathbf{A}/\partial t$ term without affecting the relation $\operatorname{div} \mathbf{A} = 0$.

The steady motion $\mathbf{v}$ in a uniform liquid can be expressed in terms of a stream function ψ by the equation

$$\mathbf{v} = -\text{curl}(\mathbf{k}\psi) = \mathbf{k} \wedge \text{grad}\,\psi, \tag{6}$$

where $\mathbf{k}$ is a unit vector parallel to Oz. Also in a normal mode of decay, $A \propto e^{-\sigma t}$; thus equation (4) becomes

$$\nabla^2 A = 4\pi\kappa\{-\sigma A + \mathbf{k}.(\text{grad}\,\psi \wedge \text{grad}\,A)\}. \tag{7}$$

This equation, together with equation (5) valid outside the cylinder and the necessary boundary conditions, determines the eigenvalues σ and the eigenfunctions A.

3. Small velocities

When $\mathbf{v}$ is small, perturbation methods can be employed. When $\mathbf{v} = 0$, equation (7) becomes

$$\nabla^2 A + 4\pi\kappa\sigma A = 0. \tag{8}$$

Functions $\mathbf{A}$ satisfying this equation inside the cylinder, equation (5) outside, and the appropriate boundary conditions, exist only for positive real eigenvalues σ_i. Let A_r, A_s be eigenfunctions (which may be assumed to be real) corresponding to different eigenvalues σ_r, σ_s. Then A_r and A_s can be shown to satisfy the orthogonality condition

$$\iint A_r A_s \, dS = 0, \tag{9}$$

the integral being over the cross-section S of the conductor. If there is degeneracy, the eigenfunctions corresponding to a given value of σ can be chosen such as also to satisfy equation (9). Eigenfunctions are also normalized to satisfy

$$\iint A_r^2 \, dS = 1. \tag{10}$$

In solving equations (7) when ψ is small but non-zero, suppose first that the unperturbed eigenvalues σ_r and eigenfunctions A_r satisfying equation (8) are all distinct. The corresponding perturbed quantities are then expressed as series

$$\begin{aligned} A &= A_r + \epsilon \sum_s a_{rs} A_s + \epsilon^2 \sum_s b_{rs} A_s + \ldots, \\ \sigma &= \sigma_r + \epsilon\mu_r + \epsilon^2 \nu_r + \ldots, \end{aligned} \tag{11}$$

where ϵ is a small constant to which ψ is assumed proportional. Substituting (11) into (7), the terms of orders ϵ and ϵ^2 give

$$\sum_s a_{rs}(\sigma_r - \sigma_s) A_s + \mu_r A_r = \epsilon^{-1}\,\mathbf{k}.(\text{grad}\,\psi \wedge \text{grad}\,A_r), \tag{12}$$

$$\sum_s b_{rs}(\sigma_r - \sigma_s) A_s + \mu_r \sum_s a_{rs} A_s + \nu_r A_r = \epsilon^{-1}\,\mathbf{k}.\Big(\text{grad}\,\psi \wedge \text{grad} \sum_s a_{rs} A_s\Big). \tag{13}$$

Equation (12) gives the first-order perturbation. Multiply this equation by A_r and integrate over S, using (9) and (10). Then

$$\begin{aligned}\mu_r &= \tfrac{1}{2}\epsilon^{-1}\iint \mathbf{k}.(\operatorname{grad}\psi\wedge\operatorname{grad}A_r^2)\,dS\\ &= -\tfrac{1}{2}\epsilon^{-1}\iint \mathbf{k}.\operatorname{curl}(A_r^2\operatorname{grad}\psi)\,dS\\ &= -\tfrac{1}{2}\epsilon^{-1}\int_C A_r^2\operatorname{grad}\psi.\,\mathbf{ds}\end{aligned} \tag{14}$$

using Stokes's theorem, where the last integral is a line-integral round the boundary C of S. But C is a streamline $\psi =$ constant of the motion; thus the integral vanishes and $\mu_r = 0$. That is, to the first order the motion does not affect the decay constant σ.

To get a_{rs} $(r \neq s)$, multiply (12) by A_s and integrate over S; then

$$a_{rs}(\sigma_r-\sigma_s) = \epsilon^{-1}\iint A_s\,\mathbf{k}.(\operatorname{grad}\psi\wedge\operatorname{grad}A_r)\,dS. \tag{15}$$

The coefficients a_{rs} are symmetric in the suffixes r and s; for

$$\begin{aligned}(a_{rs}-a_{sr})(\sigma_r-\sigma_s) &= \epsilon^{-1}\iint \mathbf{k}.(\operatorname{grad}\psi\wedge\operatorname{grad}A_rA_s)\,dS\\ &= \epsilon^{-1}\int_C A_rA_s\operatorname{grad}\psi.\,\mathbf{ds}\end{aligned}$$

which vanishes like (14).

The second-order perturbation equation (13) can be solved similarly to give ν_r and b_{rs}. Using the symmetry property $a_{rs} = a_{sr}$, the results can be put in the form

$$\nu_r = \sum_s (\sigma_s-\sigma_r)a_{rs}^2, \tag{16}$$

$$b_{rs}(\sigma_r-\sigma_s) = \sum_t (\sigma_t-\sigma_s)a_{rt}a_{ls}. \tag{17}$$

Suppose that σ_1 corresponds to the mode of slowest decay, σ_2 to the next slowest, etc.; then $\sigma_1 \leqslant \sigma_s$ for all s, and so $\nu_1 > 0$. Thus the rate of decay in the lowest mode is accelerated by the fluid motion, to the second approximation. No similar conclusion is possible for the higher modes, for which the series in equation (16) contains negative terms. However, no general reduction in the rate of decay is possible, since from equation (16) and the symmetry condition in a_{rs} it follows that the quantities

$$\nu_1,\ \nu_1+\nu_2,\ \nu_1+\nu_2+\nu_3,\ldots,$$

are all positive.

The case of simple degeneracy can also be discussed without difficulty. If two real eigenfunctions A_r, A_r' correspond to the same eigenvalue σ_r, the zero-order eigenfunctions for the purpose of perturbation theory must be

taken as $A_r \pm iA'_r$. There is now a first-order perturbation in the eigenvalues σ, given by

$$\epsilon\mu_r = \pm i \iint A_r \mathbf{k}.(\operatorname{grad}\psi \wedge \operatorname{grad} A'_r)\, dS. \tag{18}$$

Since this is purely imaginary, the rate of decay is still unchanged to the first order, but now the decaying field has something of the character of a progressive wave. To the second order, the effect of the perturbation is to increase both values of σ by the same real quantity $\epsilon^2\nu_r$, where again ν_r is positive for the slowest mode of decay.

4. Applications of perturbation method

A simple application is to the problem of decay in an infinite slab between parallel plane walls $y = \pm a$. Here the unperturbed eigenfunctions and eigenvalues are given by

$$A = (C\cos\rho y + D\sin\rho y)\begin{matrix}\cos\\ \sin\end{matrix}(\alpha x), \tag{19}$$

$$4\pi\kappa\sigma = \rho^2 + \alpha^2, \tag{20}$$

where *either*
$$D = 0, \qquad \tan(\rho a) = \alpha/\rho$$
or
$$C = 0, \qquad \cot(\rho a) = -\alpha/\rho \Big\}. \tag{21}$$

There are thus two interlacing sets of eigenvalues for any α; the larger ones are given approximately by

$$\rho a = \nu\pi/2, \qquad 4\pi\kappa\sigma = \alpha^2 + \nu^2\pi^2/4a^2, \tag{22}$$

where ν is a sufficiently large integer. Corresponding to the degeneracy indicated by equation (19), the zero-order eigenfunctions in perturbation theory must be taken as

$$A = f(y)e^{\pm i\alpha x}, \tag{23}$$

where $f(y) = C\cos\rho y + D\sin\rho y$.

Consider first the case $\psi = \epsilon\phi(y)$, when the motion is entirely in the x-direction (parallel to the faces of the slab). To avoid infinities, the integrals in equations (9), (10), etc., are limited to a region S of the slab whose length in the x-direction is the wavelength $2\pi/\alpha$ of the eigenfunction in that direction. The first-order perturbation in σ_r is found to be

$$\epsilon\mu_r = \pm i\alpha V,$$

where
$$V = \frac{\int_{-a}^{a} v_x f_r^2\, dy}{\int_{-a}^{a} f_r^2\, dy}, \tag{24}$$

v_x ($\equiv -\epsilon\, d\phi/dy$) being the velocity of streaming. Thus the dependence of

the field on x and t is through a factor $e^{\pm i\alpha(x-Vt)}$. This shows that the field drifts in the x-direction with the velocity V, which is a weighted mean of the fluid velocity.

Secondly, consider a motion periodic in x such that

$$\psi = \epsilon\phi(y)\cos(\beta x+\eta) \tag{25}$$

with $\phi(a) = 0 = \phi(-a)$. For simplicity, α and β are assumed to be commensurable; the integrations in equations (9), (10), etc., are taken over a length in the x-direction which is a multiple of the wavelengths $2\pi/\alpha$, $2\pi/\beta$. One then finds that, in spite of the degeneracy, the first-order perturbation in σ_r is always zero. Thus a succession of oppositely-directed circulations does not, to the first approximation, lead to any drift of the field in a normal mode.

The results for decay in a circular cylinder of radius a are similar. In terms of polar coordinates r, θ the unperturbed eigenfunctions are

$$A = CJ_n(Kr)\begin{matrix}\cos\\ \sin\end{matrix}(n\theta), \tag{26}$$

where n is an integer, and K ($\equiv \sqrt{(4\pi\kappa\sigma)}$) is a root of the equation

$$J_{n-1}(Ka) = 0.$$

In non-uniform rotation with angular velocity $\omega(r)$ at a distance r from the axis, the first-order perturbation indicates a field rotating with angular velocity Ω, where

$$\Omega = \frac{\int_0^a r\omega(r)[J_n(Kr)]^2\,dr}{\int_0^a r[J_n(Kr)]^2\,dr}, \tag{27}$$

so that Ω is a weighted mean of $\omega(r)$. On the other hand, a succession of oppositely directed circulations given by

$$\psi = \epsilon\phi(r)\cos(m\theta+\eta) \quad (m \neq 0) \tag{28}$$

produces no first-order perturbation of the eigenvalues, i.e. no migration of the decaying field.

5. Fast motions: an exceptional case

In the presence of a fast shearing motion, two kinds of normal decay are in general possible. In the first, there is little interaction between the motion and the field, the lines of force being almost identical with the streamlines. The decay tends to create a pattern of lines of force differing slightly from that of the streamlines; the effect of the motion is simply to push them back and so restore the original form of the field. Thus the rate of decay is similar in order of magnitude to that in the absence of the motion.

In the second kind of decay-field the lines of force run across the streamlines; the effect of the motion is to elongate the lines of force in the direction of the motion and so to bring elements containing oppositely directed fields into close proximity. Thus in this case the motion greatly increases the rate of decay of the field.

The first type of decay, which includes only a limited set of modes, will be considered in this section. In modes of this type, A is given by

$$A = A_0(\psi)+A_1, \tag{29}$$

where $A_0(\psi)$ represents the main part of the field, with lines of force coinciding with the streamlines, and A_1 is a small correcting term. If this expression is substituted in equation (7), the part involving A_0 disappears in the vector-product term on the right; in the remaining terms A_1 can be neglected compared with A_0. Thus one finds that

$$\nabla^2 A_0 = 4\pi\kappa\{-\sigma A_0+\mathbf{k}.(\operatorname{grad}\psi\wedge\operatorname{grad}A_1)\}. \tag{30}$$

Since the vector product depends only on the component of grad A_1 along the streamlines, if ds and dn denote elements of length along and normal to a streamline, this equation can be written in the form

$$\nabla^2 A_0+4\pi\kappa\sigma A_0 = 4\pi\kappa\frac{\partial\psi}{\partial n}\frac{\partial A_1}{\partial s}. \tag{31}$$

Integrate this equation over the area δS bounded by the two adjacent streamlines $\psi, \psi+\delta\psi$. Then if $C(\psi)$ denotes the streamline ψ, the right-hand side of equation (31) gives

$$4\pi\kappa\,\delta\psi\int_{C(\psi)}\frac{\partial A_1}{\partial s}\,ds = 4\pi\kappa\,\delta\psi\int_{C(\psi)}dA_1 = 0.$$

Also, by Green's theorem,

$$\iint_{\delta S}\nabla^2 A_0\,dS = \int_{C(\psi+\delta\psi)}\frac{\partial A_0}{\partial n}\,ds-\int_{C(\psi)}\frac{\partial A_0}{\partial n}\,ds$$

$$= \delta\psi\frac{d}{d\psi}\left(\int_{C(\psi)}\frac{\partial A_0}{\partial n}ds\right) = \delta\psi\frac{d}{d\psi}\left(P(\psi)\frac{dA_0}{d\psi}\right)$$

where
$$P(\psi) = \int_{C(\psi)}\frac{\partial\psi}{\partial n}\,ds. \tag{32}$$

Again
$$\iint_{\delta S}A_0\,dS = A_0\,Q(\psi)\,\delta\psi,$$

where
$$Q(\psi) = \int_{C(\psi)}\left(\frac{\partial\psi}{\partial n}\right)^{-1}ds. \tag{33}$$

Thus the result of integrating (31) is the (self-adjoint) ordinary differential equation

$$\frac{d}{d\psi}\left(P(\psi)\frac{dA_0}{d\psi}\right)+4\pi\kappa\sigma\, Q(\psi)A_0 = 0. \tag{34}$$

This equation, together with the boundary conditions

$$A_0 = 0, \qquad dA_0/d\psi = 0$$

on the surface of the conductor, determines the eigenvalues σ. Numerical values of σ are most simply obtained from a variational (Rayleigh) principle; they are the stationary values of the Rayleigh quotient

$$\Sigma = (4\pi\kappa)^{-1}\int P(\psi)\left(\frac{dA_0}{d\psi}\right)^2 d\psi \Big/ \int Q(\psi)A_0^2\, d\psi \tag{35}$$

as the function $A_0(\psi)$ is varied. An alternative expression to (35) is

$$\Sigma = (4\pi\kappa)^{-1}\iint\left(\frac{dA_0}{d\psi}\right)^2 |\operatorname{grad}\psi|^2\, dS \Big/ \iint A_0^2\, dS, \tag{36}$$

the integrations again being over the cross-section of the cylinder. The advantage of (36) is that it frequently can be applied when explicit expressions for $P(\psi)$, $Q(\psi)$ cannot be found.

Numerical results have been obtained for motion in the circular cylinder $r = a$, with the stream function $\psi = K\psi_0$, where

$$\psi_0 = r(a^2-r^2)\cos\theta/a^3. \tag{37}$$

This represents a double circulation of the fluid; to give rapid motion, the constant K must be large. Equation (36) is used, with the approximating function $A_0 = \alpha\psi_0^2+\beta\psi_0^4$. The least value of Σ then gives $\sigma\pi\kappa a^2 = 4{\cdot}41$ as an approximation (probably a good one) to the lowest eigenvalue. For comparison, in the absence of motion the lowest eigenvalues corresponding to $n = 1$ and $n = 2$ in equation (26) make $\sigma\pi\kappa a^2$ equal to $1{\cdot}45$ and $3{\cdot}67$ respectively. Thus the decay is speeded up by the motion, but remains of the same order of magnitude.

6. Fast motions: the slab problem

The second type of decay in the presence of fast motions (that in which the lines of force run across the streamlines) will be studied in two special cases. These are non-uniform streaming in an infinite slab, and non-uniform rotation in a circular cylinder.

Consider first the slab problem. As in section 4, the slab is bounded by the walls $y = \pm a$, the motion $\mathbf{v}$ between the walls being in the x-direction. For simplicity we consider a linear velocity-profile, given by

$$v = \mu y, \qquad \psi = -\tfrac{1}{2}\mu y^2. \tag{38}$$

Then equation (7) reduces to

$$\nabla^2 A + 4\pi\kappa\sigma A = 4\pi\kappa\mu y \frac{\partial A}{\partial x}. \tag{39}$$

A solution periodic in x is taken to be

$$A = f(y)e^{i\alpha x - \sigma t}, \tag{40}$$

where f satisfies the equation

$$\frac{d^2 f}{dy^2} + (4\pi\kappa\sigma - \alpha^2 - 4\pi\kappa\mu i\alpha y)f = 0. \tag{41}$$

At the walls of the slab, A must join up smoothly with solutions of Laplace's equation which vanish at $y = \pm\infty$. These are

$$\begin{aligned} A &= Ce^{\alpha(ix-y)-\sigma t} \quad (y \geqslant a), \\ &= De^{\alpha(ix+y)-\sigma t} \quad (y \leqslant a). \end{aligned}$$

Thus, to make A and its derivatives continuous at the slab walls, $f(y)$ must satisfy the boundary conditions

$$f'(a) = -\alpha f(a), \qquad f'(-a) = \alpha f(-a). \tag{42}$$

Non-dimensional combinations of the different parameters are defined by the equations

$$\left.\begin{aligned} q &= \alpha a, & p &= 4\pi\kappa a^2\mu q \\ w &= p^{-1}(4\pi\kappa a^2\sigma - q^2), & Y &= y/a \end{aligned}\right\}. \tag{43}$$

Then equations (41) and (42) become

$$\frac{d^2 f}{dY^2} + p(w - iY)f = 0 \tag{44}$$

and

$$f'(1) = -qf(1), \qquad f'(-1) = qf(-1), \tag{45}$$

where in equation (45) f is regarded as a function of Y. The fact that the motion is fast implies that p is large; the magnitude of w depends on that of σ.

Let new variables Z, X be defined by

$$Z = p(w - iY), \qquad X = \tfrac{2}{3}iZ^{\frac{3}{2}}/p. \tag{46}$$

Then the solution of equation (44) is expressible in terms of Hankel functions in the form

$$f = Z^{\frac{1}{2}}[PH_{\frac{1}{3}}^{(1)}(X) + QH_{\frac{1}{3}}^{(2)}(X)]. \tag{47}$$

On inserting this expression into equations (45), and using the recurrence relations for Hankel functions, one finds that

$$\left.\begin{aligned} Z_1^{\frac{1}{2}}[PH_{-\frac{2}{3}}^{(1)}(X_1) + QH_{-\frac{2}{3}}^{(2)}(X_1)] &= -q[PH_{\frac{1}{3}}^{(1)}(X_1) + QH_{\frac{1}{3}}^{(2)}(X_1)] \\ Z_2^{\frac{1}{2}}[PH_{-\frac{2}{3}}^{(1)}(X_2) + QH_{-\frac{2}{3}}^{(2)}(X_2)] &= q[PH_{\frac{1}{3}}^{(1)}(X_2) + QH_{\frac{1}{3}}^{(2)}(X_2)] \end{aligned}\right\}, \tag{48}$$

where

$$\left.\begin{aligned} Z_1 &= p(w-i), & Z_2 &= p(w+i) \\ X_1 &= \tfrac{2}{3}ip^{\frac{1}{2}}(w-i)^{\frac{3}{2}}, & X_2 &= \tfrac{2}{3}ip^{\frac{1}{2}}(w+i)^{\frac{3}{2}} \end{aligned}\right\}. \tag{49}$$

If the ratio P/Q is eliminated between equations (48), the result is

$$\begin{aligned}(Z_1 Z_2)^{\frac{1}{2}}[H^{(1)}_{-\frac{1}{3}}(X_1)H^{(2)}_{-\frac{1}{3}}(X_2)-H^{(2)}_{-\frac{1}{3}}(X_1)H^{(1)}_{-\frac{1}{3}}(X_2)]-\\ -Z_1^{\frac{1}{2}}q[H^{(1)}_{-\frac{1}{3}}(X_1)H^{(2)}_{\frac{1}{3}}(X_2)-H^{(2)}_{-\frac{1}{3}}(X_1)H^{(1)}_{\frac{1}{3}}(X_2)]+\\ +Z_2^{\frac{1}{2}}q[H^{(1)}_{\frac{1}{3}}(X_1)H^{(2)}_{-\frac{1}{3}}(X_2)-H^{(2)}_{\frac{1}{3}}(X_1)H^{(1)}_{-\frac{1}{3}}(X_2)]-\\ -q^2[H^{(1)}_{\frac{1}{3}}(X_1)H^{(2)}_{\frac{1}{3}}(X_2)-H^{(2)}_{\frac{1}{3}}(X_1)H^{(1)}_{\frac{1}{3}}(X_2)]=0. \qquad (50)\end{aligned}$$

This is an equation giving the eigenvalues of w, and so of the decay constant σ, for given values of p and q.

7. Asymptotic expansions

By equations (49), Z_1 and Z_2 are in general large of order p, and X_1 and X_2 of order $p^{\frac{1}{2}}$. Thus in equation (50) the Hankel functions can be replaced by their asymptotic expansions. Since for all values of X these indicate that $H^{(1)}_{-\frac{1}{3}}(X)$, $H^{(2)}_{-\frac{1}{3}}(X)$ are comparable in order of magnitude with $H^{(1)}_{\frac{1}{3}}(X)$, $H^{(2)}_{\frac{1}{3}}(X)$, the term involving $(Z_1 Z_2)^{\frac{1}{2}}$ in equation (50) dominates the other terms, so that the equation can be simplified to

$$H^{(1)}_{-\frac{1}{3}}(X_1)H^{(2)}_{-\frac{1}{3}}(X_2)-H^{(2)}_{-\frac{1}{3}}(X_1)H^{(1)}_{-\frac{1}{3}}(X_2)=0. \qquad (51)$$

The leading terms of the asymptotic expansions are as follows, for different ranges of $\arg X$:

$$H^{(1)}_\nu(X)=\left(\frac{2}{\pi X}\right)^{\frac{1}{2}}e^{i(X-\frac{1}{2}\nu\pi-\frac{1}{4}\pi)} \quad (-\pi<\arg X<2\pi) \qquad (a)$$

$$=\left(\frac{2}{\pi X}\right)^{\frac{1}{2}}\{2\cos\nu\pi\, e^{-i(X+\frac{1}{2}\nu\pi+\frac{3}{4}\pi)}+e^{i(X-\frac{1}{2}\nu\pi-\frac{1}{4}\pi)}\} \quad (-2\pi<\arg X<0) \qquad (b)$$

$$H^{(2)}_\nu(X)=\left(\frac{2}{\pi X}\right)^{\frac{1}{2}}e^{-i(X-\frac{1}{2}\nu\pi-\frac{1}{4}\pi)} \quad (-2\pi<\arg X<\pi) \qquad (c)$$

$$=\left(\frac{2}{\pi X}\right)^{\frac{1}{2}}\{2\cos\nu\pi\, e^{i(X+\frac{1}{2}\nu\pi+\frac{3}{4}\pi)}+e^{-i(X-\frac{1}{2}\nu\pi-\frac{1}{4}\pi)}\} \quad (0<\arg X<2\pi). \qquad (d)$$

In the range $-\pi<\arg X<0$, where both (a) and (b) are valid, the extra term in (b) is negligible; a similar remark applies to (c) and (d) in the range $0<\arg X<\pi$.

Using these and similar relations, equation (51) can readily be shown to possess solutions only if w has a positive real part, and an imaginary part lying between -1 and $+1$. When w lies in this range,

$$-\tfrac{1}{4}\pi<\arg X_1<\tfrac{1}{2}\pi<\arg X_2<\tfrac{5}{4}\pi. \qquad (52)$$

The expansion (a) can accordingly be used for both $H^{(1)}_\nu(X_1)$ and $H^{(1)}_\nu(X_2)$,

but (c) must be used for $H_\nu^{(2)}(X_1)$ and (d) for $H_\nu^{(2)}(X_2)$. On use of these expressions, equation (51) becomes, after simplification,

$$\exp\{\tfrac{4}{3}p^{\frac{1}{2}}(w+i)^{\frac{3}{2}}\}-\exp\{\tfrac{4}{3}p^{\frac{1}{2}}(w-i)^{\frac{3}{2}}\} = i. \tag{53}$$

The solutions of this equation fall into two groups, corresponding respectively to real and complex values of w.

8. Real eigenvalues

If w is real, let us write

$$(w\pm i)^{\frac{1}{2}} = \gamma\pm i\delta, \tag{54}$$

where γ and δ are real. Then equation (53) further simplifies to give

$$\sin(\tfrac{4}{3}p^{\frac{1}{2}}\delta) = \tfrac{1}{2}\exp(-\tfrac{4}{3}p^{\frac{1}{2}}\gamma). \tag{55}$$

In this equation, γ cannot be appreciably negative, since this would make the right-hand side large, whereas the left-hand side cannot exceed unity. Now $\gamma = 0$ corresponds to $w = w_0 \equiv 1/\sqrt{3}$; hence the possible values of w are effectively limited to the range $w \geqslant w_0$. By equation (49), this in turn implies that $4\pi\kappa a^2\sigma$ is large of order p, so that decay of the field in these modes is fast compared with that in the fundamental mode in the absence of motion.

If w is appreciably greater than w_0, $p^{\frac{1}{2}}\gamma$ is large, and the right-hand side of equation (55) is negligible. Thus in this case approximately

$$\sin(\tfrac{4}{3}p^{\frac{1}{2}}\delta) = 0, \qquad \tfrac{4}{3}p^{\frac{1}{2}}\delta = \nu\pi, \tag{56}$$

where ν is a sufficiently large integer. In particular, if the decay is very rapid, w is large and $\delta \doteq \frac{3}{2}w^{\frac{1}{2}}$, so that

$$2(wp)^{\frac{1}{2}} = \nu\pi, \qquad 4\pi\kappa\sigma = \alpha^2+\tfrac{1}{4}\nu^2\pi^2a^{-2}. \tag{57}$$

Equation (57) gives the same expression for the decay constant σ as equation (22), valid in the absence of fluid motion. This is not surprising; if the decay is sufficiently fast, the motion has insufficient time to modify it appreciably.

All save one or two values of w are given very closely by equation (56). But in this equation δ cannot be less than $(\frac{4}{3})^{\frac{1}{2}}$, its value for $w = w_0$; thus

$$\nu\pi > (\tfrac{4}{3})^{\frac{1}{2}}p^{\frac{1}{2}}. \tag{58}$$

This implies that as p increases the number of modes of decay with a real w continually decreases. In fact, the number of intersections in the (χ, w)-plane of the two curves

$$\chi = \sin(\tfrac{4}{3}p^{\frac{1}{2}}\delta), \qquad \chi = \tfrac{1}{2}\exp(-\tfrac{4}{3}p^{\frac{1}{2}}\gamma)$$

continually decreases as the increase in p compresses the sine-curve towards the axis $w = 0$, and carries progressively more and more of its arches past the value $w = w_0$ for which the exponential is unity. One can expect that

the eigenvalues of w will coalesce in pairs and then be replaced by pairs of conjugate complex eigenvalues. This conclusion is confirmed by the numerical work described later.

9. Complex eigenvalues

Consider now the complex solutions of equation (53). The assumption (52) made in deriving this equation corresponds to

$$-\tfrac{1}{2}\pi < \arg(w-i) < 0 < \arg(w+i) < \tfrac{1}{2}\pi.$$

In Fig. 1 the lines AB, CD are the lines

$$\arg(w-i) = -\tfrac{1}{3}\pi, \qquad \arg(w+i) = \tfrac{1}{3}\pi$$

in the complex w-plane; on AB, $(w-i)^{\frac{3}{2}}$ is purely imaginary; on CD, $(w+i)^{\frac{3}{2}}$ is purely imaginary. If w is appreciably above AB, the term $\exp\{\frac{4}{5}p^{\frac{1}{2}}(w-i)^{\frac{5}{2}}\}$

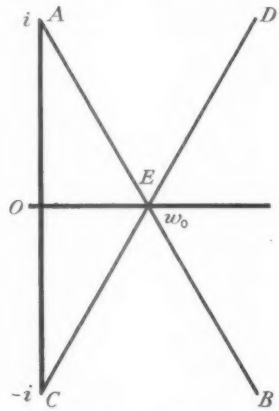

FIG. 1. Lines in the complex w-plane. w_0 is the point $w = 1/\sqrt{3}$

of equation (53) is large. Thus in this case equation (53) can be satisfied only if w is appreciably below CD, so that $\exp\{\frac{4}{5}p^{\frac{1}{2}}(w+i)^{\frac{5}{2}}\}$ is also large. But in this case the equation becomes

$$\exp\{\tfrac{4}{5}p^{\frac{1}{2}}(w+i)^{\frac{5}{2}}\} = \exp\{\tfrac{4}{5}p^{\frac{1}{2}}(w-i)^{\frac{5}{2}}\},$$

which is satisfied only by real values of w in the ranges of $\arg(w\pm i)$ under consideration. Thus no complex roots of equation (53) exist such that w is appreciably above AB; similarly, none exist such that w is appreciably below CD.

If w is appreciably below AB and above CD, both of the exponentials on the left of equation (53) are small, and their difference cannot equal i. Thus the only possibility for complex solutions of (53) is that the point w

should be very near one or both of the lines AB, CD. The intersection E of the lines is the point $w = w_0$ near which the transition from real to complex eigenvalues takes place. Only a small number of solutions of (53) can be expected to correspond to points w near to E; most of the complex eigenvalues correspond to points near AE or CE, but well away from E.

Consider, for example, values of w corresponding to a point near AE but appreciably above CE. Then the first exponential on the right of equation (53) is negligible, and the equation becomes

$$\exp\{\tfrac{4}{3}p^{\frac{1}{2}}(w-i)^{\frac{3}{2}}\} = -i.$$

This has roots

$$w = i + \left(\frac{9}{16p}\right)^{\frac{1}{3}}[(2\nu'+\tfrac{1}{2})\pi]^{\frac{2}{3}}e^{-\frac{1}{3}\pi i}, \tag{59}$$

where ν' is a positive integer or zero. Similarly, the roots of equation (53) corresponding to points near CE but appreciably below AE are given by

$$w = -i + \left(\frac{9}{16p}\right)^{\frac{1}{3}}[(2\nu'+\tfrac{1}{2})\pi]^{\frac{2}{3}}e^{\frac{1}{3}\pi i}. \tag{60}$$

The condition that the points w given by equations (59) and (60) must not reach E is that

$$(2\nu'+\tfrac{1}{2})\pi < (\tfrac{4}{3})^{\frac{1}{2}}p^{\frac{1}{2}}.$$

Thus the total number of complex eigenvalues is roughly $\pi^{-1}(\frac{4}{3})^{\frac{1}{2}}p^{\frac{1}{2}}$. This agrees, as is to be expected, with the number excluded from the set of real eigenvalues by equation (58); effectively the real eigenvalues which have disappeared have been replaced by an equal number of complex ones.

The lowest eigenvalues given by (59) make $w-i$ small, of order $p^{-\frac{1}{2}}$. This means that the asymptotic formulae used in deriving equation (53) are not strictly applicable to the lowest one or two of the eigenvalues; in fact, (59) gives

$$X_1 = \tfrac{2}{3}ip^{\frac{1}{2}}(w-i)^{\frac{3}{2}} = \tfrac{1}{2}(2\nu'+\tfrac{1}{2})\pi,$$

which is not large for the lowest eigenvalues. However, equation (58) should give all save the lowest one or two eigenvalues satisfactorily, and even for these it should at least give the correct order of magnitude.

Let $w = c+id$, where c and d are real. Then, by equations (43),

$$\sigma = \mu\alpha a(c+id)+\alpha^2/(4\pi\kappa). \tag{61}$$

The decay field is proportional to $e^{i\alpha x-\sigma t}$, and so includes a factor

$$e^{i\alpha(x-\mu adt)}.$$

This implies that the field is undergoing a translation with velocity μad. For the eigenvalues given by equation (59), $0 < d < 1$; thus the velocity is that of the fluid at a point $y = ad$ between the central plane $y = 0$ and the boundary $y = a$. Similarly, for the eigenvalues given by (60) the field

moves with the velocity of a point $y = -ad$ of the fluid below the plane $y = 0$. For the lowest eigenvalues (ν' small in (59) or (60)) the velocity of the field is very nearly that of the fluid at one boundary.

The rate of decay of the field is given by the real part of σ, which is found to be

$$(4\pi\kappa)^{-1}(\alpha^2+pc/a^2) = (4\pi\kappa)^{-1}\left\{\alpha^2+\frac{1}{2a^2}\left[\frac{3p\pi}{4}(2\nu'+\tfrac{1}{2})\right]^{\frac{2}{3}}\right\}. \tag{62}$$

Thus the rate of decay increases with p, roughly like $p^{\frac{2}{3}}$; for all the lower modes it is much faster than that in the absence of motion, given by equation (22).

The transition from real to complex eigenvalues takes place at

$$w = w_0 = 1/\sqrt{3}.$$

This corresponds to a time of decay σ^{-1} roughly equal to

$$4\pi\kappa a^2\sqrt{3}/p = \sqrt{3}/(\mu\alpha a).$$

Since the fluid at the walls $y = \pm a$ travels a wavelength $2\pi/\alpha$ of the field in time $2\pi/(\mu\alpha a)$, real eigenvalues are impossible if fluid at the walls travels more than about a quarter of a wavelength in the time of decay. When the motion is faster than this, the field is carried about with the fluid.

10. The decay fields

In modes corresponding to real values of w, the decay fields can be expected, like the eigenvalues, to be little affected by the motion. The decay fields for the complex eigenvalues have more interest.

Consider values of w corresponding in Fig. 1 to points of AE not close to E. The field corresponding to the vector-potential of equations (40) and (47) is

$$H_x = -(Z/a)[PH^{(1)}_{-\frac{2}{3}}(X)+QH^{(2)}_{-\frac{2}{3}}(X)]e^{i\alpha x-\sigma t},$$
$$H_y = i\alpha Z^{\frac{1}{2}}[PH^{(1)}_{\frac{1}{3}}(X)+QH^{(1)}_{\frac{1}{3}}(X)]e^{i\alpha x-\sigma t}.$$

Here the ratio P/Q is found to be $e^{\frac{1}{6}i\pi}$. Hence, using the asymptotic forms (a) and (c) of section (7), one finds that, except for values of y very nearly equal to a,

$$\left.\begin{aligned} H_x &= -\frac{QZ}{a}\sqrt{\left(\frac{2}{\pi X}\right)}e^{-i(X+\frac{1}{12}\pi)}e^{i\alpha x-\sigma t} \\ H_y &= -Q\alpha Z^{\frac{1}{2}}\sqrt{\left(\frac{2}{\pi X}\right)}e^{-i(X+\frac{1}{12}\pi)}e^{i\alpha x-\sigma t} \end{aligned}\right\}. \tag{63}$$

In this, $X = \frac{2}{3}ip^{\frac{1}{2}}(w-iy/a)^{\frac{3}{2}}$. Because of the factor $p^{\frac{1}{2}}$, the imaginary part of X varies rapidly as y varies, and it has a maximum value when

$$y/a = \mathrm{im}(w) = d.$$

Thus the magnetic field attains its maximum value on the plane $y = ad$,

where the fluid and the field have the same velocity. Well away from this plane, the field is negligibly small. Thus it is always small on the face $y = -a$ of the slab; it is also small on the face $y = a$, save for the lowest few eigenvalues, for which the maximum field is attained near $y = a$.

From equation (63) the ratio H_x/H_y is of order $Z^{\frac{1}{2}}$, and so is large of order $p^{\frac{1}{2}}$ (save near the boundaries of the slab). This shows that the loops in the lines of force are greatly elongated in the x-direction as a consequence of the motion.

The case when w corresponds to a point of CE in Fig. 1 can be treated similarly; the only difference is that the maximum field is attained below the central plane $y = 0$.

11. Other velocity profiles

In the problem just considered, the existence of a family of real eigenvalues depended on the skew-symmetry of the velocity-profile with respect to the central plane. No such family would exist for a less special profile, though the eigenvalues for a general velocity varying monotonically across the section can be expected to have properties generally like those for the linear velocity profile.

The properties of eigenvalues when the variation of the velocity is not monotonic can be roughly inferred from those for the 'roof-top' profile given by

$$v = \mu(a-y) \quad (0 \leqslant y \leqslant a), \qquad v = \mu(a+y) \quad (-a \leqslant y \leqslant 0). \tag{64}$$

The discussion of this profile exactly follows that for the linear profile; hence only the main results need be quoted. In the sufficiently high modes, the field is carried along with the velocity of the fluid at $y = \pm\frac{1}{2}a$; the eigenvalues for very rapid decay are given by

$$4\pi\kappa\sigma = \alpha^2 + \tfrac{1}{4}\nu^2\pi^2 a^{-2} + (4\pi\kappa)\,\tfrac{1}{2}\mu\alpha a i, \tag{65}$$

which differs from equation (57) only through the imaginary part which represents the velocity of translation of the field.

The lower modes (those corresponding to the complex eigenvalues of section 9) fall into two groups. In one group, the field moves with a velocity less than $\frac{1}{2}\mu a$, the velocity becoming small for the lowest modes. In the other group, the velocity of the field is greater than $\frac{1}{2}\mu a$, and approaches μa for the lowest modes. The field in either case attains a strong maximum on the planes where it moves with the velocity of the fluid; these planes are near the walls of the slab for the first group, near the central plane $y = 0$ for the second group. The first group corresponds to pairs of virtually) equal eigenvalues, given by

$$4\pi\kappa\sigma = \alpha^2 + \tfrac{1}{2}(1+i\sqrt{3})\{3(2\nu+\tfrac{1}{2})\pi^2\mu\alpha\kappa\}^{\frac{2}{3}}. \tag{66}$$

The appearance of these pairs of values corresponds to the fact that the field is vanishingly small near $y = 0$, so that effectively decay modes exist such that the field is limited to one or the other of the regions $y > 0$, $y < 0$. No such pairs exist for the second group, for which the eigenvalues are given by

$$4\pi\kappa\sigma = \alpha^2 + 4\pi\kappa\mu\alpha a i + \tfrac{1}{2}(1 - i\sqrt{3})\{3(\nu + \tfrac{1}{2})\pi^2\mu\alpha\kappa\}^{\frac{2}{3}}. \tag{67}$$

As regards other velocity-profiles, when the velocity is an analytic function of y, general methods of the theory of functions of complex variables can be used to determine the eigenvalues (**4**). Such methods are, however, of limited application here, and will not be discussed.

12. The cylinder problem

Non-uniform rotation in a circular cylinder can be discussed like the streaming in a slab. For illustration, consider the case when the angular velocity at a distance r from the axis of the cylinder is λr. In terms of polar coordinates r, θ equation (4) then becomes

$$\frac{\partial^2 A}{\partial r^2} + \frac{1}{r}\frac{\partial A}{\partial r} + \frac{\partial^2 A}{r^2 \partial\theta^2} = 4\pi\kappa\left(\frac{\partial A}{\partial t} + \lambda r \frac{\partial A}{\partial\theta}\right). \tag{68}$$

Assume a solution of form

$$A = r^{-\frac{1}{2}} f(r) e^{in\theta - \sigma t},$$

where n is a positive integer. Then the radial function $f(r)$ must satisfy

$$\frac{d^2 f}{dr^2} + \left\{4\pi\kappa(\sigma - in\lambda r) - \frac{n^2 - \frac{1}{4}}{r^2}\right\} f = 0. \tag{69}$$

This has to be solved subject to the boundary conditions that f is finite at $r = 0$, and $df/dr = -(n - \frac{1}{2})f/r$ at the boundary $r = a$ of the cylinder.

If λ is large, we may expect from the results of the slab problem that σ is in general of order $n\lambda a$. Thus, within a range $0 < r \leqslant (4\pi\kappa\lambda)^{\frac{1}{2}}$, the term involving $n\lambda r$ in equation (69) is negligible compared with the σ-term; in the range $(4\pi\kappa\lambda)^{\frac{1}{2}} < r < a$, the term $(n^2 - \frac{1}{4})/r^2$ is negligible compared with the σ-term. Approximating by neglecting these terms in the appropriate ranges, we can obtain asymptotic expressions for the solutions of equation (69) in the two ranges; both asymptotic expressions are valid near

$$r = (4\pi\kappa\lambda)^{-\frac{1}{4}},$$

which enables the arbitrary constants in the two to be linked up.

When this is done one finds that, in order to satisfy the boundary conditions, an equation must be satisfied of the form

$$\exp\{\tfrac{4}{3}p^{\frac{1}{2}}(w+i)^{\frac{3}{2}} - in\pi - \tfrac{1}{2}i\pi\} - \exp\{\tfrac{4}{3}p^{\frac{1}{2}}(w-i)^{\frac{3}{2}}\} = i, \tag{70}$$

where

$$p = \tfrac{1}{2}\pi\kappa a^3 n\lambda, \qquad w = -i + 2\sigma/\lambda a n. \tag{71}$$

Equation (70) corresponds to equation (53) for the slab problem.

As in the slab problem, there are two sets of solutions. For the modes of very fast decay, w is real; this implies that the field rotates with the angular velocity $\frac{1}{2}\lambda a$ of the fluid at $r = \frac{1}{2}a$. For modes of less rapid decay, the field rotates faster or slower than this; for the low modes, it rotates with the angular velocity of fluid near the axis of the cylinder or near the surface. The decay field is small save where the field and fluid are rotating with the same angular velocity.

13. Moderate velocities

In order to indicate how the results for low and high velocities join up, the slab problem of section 6 has been studied numerically for moderate velocities. The range of velocities considered is that in which takes place the transition of the lowest pair of eigenvalues from real to complex values

The equation to be studied is (44), i.e.

$$\frac{d^2f}{dY^2}+(\rho^2-ipY)f = 0, \tag{72}$$

where $\rho^2 = pw$; the boundary conditions are

$$f'(1) = -qf(1), \qquad f'(-1) = qf(-1). \tag{73}$$

If ρ^2 is real, any function f satisfying these conditions can be shown to be of the form

$$f = e^{i\phi}(U+iV), \tag{74}$$

where U is even and V odd in Y, and ϕ is a constant. This implies that, if u and v are the real and imaginary parts of f,

$$u'(0)/v'(0) = -v(0)/u(0), \tag{75}$$

each of these expressions being in fact equal to $-\tan\phi$.

Accordingly the calculation for real eigenvalues proceeded as follows. For simplicity the quantity $q = \alpha a$ was taken to be unity. A solution satisfying the boundary condition $f'(-1) = f(-1)$ was begun at $Y = -1$, the Taylor series at $Y = -1$ being used to give the values at $Y = -0{\cdot}9$ and $-0{\cdot}8$. The values at $Y = -0{\cdot}7$, $-0{\cdot}6$, $-0{\cdot}5$,..., were then found by repeated use of the approximate formula

$$h^2f''(a) = f(a+h)+f(a-h)-2f(a) \tag{76}$$

with $h = 0{\cdot}1$. This formula neglects terms of order h^4, but is sufficiently accurate for present purposes; its use is far less laborious than using the Taylor series. Corresponding to a suitable value of p, solutions were tabulated for several different values of ρ^2. The correct value of ρ^2 is that for which the solution satisfies equation (75).

The variation of ρ^2 with p is shown in Table 1 for the lowest two modes. The values corresponding to $p = 0$ are those given by equation (21). As

p increases, the two values of ρ^2 come together, and finally coalesce at $p = 3{\cdot}6$, which therefore corresponds to the transition to complex eigenvalues. This value of p implies that fluid at the slab walls travels about one-sixth of the wavelength $2\pi/\alpha$ of the field in the decay time σ^{-1}.

TABLE 1

p	$0{\cdot}0$	$2{\cdot}0$	$3{\cdot}3$	$3{\cdot}6$
ρ^2	$0{\cdot}7$	$1{\cdot}1$	$1{\cdot}9$	$2{\cdot}7$
	$4{\cdot}1$	$3{\cdot}9$	$3{\cdot}2$	$2{\cdot}7$

Complex eigenvalues are less easy to discuss, because of the absence of a symmetry condition like that of equation (74). The method finally adopted involved abandoning assigning a value to q beforehand. Put

$$\rho^2 = q^2(\gamma+i\delta), \qquad Y = q^{-1}\eta+\delta/p, \qquad \Omega = p/q^3. \tag{77}$$

Then the equation satisfied by f is

$$d^2f/d\eta^2+(\gamma-i\Omega\eta)f = 0 \tag{78}$$

and the boundary conditions are

$$\left.\begin{aligned} f'(\eta)/f(\eta) &= 1 \quad \text{at} \quad \eta = -q(1+\delta/p) = b, \text{ say} \\ &= -1 \quad \text{at} \quad \eta = \quad q(1-\delta/p) = c, \text{ say} \end{aligned}\right\}. \tag{79}$$

If f_1 and f_2 are two independent solutions of equation (78), the general solution is $f = Af_1+Bf_2$. On elimination of the ratio A/B between the two equations (79), one gets

$$\frac{f_1'(b)+f_1(b)}{f_2'(b)+f_2(b)} = \frac{f_1'(c)-f_1(c)}{f_2'(c)-f_2(c)}. \tag{80}$$

Accordingly, to obtain complex eigenvalues assigned values were adopted for Ω and γ. The two independent solutions f_1, f_2 were obtained by numerical integration of equation (78). The (complex) functions on either side of equation (80) were then tabulated for negative values of b and positive values of c. If Ω was large enough, values of b and c could be found graphically to satisfy equation (80); knowing these and Ω, values of q, p, and δ could then be derived.

When $q = 1$, the transition from real eigenvalues to complex was found to occur at $\Omega = p = 3{\cdot}6$, $\rho^2 = \gamma = 2{\cdot}7$. Thus to get complex eigenvalues the values $\Omega = 4{\cdot}0$, $\gamma = 2{\cdot}7$ were adopted; this gave

$$q = 0{\cdot}99, \qquad \delta/\Omega = \pm 0{\cdot}16.$$

The value of δ implies that the field moves with an x-velocity equal to that of the fluid at $y = \pm 0{\cdot}16a$. Since q differs so little from unity, the results so obtained can be regarded as continuing those for real eigenvalues with $q = 1$.

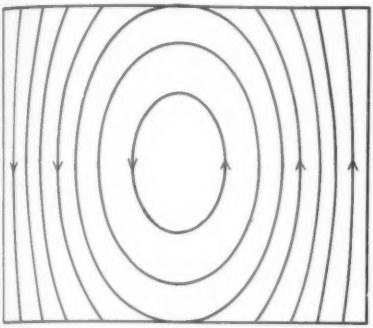

FIG. 2.

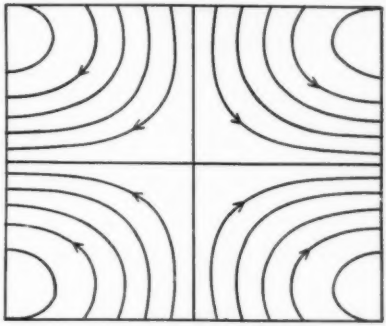

FIG. 3.

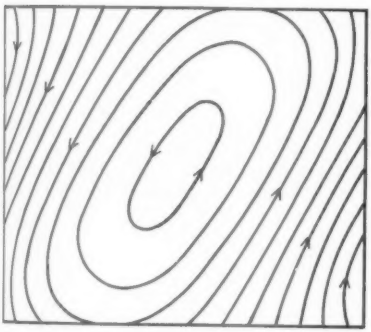

FIG. 4.

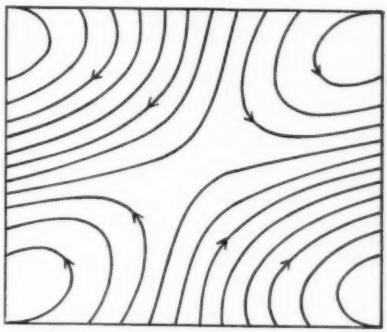

FIG. 5.

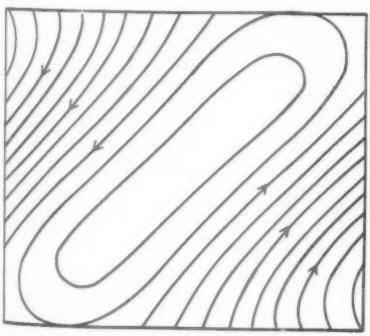

FIG. 6.

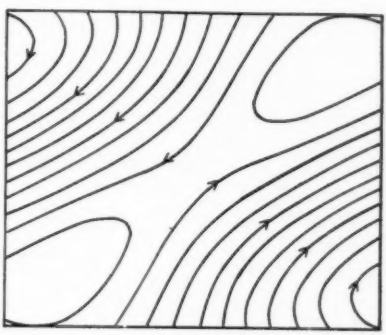

FIG. 7.

FIGS. 2–7. Lines of force for first and second decay modes in the slab problem, for different values of the velocity parameter p. Figs. 2 and 3, $p = 0$; Figs. 4 and 5, $p = 2$; Figs. 6 and 7, $p = 3{\cdot}3$

Lines of force for both real and complex eigenvalues are shown in Figs. 2–9, where the curves correspond to different constant values of the real part of A. In each diagram, the upper and lower boundaries are the walls $y = \pm a$ of the fluid; the breadth is one-half of a wavelength of the field. It can be seen that increased values of the velocity parameter p

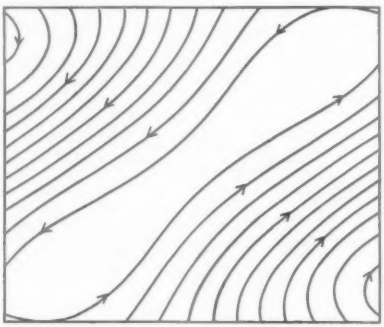

FIG. 8. Lines of force corresponding to $p = 3{\cdot}6$, for which first and second decay modes coalesce

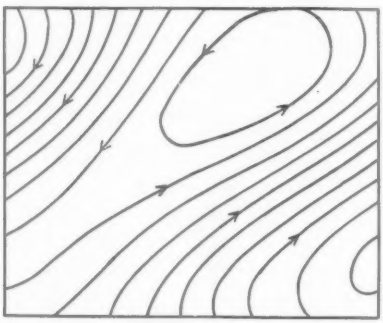

FIG. 9. Lines of force corresponding to $\Omega = 4$, $\gamma = 2{\cdot}7$, for which fields in the first pair of decay modes are being transported with the fluid

at first lead to a stretching of the lines of force in the direction of motion, and to a closer approach of the patterns representing the first and second modes to each other. After the coalescence of these two modes, complex eigenvalues appear which correspond to a good deal of asymmetry of the field with respect to the plane $y = 0$.

14. Conclusions

The results outlined above make it possible to predict the nature of decay fields in the presence of an arbitrary two-dimensional motion. Such a

motion can be divided up into circulations in separate regions, bounded by streamlines passing through stagnation points. In the interior of any such region, the decay fields will vary roughly as in the problems considered above. In slow motion, or in fast motion when there is very rapid decay, the field in any region will be carried round with a period of circulation which is a mean of periods of circulation in all the regions.

In fast motion when the decay is less rapid, the difficulty of transporting lines of force through the stagnation points can be overcome only by supposing that very few of the lines of force cross the boundaries of the regions, and that these are mainly concentrated just in front of the stagnation points. In this case the lines of force, when not nearly coincident with the streamlines, will be greatly extended in the direction of the motion. The field will be transported by the circulations, and will attain maximum strength on streamlines where its period of circulation equals that of the fluid. The modes of slowest decay will circulate with nearly the period of circulation characteristic of streamlines on which this period is a maximum or a minimum. These may include streamlines immediately surrounding, or passing through, a stagnation point. In the first case the decay modes can effectively be taken as modes in which the field is confined to one of the regions; in the second, when the field circulates with the fluid near the boundary of the regions, some slight interdependence of the regions is possible. As the velocity increases, the period of decay in the lowest modes varies roughly inversely as the $\frac{2}{3}$ power of the velocity (save for the special modes for which the lines of force and streamlines nearly coincide).

REFERENCES

1. E. C. Bullard and H. Gellman, *Phil. Trans.* A, **247** (1954) 213.
2. T. G. Cowling, *Monthly Notices R.A.S.* **94** (1934) 39; *Quart. J. Mech. App. Math.* **10** (1957) 129.
3. S. Chandrasekhar, *Astrophys. J.* **124** (1956) 234 and 244.
4. R. E. Langer, *Trans. American Math. Soc.* **34** (1932) 447.

NON-UNIFORM SHEAR FLOW PAST CYLINDERS

By JAMES D. MURRAY

(*Harvard University, Massachusetts, U.S.A.*)

[Received 24 May 1956; revise received 17 December 1956]

SUMMARY

A general method is described whereby an approximation of any desired degree of accuracy to the stream functions for two types of variable shear flows past finite cylinders can be obtained. The two shear distributions in the free stream can be approximated to the linear shear distribution and the shear present in an unretarded incompressible boundary layer respectively. In every case the stagnation streamline is displaced from the position opposite the line of symmetry of the cylinder, and general expressions are obtained for this displacement. The line of symmetry may be in the direction of or perpendicular to the direction of flow. The two particular examples cited are those of a general elliptic cylinder and cylinders of the form $r = p(1+\gamma\cos\theta)$, where $|\gamma| < 1$, r and θ being the polar coordinates, and $2p$ the maximum width of the cylinder.

Nomenclature

J	Bessel function of the first kind.
I	Modified Bessel function of the first kind.
Y	Bessel function of the second kind.
K	Modified Bessel function of the second kind.
l	Typical linear dimension.
L	Perimeter of the cylinder.
N	Rotational flow parameter ($= U/\omega_0 l$).
p	Typical length in the cylinder.
q	Velocity.
$q_\|$	Velocity on the cylinder.
q_x, q_y	Velocity components in the x- and y-directions.
q_r, q_θ	Radial and transverse velocity components.
r, θ	Polar coordinates.
U	Standard velocity.
x, y	Cartesian coordinates.
y_s	Deflexion of the stagnation streamline in the free stream.
α	Angle the tangent to the cylinder makes with the x-axis.
γ	General parameter.
Γ	Circulation.
δ	Thickness of the incompressible boundary layer.
ϵ	Eccentricity of the ellipse.
ψ	Stream function.

Ψ Disturbance stream function.
ω Vorticity.
∇^2 Laplacian operator.

1. Introduction

THE stream function ψ for the steady, rotational two-dimensional flow of an incompressible inviscid fluid satisfies

$$\frac{\partial^2\psi}{\partial x^2}+\frac{\partial^2\psi}{\partial y^2}+\omega=0, \tag{1}$$

where the vorticity ω, given by

$$\omega=\frac{\partial q_y}{\partial x}-\frac{\partial q_x}{\partial y}, \tag{2}$$

satisfies the equation

$$q_x\frac{\partial\omega}{\partial x}+q_y\frac{\partial\omega}{\partial y}=0, \tag{3}$$

and $q_x=\dfrac{\partial\psi}{\partial y}$, $q_y=-\dfrac{\partial\psi}{\partial x}$ are the velocity components parallel to the x- and y-axis respectively.

In a previous paper, Mitchell and the author (**1**) obtained the stream functions for some variable shear flows past circular cylinders, and compared certain aspects of these flows with experimental results. As far as the author is aware, no theoretical solutions of (1) and (3) exist, with the exception of those obtained in (**1**) and those for constant shear flow. In the present paper, a method is derived for obtaining an approximation to the stream functions for some non-uniform shear flows past general cylinders, and the method is outlined for obtaining the flows past an elliptic cylinder and any cylinder whose equation is of the form $r=p(1+\gamma\cos\theta)$.

2. The variable shear distributions

The general solution of (3) is

$$\omega=f(\psi),$$

and so the vorticity is constant along a streamline. In the particular case when

$$\omega=f(\psi)=\mp\psi/l^2,$$

where l is some arbitrary length, equation (1) becomes

$$\frac{\partial^2\psi}{\partial x^2}+\frac{\partial^2\psi}{\partial y^2}=\pm\psi/l^2. \tag{4}$$

The two cases incorporated in (4) give an approximation to a linear shear distribution taking the positive sign, and a shear distribution approximating to that present in an unretarded incompressible boundary layer, taking the negative sign.

(*a*) *The 'linear' shear distribution*

The appropriate equation (4) is

$$\frac{\partial^2\psi}{\partial x^2}+\frac{\partial^2\psi}{\partial y^2}=\psi/l^2. \tag{5}$$

A flow distribution parallel to the x-axis in the free stream near $x=-\infty$, consistent with this equation is given by

$$\psi=ae^{y/l}+be^{-y/l}, \tag{6}$$

which on differentiating gives the velocity distribution as

$$q_x=l^{-1}[ae^{y/l}-be^{-y/l}], \tag{7}$$

and the vorticity distribution as

$$\omega=-l^{-2}[ae^{y/l}+be^{-y/l}], \tag{8}$$

where the constants a and b are arbitrary. Introducing a standard rotation ω_0 and a standard velocity U as the values of ω and q_x at $y=0$, it follows from equations (7) and (8) that

$$a=\tfrac{1}{2}l(U-\omega_0 l), \qquad b=-\tfrac{1}{2}l(U+\omega_0 l).$$

With these values for a and b substituted in (7) and (8), the velocity and vorticity distributions in the free stream near $x=-\infty$ become

$$q_x/U=\cosh y/l-(1/N)\sinh y/l, \tag{9}$$

and

$$\omega/\omega_0=\cosh y/l-N\sinh y/l, \tag{10}$$

respectively, where $N=U/\omega_0 l$. In order to keep the velocity positive everywhere, the parameter N must satisfy the inequality $N>1$. Expanding the above distributions in terms of y/l, and neglecting higher powers of y/l, they become

$$q_x/U=1-(1/N)(y/l)+\tfrac{1}{2}(y/l)^2 \tag{11}$$

and

$$\omega/\omega_0=1-N(y/l) \tag{12}$$

for the velocity and vorticity respectively, and so the free stream shear distribution (10) is approximately linear in the vicinity of the x-axis.

(*b*) *The 'boundary layer' shear distribution*

The appropriate equation (4) is now

$$\frac{\partial^2\psi}{\partial x^2}+\frac{\partial^2\psi}{\partial y^2}=-\psi/l^2. \tag{13}$$

A flow distribution parallel to the x-axis in the free stream near $x=-\infty$ consistent with (13) is

$$\psi=a\cos y/l+b\sin y/l, \tag{14}$$

which on differentiating gives

$$q_x=l^{-1}[b\cos y/l-a\sin y/l], \tag{15}$$

and

$$\omega=l^{-2}[a\cos y/l+b\sin y/l], \tag{16}$$

where a and b are arbitrary constants. If a standard rotation ω_0 and a standard velocity U are introduced as the value of $-\omega$ at $y = 0$, and the value of q_x at $y = \delta - y_0$ respectively, it follows from (15) and (16) that

$$a = -\omega_0 l^2, \qquad b = \omega_0 l^2[N - \sin(\delta - y_0)/l]\sec(\delta - y_0)/l,$$

where $N = U/\omega_0 l$, and y_0 is a variable parameter lying in the range $0 \leqslant y_0 \leqslant \delta$. If

$$\cos y_0/l = 1/N,$$

and the arbitrary length l is chosen to be

$$l = (2/\pi)\delta$$

the velocity and vorticity distributions in the free stream near $x = -\infty$ become

$$q_x/U = \sin \tfrac{1}{2}\pi(y + y_0)/\delta, \tag{17}$$

and

$$\omega/\omega_0 = -N \cos \tfrac{1}{2}\pi(y + y_0)/\delta, \tag{18}$$

respectively. In the range $0 \leqslant y + y_0 \leqslant \delta$, the free stream velocity distribution (17) is Lamb's approximation for the flow in an unretarded incompressible boundary layer of thickness δ (**2**).

3. The general cylinder with its line of symmetry in the direction of the stream

A cylinder is now introduced into the flow, in such a way that the line of symmetry lies on the x-axis, the origin lying within the cross-section of the cylinder, the equation of which may be written as

$$r = p\phi(\theta), \tag{19}$$

where r and θ are the polar coordinates and p is some typical length in the cylinder. The function $\phi(\theta)$ must be an even function with no zeros or singularities in the range $-\pi < \theta \leqslant \pi$. As the method is developed, it is seen that these restrictions are necessary. The problem, which is illustrated in Fig. 1, is to find the stream function which satisfies in the first instance equation (5) and takes a constant value on the cylinder. Considering the 'linear' distribution in the first case, and retaining the general a and b in (6), the function Ψ is introduced by the transformation

$$\psi = ae^{y/l} + be^{-y/l} + \Psi. \tag{20}$$

From (5), Ψ, which tends to zero as x tends to $-\infty$, satisfies the equation

$$\frac{\partial^2\Psi}{\partial x^2} + \frac{\partial^2\Psi}{\partial y^2} = \Psi/l^2. \tag{21}$$

Using polar coordinates r and θ, and the method of separation of variables, (21) is solved to give

$$\Psi = B_0\theta K_0(r') + \sum_{n=0}^{\infty} (A_n \cos n\theta + B_n \sin n\theta)K_n(r'), \tag{22}$$

where A_n and B_n ($n = 0, 1, 2,...$) are constants, K_n is the modified Bessel function of the second kind, and $r' = r/l$. Thus, from (20), the required stream function ψ is given by

$$\psi = ae^{y/l} + be^{-y/l} + B_0\theta K_0(r') + \sum_{n=0}^{\infty} (A_n \cos n\theta + B_n \sin n\theta) K_n(r').$$

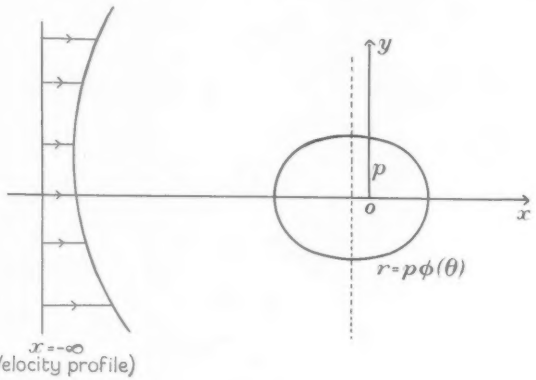

FIG. 1

Now ψ must take the constant value, say c, on the cylinder given by (19), and taking for convenience $l = p$, this gives

$$c = a\exp\{\phi(\theta)\sin\theta\} + b\exp\{-\phi(\theta)\sin\theta\} + B_0\theta K_0\{\phi(\theta)\} + \\ + \sum_{n=0}^{\infty} (A_n \cos n\theta + B_n \sin n\theta) K_n\{\phi(\theta)\}. \quad (23)$$

The constants A_n and B_n ($n = 0, 1, 2,...$) are found by equating coefficients of $\sin n\theta$ and $\cos n\theta$, the requisite functions $\exp\{\pm\phi(\theta)\sin\theta\}$ and $K_n\{\phi(\theta)\}$ being expanded as Fourier series. Write

$$\exp\{\pm\phi(\theta)\sin\theta\} = \sum_{m=0}^{\infty} X_m \cos m\theta \pm \sum_{m=1}^{\infty} Y_m \sin m\theta, \quad (24)$$

where X_m and Y_m ($m = 0, 1, 2,...$) are evaluated by the usual methods. Appendix (a) illustrates how this is carried out in the case of an elliptic cylinder, where $r = p/(1+\epsilon\cos\theta)$, p being the semi-latus rectum and ϵ the eccentricity. The Bessel function is written as

$$K_n\{\phi(\theta)\} = \lambda_{n,0} + \lambda_{n,1}\cos\theta, \quad (25)$$

where $\lambda_{n,0}$ and $\lambda_{n,1}$ are the first two terms of a series expansion of the form $\sum_{\gamma=0}^{\infty} \lambda_{n,\gamma}\cos\gamma\theta$, amended to give a good approximation to $K_n\{\phi(\theta)\}$ in the range $-\pi < \theta \leqslant \pi$, when this series is terminated at $\gamma = 1$.

The expressions given by (24) and (25) are now substituted in equation (23), resulting in

$$c = (a+b)\sum_{m=0}^{\infty} X_m \cos m\theta + (a-b)\sum_{m=1}^{\infty} Y_m \sin m\theta + B_0\theta(\lambda_{0,0}+\lambda_{0,1}\cos\theta) + \\ + \sum_{n=0}^{\infty}(A_n \cos n\theta + B_n \sin\theta)(\lambda_{n,0}+\lambda_{n,1}\cos\theta).$$

The constant c in the above expression is as yet arbitrary, and in fact, as is seen from the subsequent analysis, remains so, unless use is made of the following hypothesis (as in the case described in (**1**)). The hypothesis is that the introduction of a cylinder into an inviscid, incompressible, rotational flow does not alter the circulation round a path L, which coincides with the perimeter of the cylinder. This assumption was used by Tsien (**3**) (see also Richardson (**4**)) and Mitchell and the author (**5**) in the case of constant shear flow past cylinders. Equating coefficients of the sine and cosine terms, from which it is seen immediately that $B_0 = 0$, two sets of equations are obtained, whose solutions give expressions for A_n and B_n. The equations, being of the following form, do not give direct values. Considering the cosine terms in the first instance,

$$\begin{aligned}
\lambda_{0,0}A_0 + \tfrac{1}{2}\lambda_{1,1}A_1 &= c-(a+b)X_0 \\
\lambda_{0,1}A_0 + \lambda_{1,0}A_1 + \tfrac{1}{2}\lambda_{2,1}A_2 &= -(a+b)X_1 \\
\tfrac{1}{2}\lambda_{1,1}A_1 + \lambda_{2,0}A_2 + \tfrac{1}{2}\lambda_{3,1}A_3 &= -(a+b)X_2 \\
&\cdots\cdots\cdots\cdots \\
\tfrac{1}{2}\lambda_{m-1,1}A_{m-1} + \lambda_{m,0}A_m + \tfrac{1}{2}\lambda_{m+1,1}A_{m+1} &= -(a+b)X_m \quad (m>1). \qquad (26)
\end{aligned}$$

A similar series is obtained by equating the coefficients of the sine terms to give

$$\begin{aligned}
\lambda_{1,0}B_1 + \tfrac{1}{2}\lambda_{2,1}B_2 &= -(a-b)Y_1 \\
\tfrac{1}{2}\lambda_{1,1}B_1 + \lambda_{2,0}B_2 + \tfrac{1}{2}\lambda_{3,1}B_3 &= -(a-b)Y_2 \\
\tfrac{1}{2}\lambda_{2,1}B_2 + \lambda_{3,0}B_3 + \tfrac{1}{2}\lambda_{4,1}B_4 &= -(a-b)Y_3 \\
&\cdots\cdots\cdots\cdots \\
\tfrac{1}{2}\lambda_{m-1,1}B_{m-1} + \lambda_{m,0}B_m + \tfrac{1}{2}\lambda_{m+1,1}B_{m+1} &= -(a-b)Y_m \quad (m>1). \qquad (27)
\end{aligned}$$

The dependence of the solution on c is illustrated in (26), the A_n being a function of the constant c. Using the hypothesis stated above, therefore, the constant c is evaluated as follows.

The stream function is given by

$$\psi = ae^{y/p} + be^{-y/p} + \sum_{n=0}^{\infty}(A_n \cos n\theta + B_n \sin n\theta)K_n(r/p), \qquad (28)$$

from which the velocity components in polar coordinates are given by

$$q_r = \frac{1}{r}\frac{\partial \psi}{\partial \theta}, \qquad q_\theta = -\frac{\partial \psi}{\partial r}.$$

The velocity at any point is given by $q^2 = q_r^2 + q_\theta^2$. In particular, the velocity on the cylinder is given by $q_\parallel$, the velocity parallel to the tangent to the cylinder at its point of contact, as illustrated in Fig. 2. The velocity perpendicular to the tangent at its point of contact is necessarily equal to zero, as may be easily checked.

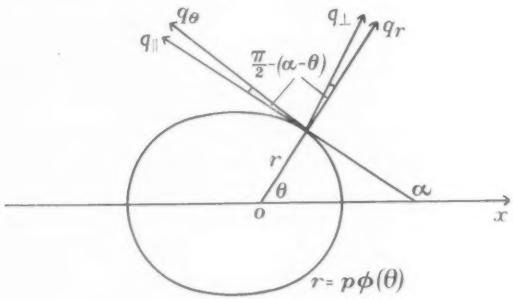

FIG. 2

The cylinder in cartesian coordinates is given by

$$(x^2+y^2)^{\frac{1}{2}} = p\phi(\tan^{-1}y/x),$$

from which $$\frac{dy}{dx} = \tan\alpha = -\left[\frac{\phi(\theta)\cos\theta + \phi'(\theta)\sin\theta}{\phi(\theta)\sin\theta - \phi'(\theta)\cos\theta}\right],$$

with α as shown in Fig. 2 and $\phi'(\theta) = d/d\theta[\phi(\theta)]$. This relation defines $\sin\alpha$ and $\cos\alpha$ in terms of θ and $\phi(\theta)$. Resolving the velocity components parallel to the tangent at the point of contact

$$q_\parallel = [q_r\cos(\alpha-\theta) + q_\theta\sin(\alpha-\theta)]_{r=p\phi(\theta)} \tag{29}$$

with $\sin\alpha$ and $\cos\alpha$, obtained from above, substituted in equation (29). Stagnation points on the cylinder are given by $q_\parallel = 0$. The circulation Γ, taken round the perimeter L of the cylinder is given by

$$\Gamma = \Gamma_0 + \Gamma_1 = \oint_L q_\parallel \, dl,$$

where dl is the element of length on the cylinder, and Γ_0 and Γ_1 are the circulations arising from the undisturbed flow and the disturbance flow respectively. The element dl is given by

$$\begin{aligned} dl &= [(dr)^2 + r^2(d\theta)^2]^{\frac{1}{2}} \\ &= p[\{\phi'(\theta)\}^2 + \{\phi(\theta)\}^2]^{\frac{1}{2}} \, d\theta. \end{aligned}$$

From equations (28) and (29), the circulation Γ_1 becomes

$$\Gamma_1 = \int_{-\pi}^{\pi} \left[\frac{\cos(\alpha-\theta)}{\phi(\theta)} \sum_{n=0}^{\infty} (-nA_n \sin n\theta + nB_n \cos n\theta)(\lambda_{n,0}+\lambda_{n,1}\cos\theta) + \right.$$
$$+\sin(\alpha-\theta) \sum_{n=0}^{\infty} (A_n \cos n\theta + B_n \sin n\theta) \left\{ \frac{n}{\phi(\theta)} (\lambda_{n,0}+\lambda_{n,1}\cos\theta) + \right.$$
$$\left. \left. + (\lambda_{n-1,0}+\lambda_{n-1,1}\cos\theta) \right\} \right] [\{\phi(\theta)\}^2+\{\phi'(\theta)\}^2]^{\frac{1}{2}}\, d\theta, \qquad (30)$$

where in (30) $K_n\{\phi(\theta)\}$ and $\left[\dfrac{dK_n(r')}{dr'}\right]_{r'=\phi(\theta)}$ have been replaced by the approximations given by (25), since the velocity $q_{\|}$ is that velocity on the cylinder, with $\sin\alpha$ and $\cos\alpha$ replaced from the above expression for $\tan\alpha$ in terms of θ. The condition that $\Gamma_1 = 0$ from (30) gives a relation involving only A_0 and c, where the A_n are replaced by the appropriate known functions of A_0 and c from (26), resulting in an expression of the form

$$c = g(a, b, X_m, \lambda_{m,0}, \lambda_{m,1}, A_0), \qquad (31)$$

where $g(A_0)$ is a known function.

If this value for c is substituted in equations (26), they become

$$\begin{aligned} \lambda_{0,0}A_0 - g(A_0) + \tfrac{1}{2}\lambda_{1,1}A_1 &= -(a+b)X_0 \\ \lambda_{0,1}A_0 + \lambda_{1,0}A_1 + \tfrac{1}{2}\lambda_{2,1}A_2 &= -(a+b)X_1 \\ \cdots\cdots\cdots\cdots\cdots\cdots\cdots \\ \tfrac{1}{2}\lambda_{m-1,1}A_{m-1} + \lambda_{m,0}A_m + \tfrac{1}{2}\lambda_{m+1,1}A_{m+1} &= -(a+b)X_m. \end{aligned} \qquad (32)$$

The systems of equations (27) and (32) are of the same type. It is seen that if either system is terminated at a given value of n, it contains $(n+1)$ unknowns and only n equations. Thus, unless the number of equations is infinite, there is not a unique solution to the system. There are several methods of approach, but since the equations in each system are not all of equal weight, the A_n and B_n are assumed, as is necessary, to form a decreasing sequence, and accordingly an iterative process is most appropriate. The method is described with reference to the system (32), but is applied in exactly the same manner to the system (27).

The constants are evaluated on the basis of equality in the two series for all values of θ. If the X_m-series, which is convergent, is terminated at $m = s$ (that is, at the value of m such that $X_{m+1} \doteq 0$ for all practical purposes), then the A_n-series must be terminated at $n = s-1$, and the constants evaluated by equating the two series, the final term in each being then $\cos s\theta$. The iterative method is to express A_r $(r > 0)$ in equations (32) in terms of A_0 and the known X_m, and then assign values to A_0 in such

a way that the two terminated series correspond exactly for values of θ between 0 and 2π. Thus, from equations (32),

$$A_1 = 2/\lambda_{1,1}[g(A_0)-\lambda_{0,0}A_0-(a+b)X_0]$$

$$A_2 = -2/\lambda_{2,1}\left[-\lambda_{0,1}A_0-(a+b)X_1-\frac{2\lambda_{1,0}}{\lambda_{1,1}}\{g(A_0)-\lambda_{0,0}A_0-(a+b)X_0\}\right]$$

. . . . . .

are substituted in the A_n-series, A_0 being chosen to make the two series equal for $\theta = \theta_0, \theta_1, \ldots$ and A_0 averaged over these values of θ. In practice the values of θ are chosen to give points equally placed round the perimeter of the cylinders as shown in Fig. 3.

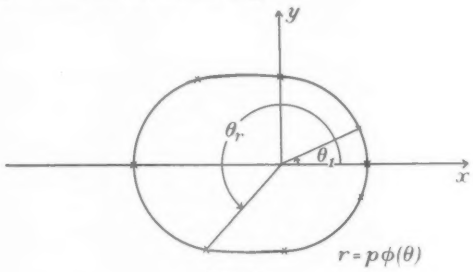

FIG. 3

As an example, if the X_m-series is terminated at $m = 3$ (which is the minimum for any practical problem) and accordingly the A_n-series at $n = 2$, the two expressions equated are

$$c-(a+b)X_0-(a+b)[X_1\cos\theta+X_2\cos 2\theta+X_3\cos 3\theta],$$

and

$$A_0(\lambda_{0,0}+\lambda_{0,1}\cos\theta)+2/\lambda_{1,1}[g(A_0)-\lambda_{0,0}A_0-(a+b)X_0](\lambda_{1,0}+\lambda_{1,1}\cos\theta)\cos\theta-$$

$$-2/\lambda_{2,1}\left[-\lambda_{0,1}A_0-(a+b)X_1-\frac{2\lambda_{1,0}}{\lambda_{1,1}}\{g(A_0)-\lambda_{0,0}A_0-(a+b)X_0\}\right]\times$$

$$\times(\lambda_{2,0}+\lambda_{2,1}\cos\theta)\cos 2\theta.$$

In practice, this method of evaluating the A_n is sufficiently accurate. The constants B_n are similarly evaluated, the numerical work being slightly easier since the constant c does not appear in the equations.

In view of the above analysis, it is easily seen that, although inclusion of further terms $\lambda_{n,\gamma}$ ($\gamma > 1$) in (1 b) gives a more accurate representation of the Bessel function, the subsequent evaluation of the constants A_n, B_n ($n = 0, 1, 2, \ldots$) is correspondingly more difficult analytically.

The stream function ψ given by

$$\psi = ae^{y/p}+be^{-y/p}+\sum_{n=0}^{\infty}(A_n\cos n\theta+B_n\sin n\theta)K_n(r/p), \qquad (33)$$

with the A_n and B_n ($n = 0, 1, 2, \ldots$) determined as accurately as desired by the above method, represents the flow past a general cylinder with line of symmetry in the direction of the flow. The stream function satisfies the necessary conditions

(i) $\nabla^2\psi = \psi/p^2$,

(ii) $\psi \to ae^{y/p} + be^{-y/p}$ as $r \to \infty$,

(iii) $\psi = c$ on the cylinder $r = p\phi(\theta)$,

(iv) $\Gamma_1 = 0$, where the circulation is taken around the perimeter of the cross-section of the cylinder. The velocity on the cylinder is given by $q_\parallel$, where the q_r and q_θ in equation (29) are obtained from equation (33). Stagnation points on the cylinder are given by $q_\parallel = 0$. The stagnation streamline is given by

$$\psi = c = g(a, b, X_m, \lambda_{m,0}, \lambda_{m,1}, A_0),$$

which in the free stream near $x = -\infty$, comes from y_s, where

$$y_s/p = \log_e[\tfrac{1}{2}c/a + \{(\tfrac{1}{2}c/a)^2 - b/a\}^{\frac{1}{2}}], \tag{34}$$

with c given by equation (31). For numerical comparison with the results for constant shear (**5**), we recall that in (**5**) the parameter N ($= U/\omega_0 l$) is defined with l equal to y_m, where $2y_m$ is the maximum width of the cylinder perpendicular to the flow. The formulae in that case have y/y_m as dimensionless length, so dimensionless quantities here must be multiplied by p/y_m.

If a and b (the free stream constants) are given the values which result in the free stream vorticity distribution being approximately a linear shear distribution, the stream function (33) gives an approximation, to any desired degree of accuracy, to the requisite stream function for a general cylinder in such a flow.

The case of the circular cylinder in such a flow, derived in a previous paper (**1**), is a particular case of the above method, with $\phi(\theta) = 1$.

4. The general cylinder with line of symmetry perpendicular to the direction of the stream

Flow with the type of free stream vorticity distribution given by equation (8), past a general cylinder with its line of symmetry perpendicular to the direction of the flow, can be obtained very quickly by taking the cylinder as that given by (19) illustrated in Fig. 1. Since the y-axis need not coincide with the line of maximum width of the cylinder, a simple replacement of y by x in equation (8) will not, in general, be sufficient. In Fig. 1 let the line of maximum width be at a distance x_0 from the axis. The vorticity given by equation (8) is to be replaced by

$$\omega = -p^{-2}[ae^{(x_0+x)/p} + be^{-(x_0+x)/p}], \tag{35}$$

where p is again taken as the most convenient typical length for the particular cylinder under consideration, and a and b are the free stream constants. Thus, the vorticity in the free stream on the line of maximum width is $-(a+b)/p^2$ as before. Define the number s by $s = x_0/p$. Then from (35),

$$\omega = -p^{-2}[Ae^{x/p}+Be^{-x/p}] \tag{36}$$

where $A = ae^s$, and $B = be^{-s}$. Fig. 4 illustrates the problem.

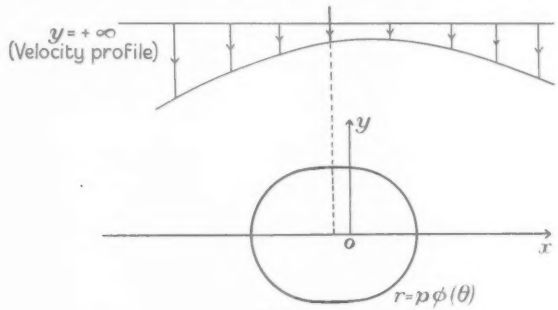

FIG. 4

The procedure for obtaining the stream function is that described in section 3, with A and B defined above taking the place of a and b respectively. In this case the Fourier expansion of $\exp\{\pm\phi(\theta)\cos\theta\}$ is needed in place of (24) and the stream function is of the form

$$\psi = Ae^{x/p}+Be^{-x/p}+\sum_{n=0}^{\infty} A_n \cos n\theta\, K_n(r/p), \tag{37}$$

where the A_n $(n = 0, 1, 2,...)$ are obtained as before. All the physical features of the flow can be determined, and the general remarks made in the last section are applicable.

5. The general cylinder in the 'boundary layer' shear distribution

The general cylinder is again given by equation (19), and the function Ψ is introduced by the transformation

$$\psi = a\cos y/l+b\sin y/l+\Psi,$$

where, from equation (13), Ψ satisfies

$$\frac{\partial^2\Psi}{\partial x^2}+\frac{\partial^2\Psi}{\partial y^2} = -\Psi/l^2 \tag{38}$$

and $\Psi \to 0$ as $x \to -\infty$. Fig. 5 illustrates the problem with a and b the values resulting in the approximation to the 'boundary layer' shear distribution in the free stream. Proceeding as in section 3, a solution of (38) is

$$\Psi = B_0\theta Y_0(r/l)+\sum_{n=0}^{\infty}(A_n\cos n\theta+B_n\sin n\theta)Y_n(r/l),$$

where A_n and B_n ($n = 0, 1, 2,...$) are constants, and Y_n is the Bessel function of the second kind. It is assumed that $J_n(r/l)$ does not appear in the solution from consideration of the case of the circular cylinder $\phi(\theta) = 1$, where

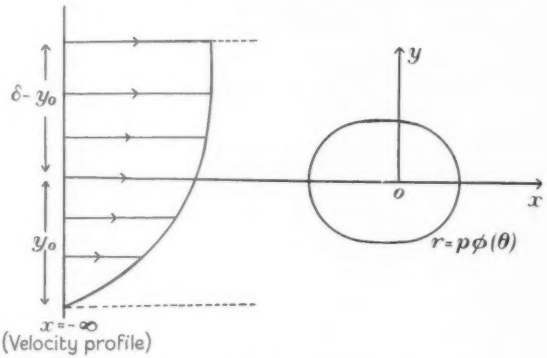

FIG. 5

inclusion of $J_n(r/l)$ leads to a contradiction of the independence of the Bessel functions. The equation corresponding to (23) is then

$$c = a\cos\{p/l\,\phi(\theta)\sin\theta\} + b\sin\{p/l\,\phi(\theta)\sin\theta\} + B_0\theta Y_0\{p/l\phi(\theta)\} + \\ + \sum_{n=0}^{\infty}(A_n\cos n\theta + B_n\sin n\theta)Y_n\{p/l\phi(\theta)\}, \quad (39)$$

where c is the constant value taken by ψ on the cylinder. The constants A_n and B_n ($n = 0, 1, 2,...$) are obtained by equating the coefficients of $\sin n\theta$ and $\cos n\theta$ as before. As in Appendix (a), the expansions of the sine and cosine terms are obtained by expanding the functions in the form:

$$\cos\left\{\frac{p}{l}\phi(\theta)\sin\theta\right\} = \sum_{r=0}^{\infty}\frac{(-1)^r(p/l)^{2r}}{(2r)!}\{\phi(\theta)\sin\theta\}^{2r},$$

and

$$\sin\left\{\frac{p}{l}\phi(\theta)\sin\theta\right\} = \sum_{r=0}^{\infty}\frac{(-1)^r(p/l)^{2r+1}}{(2r+1)!}\{\phi(\theta)\sin\theta\}^{2r+1}.$$

The Bessel function $Y_n\{p/l\phi(\theta)\}$ is obtained as a cosine series using a comparable method to that in Appendix (b), resulting in a similar equation to (5 b).

Thus, following the method of section 3, the required stream function is obtained, and is of the form

$$\psi = a\cos y/l + b\sin y/l + \sum_{n=0}^{\infty}(A_n\cos n\theta + B_n\sin n\theta)Y_n(r/l), \quad (40)$$

where the A_n and B_n are known, and are such that ψ satisfies

(i) $\nabla^2\psi = -\psi/l^2$,

(ii) $\psi \to a\cos y/l + b\sin y/l$ as $r \to \infty$,

(iii) $\psi = c$ on the cylinder $r = p\phi(\theta)$,

(iv) $\Gamma_1 = 0$, where the circulation is taken round the perimeter of the cylinder.

The velocity at any point in the flow can be obtained, and in particular on the cylinder by $q_{||}$, defined by equation (29). If a and b are given the values obtained from (18), and if the length l used above is taken equal to $(2/\pi)\delta$, the field of flow represented by (40) gives an approximation to the flow past such a cylinder when the flow due to the presence of the cylinder is that in an unretarded incompressible boundary layer of thickness δ, provided that, in the case when the axis of the cross-section of the cylinder is in the direction of the flow, (i) the length $2y_m$ is small compared with δ, and (ii) y_0/δ has a value not too near the end values 0 and 1 of its allowable range.

Davies (**6**) has recently sought to determine the magnitude of the displacement of the stagnation streamline in flows by traverses across boundary layers on a flat plate and a cone in sub- and supersonic flows. He used pitot tubes with circular cross-sections which he suggested must have a radius less than $0{\cdot}1\delta$. Thus, such a condition on p/l gives

$$y_m/l < 0{\cdot}05\pi. \tag{41}$$

The corresponding deflexion y_s, in the free stream, of the stagnation streamline is given by equation (14) in the form

$$c = a\cos(y_s/l) + b\sin(y_s/l), \tag{42}$$

where c is obtained from the circulation consideration, and a and b are replaced by the appropriate expressions for the approximation to the shear flow in an incompressible boundary layer. Use of condition (41) in the numerical results is reasonable for comparison with Davies, since the deflexion in the free stream is in each case a result of the vorticity present in the flow.

The flow past a cylinder with the line of symmetry of its cross-section perpendicular to the direction of the flow, can be obtained in a similar manner to that described in section 4, with the appropriate changes in the flow in the free stream at infinity. For means of comparison, equation (41) must be altered so that the maximum length on the axis conforms with the condition given by Davies.

6. The elliptic cylinder $r = p/(1+\epsilon\cos\theta)$

The ellipse has p as the semi-latus rectum and ϵ as the eccentricity. Thus $\phi(\theta) = (1+\epsilon\cos\theta)^{-1}$, from which it is easily seen that $0 \leqslant \epsilon < 1$ is a necessary limitation on ϵ. The practical difficulties which arise are in the evaluation of the series (24) and (25). The appendix shows how this is carried out in this particular case. By using the appropriate equations, the

flows can be obtained when the major axis of the cross-section of the cylinder is perpendicular to and in the direction of the flow respectively, where the flow may be that with the 'linear' shear distribution or the 'boundary layer' distribution in the free stream.

This particular case could be evaluated using elliptic coordinates and Mathieu functions, but it serves as a practical example of the general method given above.

7. The general cylinder of the form $r = p(1+\gamma\cos\theta)$ where $|\gamma| < 1$

In this case, $\phi(\theta) = (1+\gamma\cos\theta)$. The appropriate equations (24) will be the product of the two series

$$\exp(\sin\theta) \quad \text{and} \quad \exp(\gamma\cos\theta\sin\theta)\ \{= \exp(\gamma/2)\sin 2\theta\}$$

expressed in their Bessel function expansion form, and (25) is the direct application of the method in the reference to Gray and Mathews (**8**) made in Appendix (*b*).

This particular example illustrates the use of the general method when the cylinder has no natural coordinates.

In each of the above examples implicit relations can be obtained for the deflexions of the stream lines and stagnation points on the cylinder.

8. Discussion of results

A method is derived whereby the stream functions for various shear flows can be obtained for any cylinder whose cross-sectional equation can be written in the form $r = p\phi(\theta)$, where $\phi(\theta)$ must satisfy certain conditions. The free stream flows are in terms of the general exponential and sine and cosine distributions of vorticity. By suitable choice of the constants involved, these can be favourably compared with a linear shear distribution and that shear present in an unretarded boundary layer.

The method is discussed in detail and the assumptions necessary for a solution to be uniquely defined are outlined. One important feature of all the flows is that the stagnation stream line is displaced in the free stream from the point on the axis opposite the line of symmetry of the cylinder.

The two particular examples considered are those of the elliptic cylinder and the cylinder with equation of the form $r = p(1+\gamma\cos\theta)$, where $|\gamma| < 1$ is necessary to exclude singularities of the Bessel functions. In comparison with the former example, the latter is quite straightforward. The analytical difficulties in the elliptic cylinder are considerable, and the detailed analysis is given in the appendix. As shown in section 4, with only slight change in notation from the flow with the major axis in the direction of flow, the stream function can be obtained very quickly when the major axis is perpendicular to the flow direction.

If comparison is made with the experimental results obtained from pitot traverses in the boundary layers on flat plates and cones in supersonic and subsonic flows, certain restrictions on the dimensions of the cylinders in comparison with the 'boundary layer thickness' must be imposed.

The examples cited do not exhaust the possible cross-sections for which the stream functions can be obtained using the general method described in this paper. They do, however, illustrate the difficulties involved in obtaining stream functions for non-uniform shear flows past cylinders whose cross-sections are other than circular. Further, it illustrates the difficulties which may be expected to arise in attempting to derive analytically the stream functions for variable shear flows of a more complicated nature, either compressible or incompressible.

Acknowledgement

The author would like to thank Dr. A. R. Mitchell of the Mathematics Department, St. Andrews University, for helpful discussions in the preparation of this paper.

APPENDIX

(*a*) *The Fourier expansion of* $\exp[\pm\sin\theta/(1+\epsilon\cos\theta)]$

The exponential function is

$$\exp[\pm\sin\theta/(1+\epsilon\cos\theta)] = 1+\sum_{r=1}^{\infty}\frac{(\pm 1)^r}{r!}[\sin\theta/(1+\epsilon\cos\theta)]^r. \tag{1a}$$

Each term in the summation is expressed as a Fourier series, and these are then summed over r in the form given by (1 a).

The expression $(1+\epsilon\cos\theta)^{-r}$ $(r = 1, 2,...)$ can be expanded as a half-range cosine series in the form

$$(1+\epsilon\cos\theta)^{-r} = a_{r,0}/2+\sum_{n=1}^{\infty}a_{r,n}\cos n\theta, \tag{2a}$$

where, using Integral Tafel (**7**), $a_{r,n}$ is given by

$$a_{r,n} = 2(1-a^2)^{1-2r}(1+a^2)^r a^{2r+n-2}\sum_{\gamma=0}^{r-1}\binom{r+n-1}{\gamma}\binom{2r-\gamma-2}{r-1}\left(\frac{1-a^2}{a^2}\right)^{\gamma}, \tag{3a}$$

where

$$a = -1/\epsilon+(1/\epsilon^2-1)^{\frac{1}{2}}, \tag{4a}$$

and $\binom{r}{s}$ are the binomial coefficients.

The function $[\sin\theta/(1+\epsilon\cos\theta)]^r$ is an odd or even function of θ according as r is an odd or an even integer respectively. If r is even, the function is expanded as a half-range cosine series, and if r is odd, as a half-range sine series.

r even

The function is an even function and can thus be expressed as

$$[\sin\theta/(1+\epsilon\cos\theta)]^r = \sin^r\theta\left(a_{r,0}/2+\sum_{n=1}^{\infty}a_{r,n}\cos n\theta\right)$$

$$= A_{r,0}/2+\sum_{m=1}^{\infty}A_{r,m}\cos m\theta, \tag{5a}$$

where

$$A_{r,m} = (2/\pi)\int_0^{\pi} [\sin\theta/(1+\epsilon\cos\theta)]^r \cos m\theta\, d\theta$$

$$= (2/\pi)\int_0^{\pi} \sin^r\theta\Big(a_{r,0}/2 + \sum_{n=1}^{\infty} a_{r,n}\cos n\theta\Big)\cos m\theta\, d\theta,$$

$$= (1/\pi)\int_0^{\pi} a_{r,0}\sin^r\theta\cos m\theta\, d\theta + (2/\pi)\sum_{n=1}^{\infty} a_{r,n}\int_0^{\pi}\sin^r\theta\cos n\theta\cos m\theta\, d\theta.$$

After a little manipulation, these integrals are evaluated using (7) to give

$$A_{r,m} = \sum_{n=0}^{r-m} a_{r,n}\frac{(-1)^{(m+n)/2}}{2^r}\binom{r}{\tfrac{1}{2}(r-m-n)} + \left.\begin{matrix} \\ +\sum_{n=1}^{m} a_{r,n}\dfrac{(-1)^{(m-n)/2}}{2^r}\binom{r}{\tfrac{1}{2}(r-m+n)} \\ +0 \end{matrix}\right\}\begin{matrix} m-n\leqslant r \\ m-n>r \end{matrix} \quad (\text{if } m \geqslant n)$$

$$+\sum_{n=m+1}^{r+m} a_{r,n}\frac{(-1)^{(n-m)/2}}{2^r}\binom{r}{\tfrac{1}{2}(r-n+m)} \quad (\text{if } n > m) \qquad (6\,\text{a})$$

where it must be remembered that r, $m+n$, $m-n$ are *even* integers, and $a_{r,n}$ for all $n \geqslant 0$ is given by (3 a). In any calculation, r and m are given, and the varying n in the above series is chosen so that $m+n$, $m-n$ are *even*.

r odd

The function in this case is an odd function and is expressed as

$$[\sin\theta/(1+\epsilon\cos\theta)]^r = \sum_{m=1}^{\infty} B_{r,m}\sin m\theta. \qquad (7\,\text{a})$$

Proceeding as above, the coefficients $B_{r,m}$ are given by

$$B_{r,m} = \sum_{n=0}^{r-m} a_{r,n}\frac{(-1)^{(m+n-1)/2}}{2^r}\binom{r}{\tfrac{1}{2}(r-m-n)} + \left.\begin{matrix} \\ +\sum_{n=1}^{m-1} a_{r,n}\dfrac{(-1)^{(m-n-1)/2}}{2^r}\binom{r}{\tfrac{1}{2}(r-m+n)} \\ +0 \end{matrix}\right\}\begin{matrix} m-n\leqslant r \\ m-n>r \end{matrix} \quad (\text{if } m > n)$$

$$-\sum_{n=m+1}^{m+r} a_{r,n}\frac{(-1)^{(n-m-1)/2}}{2^r}\binom{r}{\tfrac{1}{2}(r-n+m)} \quad (\text{if } m < n) \qquad (8\,\text{a})$$

where r, $m+n$, $m-n$, are *odd* integers.

Using equations (5 a) and (7 a), the required Fourier expansion of (1 a) is now given as

$$\exp[\pm\sin\theta/(1+\epsilon\cos\theta)]$$

$$= 1 + \tfrac{1}{2}\sum_{r=1}^{\infty}\frac{A_{2r,0}}{(2r)!} + \sum_{r=1}^{\infty}\sum_{m=1}^{\infty}\frac{A_{2r,m}}{(2r)!}\cos m\theta \pm \sum_{r=0}^{\infty}\sum_{m=1}^{\infty}\frac{B_{2r+1,m}}{(2r+1)!}\sin m\theta, \qquad (9\,\text{a})$$

where $A_{r,m}$ and $B_{r,m}$ for all r and m are given by equations (6a) and (8a) respectively. It should be noted that (9a) is only valid for $0 \leqslant \epsilon < 1$. For convenience, defining X_m and Y_m by the following expression, equation (9a) is written in the form

$$\exp[\pm \sin\theta/(1+\epsilon\cos\theta)] = \sum_{m=0}^{\infty} X_m \cos m\theta \pm \sum_{m=1}^{\infty} Y_m \sin m\theta. \tag{10a}$$

These summations converge strongly, with stronger convergence for smaller values of ϵ. The numerical values of the coefficients X_m and Y_m are easily calculated: as an example, when $\epsilon = 0{\cdot}25$,

$$\exp[\pm \sin\theta/(1+0{\cdot}25\cos\theta)] = 1{\cdot}2799 - 0{\cdot}0727\cos\theta - 0{\cdot}2715\cos 2\theta + \\ + 0{\cdot}0732\cos 3\theta - 0{\cdot}0088\cos 4\theta \ldots \pm 1{\cdot}1495\sin\theta \mp 0{\cdot}1630\sin 2\theta \mp 0{\cdot}0210\sin 3\theta \ldots.$$

(*b*) *The Bessel function* $K_n[1/(1+\epsilon\cos\theta)]$ *as a cosine series.*

To a first approximation $K_n(1)$ may be used, since the argument has limits $1/(1\pm\epsilon)$. Thus, for small ϵ ($\epsilon < 0{\cdot}1$) K_n may be considered constant, and the method outlined in (**1**) is directly applicable. The discrepancy from the true value increases with ϵ and n. Writing $K_n[1/(1+\epsilon\cos\theta)]$ in the form

$$K_n[1/(1+\epsilon\cos\theta)] = \sum_{\gamma=0}^{\infty} \lambda_{n,\gamma} \cos\gamma\theta, \tag{1b}$$

the procedure for determining $\lambda_{n,\gamma}$ as a function of ϵ is carried out as follows, using Gray and Mathews' *Treatise on Bessel Functions* (**8**). The expansion of $K_n(R)$ as a cosine series is given as

$$K_n(R) = (2R/(ab))^n (n-1)! \sum_{p=0}^{\infty} (n+p) C_p^n(\cos\theta) K_{n+p}(b) I_{n+p}(a), \tag{2b}$$

where $R^2 = a^2+b^2-2ab\cos\theta$, I is the Bessel function of the first kind, $n \neq 0$, $|a| < |b|$, and $C_p^n(\cos\theta)$ is Gegenbauer's polynomial, which for integral p and n may be defined by

$$C_p^n(v) = \frac{(n+p-1)!}{(n-1)!} \frac{(2v)^p}{p!}\left[1 - \frac{p(p-1)}{(n+p-1)}(2v)^{-2} + \frac{p(p-1)(p-2)(p-3)}{2!(n+p-1)(n+p-2)}(2v)^{-4} \ldots\right],$$

from which $C_0^n(v) = 1$, and $C_1^n(v) = 2nv$. The case $n = 0$ is given by

$$K_0(R) = I_0(a)K_0(b) + 2\sum_{p=1}^{\infty} K_p(b) I_p(a) \cos p\theta, \tag{3b}$$

where $|a| < |b|$. Comparing these formulae with the Bessel function in question

$$R^2 = (1+\epsilon\cos\theta)^{-2} = \tfrac{1}{2}a_{2,0} + a_{2,1}\cos\theta,$$

to a first approximation from (2a), with $a_{2,0}$ and $a_{2,1}$ given by (3a). This gives reasonably good results if $\epsilon < 0{\cdot}5$, the smaller the value of ϵ the better is the approximation. Using the last relation, comparison with R^2 in (2b) and (3b) gives

$$a^2+b^2 = \tfrac{1}{2}a_{2,0}, \qquad 2ab = -a_{2,1},$$

which gives

$$a = \tfrac{1}{2}[(\tfrac{1}{2}a_{2,0} - a_{2,1})^{\frac{1}{2}} - (\tfrac{1}{2}a_{2,0} + a_{2,1})^{\frac{1}{2}}]$$

and

$$b = \tfrac{1}{2}[(\tfrac{1}{2}a_{2,0} - a_{2,1})^{\frac{1}{2}} + (\tfrac{1}{2}a_{2,0} + a_{2,1})^{\frac{1}{2}}], \tag{4b}$$

since $|a| < |b|$. If a and b are to be real, it can be easily shown from (3a) and (4a) that ϵ must be less than 0·5. For larger values than 0·5 the first approximations give poor results and the values must be suitably amended by trial and error. In equation (2b) R appears in the form R^n, and so further use of (2a) must be made, the case $n = 1$ being

$$R = 1/(1+\epsilon\cos\theta) = \tfrac{1}{2}a_{1,0} + a_{1,1}\cos\theta.$$

Substituting the required quantities in (2b) and (3b), approximate expressions for $\lambda_{n,\gamma}$ are obtained. Table 1 (*b*) illustrates the form of $\lambda_{n,0}$ and $\lambda_{n,1}$ for various values of n,

where a and b are given by (4 b). Terms with $\gamma > 1$ are similarly obtained from equation (2 b).

TABLE 1 (b)

n	$\lambda_{n,0}$
0	$I_0(a)K_0(b)$
1	$(2/ab)[a_{1,0}\, I_1(a)K_1(b)+2a_{1,1}\, I_2(a)K_2(b)]$
2	$(2/ab)^2[2a_{2,0}\, I_2(a)K_2(b)+6a_{2,1}\, I_3(a)K_3(b)]$
n	$\lambda_{n,1}$
0	$2I_1(a)K_1(b)$
1	$(2/ab)[a_{1,1}\, I_1(a)K_1(b)+4a_{1,0}\, I_2(a)K_2(b)]$
2	$(2/ab)^2[12a_{2,0}\, I_3(a)K_3(b)+2a_{2,1}\, I_2(a)K_2(b)]$

In the evaluation of the constants A_n and B_n in equation (23), certain analytical difficulties arise as a result of $K_n[1/(1+\epsilon\cos\theta)]$ being itself a function of θ. Accordingly, if the series (1 b) is terminated at $\gamma = 1$, $\lambda_{n,0}$ and $\lambda_{n,1}$ must be amended by trial and error to give a reasonable approximation to $K_n[1/(1+\epsilon\cos\theta)]$. The procedure is to evaluate $\lambda_{n,0}$ and $\lambda_{n,1}$ from the formulae given above, and to amend the numerical values for each n and ϵ. Table 2 (b) illustrates the numerical changes necessary in the case of $K_n[1/(1+0{\cdot}25\cos\theta)]$.

TABLE 2 (b)

	$\lambda_{n,0}$		$\lambda_{n,1}$	
n	*Theoretical values*	*Amended values*	*Theoretical values*	*Amended values*
0	0·4227	0·4227	0·1603	0·1603
1	0·5665	0·5978	0·1174	0·2424
2	0·7701	1·7101	0·7004	0·8954

Figs. 1 (b), 2 (b) illustrate the graphs of $K_n[1/(1+\epsilon\cos\theta)]$ with $\epsilon = 0{\cdot}25$ and $n = 0, 1$ respectively, with the various approximations to the exact curve.

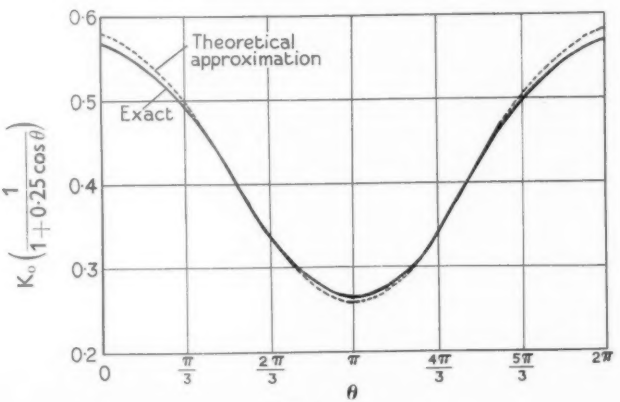

FIG. 1 (b)

A more accurate representation of $K_n[1/(1+\epsilon\cos\theta)]$ is obtained if $\lambda_{n,\gamma}$ ($\gamma > 1$) are included in the summation, but with a proportional increase in analytical labour. It is sufficient, however, for the purposes of illustrating the method and analytical

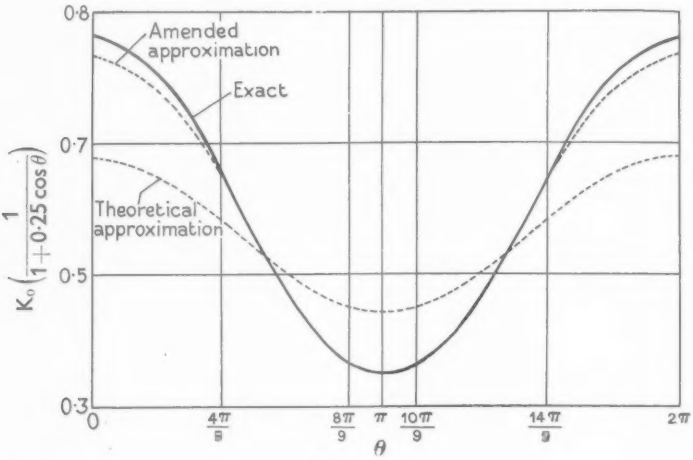

FIG. 2 (*b*)

difficulties involved to assume that the series given by (1 b) terminates at $\gamma = 1$, giving

$$K_n[1/(1+\epsilon\cos\theta)] = \lambda_{n,0}+\lambda_{n,1}\cos\theta, \tag{5 b}$$

where $\lambda_{n,0}$ and $\lambda_{n,1}$ are the amended values giving the best approximation to the Bessel function for a given ϵ. Equation (5 b) gives a good approximation without amendment to $\lambda_{n,\gamma}$ for small values of ϵ, the accuracy decreasing with increasing ϵ. The particular case of $\epsilon = 0$ (that of the circular cylinder), gives, as may be easily checked $\lambda_{n,\gamma} = 0$ for $\gamma \geqslant 1$.

REFERENCES

1. J. D. MURRAY and A. R. MITCHELL, *Quart. J. Mech. App. Math.* **10** (1957) 13.
2. H. LAMB, *Hydrodynamics* (Cambridge, 1932) 686.
3. H. S. TSIEN, *Quart. J. App. Math.* **1** (1943) 130.
4. M. RICHARDSON, ibid. **3** (1945) 175.
5. A. R. MITCHELL and J. D. MURRAY, *Z. angew. Math. Phys.* **6** (1955) 223.
6. F. V. DAVIES, R.A.E. Technical Note, Aero. 2179 (1952).
7. W. GRÖBNER and H. HOFREITER, *Integral Tafel II* (1950).
8. A. GRAY and G. B. MATHEWS, *A Treatise on Bessel Functions* (Cambridge, 1952).

THE STEADY TWO-DIMENSIONAL FLOW OF VISCOUS FLUID AT LOW REYNOLDS NUMBERS PASSING THROUGH AN INFINITE ROW OF EQUAL PARALLEL CIRCULAR CYLINDERS

By K. TAMADA

(*Department of Aeronautics, University of Kyoto, Kyoto, Japan*)

and H. FUJIKAWA

(*Jr. C. of Eng., University of Osaka Pref., Osaka, Japan*)

[Received 10 May 1956; revise received 21 February 1957]

SUMMARY

A detailed discussion based upon Oseen's equations of motion has been made of the steady two-dimensional flow of a viscous fluid passing perpendicularly through an infinite row of equal parallel circular cylinders regularly spaced. It has thus been found that the drag acting on any one of the cylinders in the row is always greater than that acting on the same cylinder when it is immersed alone in an unlimited uniform flow with the same velocity. In particular, when the Reynolds number of the flow is sufficiently small, the drag is found to be proportional to the flow speed U, while it is proportional to $U/\log U$ in the case of a single cylinder. Thus, the interference effect between the cylinders in the row is very remarkable at low Reynolds numbers.

1. Introduction

THE steady flow of a viscous fluid past a cylindrical obstacle at small Reynolds numbers has hitherto been studied theoretically by many authors on the basis of Oseen's linearized equations of motion. However, so far as the present writers are aware, most of these investigations concern the case of flow around a single obstacle.

It is natural to expect that the disturbance due to an obstacle will spread very far in the flow field at low Reynolds numbers (e.g. the flow of very viscous fluid). Therefore, when two or more obstacles are present in the otherwise uniform stream, the interference effect between them will be very conspicuous at low Reynolds numbers. In this respect, the present writers have studied the steady two-dimensional flow of incompressible viscous fluid past an infinite row of equal regularly spaced circular cylinders lying in a plane perpendicular to the uniform stream. The flow of this type seems to be of considerable interest both from theoretical and practical points of view. The whole analysis is based on the Oseen approximation. Denoting by R and R_h the Reynolds numbers referred to the diameter of each cylinder and the central distance between the two neighbouring

cylinders respectively, we may distinguish the case in which R is small but R_h is not small from the case where R and R_h are both small. In the former case, a solution in the form of R-expansion is obtained correct to the order of R^2, the lowest order term being $O(1)$. In the latter case, the solution is expressed in the form of power series in the diameter-distance ratio of the row.

Detailed numerical calculations are made for the drag coefficient at various Reynolds numbers ranging from 0 to 8, and for values of $\frac{1}{5}$, $\frac{1}{10}$, $\frac{1}{50}$, $\frac{1}{500}$, for the diameter-distance ratio of the row.

2. Fundamental equations and boundary conditions

Let us consider the steady two-dimensional flow of a viscous fluid passing through an infinite row of equal circular cylinders of radius a, spaced regularly at a distance h between the centres and lying in a plane perpendicular to the uniform stream. We take the rectangular coordinates (x, y) in the plane of fluid motion, in such a way that the origin coincides with the centre of any cylinder of the row, and the x-axis is along the direction of the uniform stream.

Let U be the undisturbed velocity, u, v the x, y components of the velocity at any point, and ζ the vorticity defined as

$$\left.\begin{aligned} \zeta &= (\partial v/\partial x)-(\partial u/\partial y) = 2i(\partial w/\partial \bar{z}) \\ w &= u-iv, \quad z = x+iy, \quad \bar{z} = x-iy \end{aligned}\right\}. \tag{1}$$

Then Oseen's equation of motion may be written as

$$(\nabla^2-2k\partial/\partial x)\zeta = 0, \qquad k = U/2\nu, \tag{2}$$

where ν is the kinematic viscosity.

From these equations it will be seen that the complex velocity w for the present problem may be put in the form:

$$w = U+\epsilon+\sum_{s=-\infty}^{\infty}(W_s+w_s), \tag{3}$$

where

$$\left.\begin{aligned} W_s &= \sum_{m=1}^{\infty} A_m(a/z_s)^m \\ w_s &= e^{kr_s\cos\theta_s}\sum_{m=-\infty}^{\infty} a_m K_m(kr_s)e^{im\theta_s} \\ z &= re^{i\theta}, \quad z_s = z-ish = r_s e^{i\theta_s} \end{aligned}\right\}, \tag{3a}$$

and ϵ, A_m, and a_m are arbitrary real constants to be determined by the boundary conditions and $K_m(kr_s)$ denotes the modified Bessel function.

Further, since the vorticity ζ should be real, $\mathrm{re}(\partial w/\partial\bar{z}) = 0$, whence

$$a_{-j} = a_{j-1} \qquad (j = 1, 2,...). \tag{4}$$

Now, for $|x| \to \infty$, w should be equal to the undisturbed velocity U. From (3) it will be seen that when $x \to -\infty$

$$w \cong U+\epsilon+\sum_{s=-\infty}^{\infty}(A_1 a/z_s) \cong U+\epsilon-(\pi a/h)A_1.$$

Hence
$$\epsilon = (\pi a/h)A_1. \tag{5}$$

Also, it can be shown after some calculation that

$$w \to U+(2\pi a/h)A_1+(2\pi/kh)\sum_{m=0}^{\infty} a_m$$

for $x \to +\infty$. Therefore the following relation is expected to hold:

$$A_1+(ka)^{-1}\sum_{m=0}^{\infty} a_m = 0. \tag{6}$$

The relations (3) together with (5) and (6) already satisfy the condition at infinity as well as the condition of periodicity in the y-direction. The only remaining condition to be satisfied is that $w = 0$ on a cylinder $r = a$. For the fulfilment of this condition, we expand w in a Fourier series† in θ on $r = a$. Then we equate every coefficient of $\exp(in\theta)$ $(n = 0, \pm 1, \pm 2, \ldots)$ to zero. Thus, after some calculations, we get the following simultaneous equations:

$$A_n+{\sum_{m=-\infty}^{\infty}}'(g_{m(-n)}+G_{m(-n)})a_m = 0 \quad (n = 1, 2, \ldots), \tag{7}$$

$$\sum_{s=1}^{\infty} F_{sn}A_s+\sum_{m=-\infty}^{\infty}(g_{mn}+G_{mn})a_m = \begin{cases} -U & (n = 0), \\ 0 & (n = 1, 2, \ldots), \end{cases} \tag{8}$$

where

$$\left.\begin{aligned} F_{1,0} &= \pi a/h \\ F_{sn} &= \begin{cases} (-1)^{s+\frac{1}{2}(s+n)}\dfrac{s}{s!\,n!(s+n)}B_{\frac{1}{2}(s+n)}\left(\dfrac{2\pi a}{h}\right)^{s+n} & (s+n = \text{even}) \\ 0 & (s+n = \text{odd} \geqslant 3) \end{cases} \\ g_{mn} &= K_m(ka)I_{m-n}(ka) \\ G_{mn} &= 2\sum_{l=-\infty}^{\infty}(-1)^{l+\frac{1}{2}(l+m)}T_{l+m}(kh)I_l(ka)I_{l+n}(ka) \\ T_{l+m}(kh) &= \begin{cases} \sum_{s=1}^{\infty} K_{l+m}(skh) & (l+m = \text{even}) \\ 0 & (l+m = \text{odd}) \end{cases} \end{aligned}\right\} \tag{9}$$

and B_n denotes Bernoulli's number.

† For this purpose, it is convenient to use the addition theorem for $K_m(kr_s)\exp(in\theta_s)$. See, for example, G. N. Watson, *Theory of Bessel Functions*, p. 361.

The first equation of (7) verifies (6), as expected. Elimination of the A_s from (7) and (8) gives

$$\sum_{m=-\infty}^{\infty} \chi_{mn} a_m = \begin{cases} -U & (n=0), \\ 0 & (n=1,2,\ldots), \end{cases} \tag{10}$$

where

$$\chi_{mn} = g_{mn} + G_{mn} - \sum_{s=1}^{\infty} F_{sn}\{g_{m(-s)} + G_{m(-s)}\}. \tag{10a}$$

Also, the a_m must satisfy the equation (4). Thus, equations (4), (7), and (10) determine in principle the constants a_m, A_m and hence the solution of the present problem. It is, however, difficult in practice to solve these equations exactly. On the other hand, Oseen's equation itself is valid only at small Reynolds numbers, and our main interest in the present work lies also in such flows. In what follows we accordingly seek for approximate solutions valid for the flow at low Reynolds number.

3. Approximate solutions for small Reynolds numbers

There are two parameters ka and kh in the present problem, and we shall first treat the case in which ka is very small but kh is not. In this case we expand the coefficients χ_{mn} in (10) in powers of ka by expanding $I_m(ka)$ and $K_m(ka)$. Then it is found that $a_m = O[(ka)^{2m}]$ and the unknowns a_m can be determined successively in the form of power series in ka. Thus, after simple but tedious calculations, we obtain the following result:

$$\left.\begin{aligned} (a_0/U) &= -(2/Z)+(2/Z^2)\{Q^2-QZ+(\tfrac{2}{3})(2\pi/kh)^2+1\}(ka/2)^2+\ldots \\ (a_1/U) &= (2/Z)(Z-Q)(ka/2)^2+\ldots \\ &\cdots\cdots\cdots\cdots\cdots\cdots\cdots\cdots\cdots \end{aligned}\right\} \tag{11}$$

where

$$\left.\begin{aligned} Z &= 4T_0-(2\pi/kh)+2S+1 \\ Q &= -4T_2+(\tfrac{1}{3})(2\pi/kh)^2-(2\pi/kh)+(\tfrac{1}{2}) \\ T_{2j} &= \sum_{s=1}^{\infty} K_{2j}(skh) \quad (j=0,1,\ldots) \\ S &= \log(2/ka)-\gamma \quad (\gamma\text{: Euler's constant}) \end{aligned}\right\}. \tag{11a}$$

Further, (7) combined with (11) determine the constants A_m. But we shall only note here that $A_m = O[(ka)^{m-2}]$.

We now proceed to the evaluation of the drag D per unit length of a cylinder in the row. By summing up the stress acting on the surface of a cylinder, it can be shown without difficulty that

$$D = 2\pi\rho a U A_1. \tag{12}$$

Substituting A_1 from (6) and (11) we arrive at the result:

$$\left.\begin{aligned} C_D = \frac{D}{2a\rho U^2} = \frac{8\pi}{RZ}\left[1-\frac{1}{Z}\left\{(Z-Q)^2+\frac{32}{3}\left(\frac{\pi}{R_h}\right)^2+1\right\}\frac{R^2}{64}+\ldots\right] \\ R = 4ka = 2aU/\nu, \qquad R_h = 2kh = hU/\nu \end{aligned}\right\}, \quad (13)$$

where Z and Q are given in (11 a). If we here take the limit as $h \to \infty$, we obtain a formula for the case of a single cylinder in an unbounded stream, which is seen to agree, up to the order considered, with the result given by Tomotika and Aoi (**1**).

Further, it can be shown that the pressure drop in the far down-stream from the row of cylinders is given by the formula

$$(p_{-\infty}-p_{+\infty})/\rho U^2 = (2a/h)C_D,$$

where $p_{-\infty}$ and $p_{+\infty}$ are the pressures at $x = -\infty$ and $x = +\infty$ respectively.

We next treat the case in which ka and kh are both small. We begin as before with an approximate evaluation of the coefficients χ_{mn} in (10).

First, it is necessary to get asymptotic expansions for the function $T_{2j}(kh)$ for small values of kh. To this end we rewrite $T_{2j}(\lambda)$ in the form

$$T_{2j}(\lambda) = T_{-2j}(\lambda) = \sum_{s=1}^{\infty} K_{2j}(s\lambda) = \frac{1}{2}\int_0^{\infty}\left[\exp\left\{\frac{\lambda}{2}\left(t+\frac{1}{t}\right)\right\}-1\right]^{-1} t^{2j-1}\,dt. \quad (14)$$

Expanding the integrand in powers of λ, carrying out term-wise integration, and summing up the resulting series, we get the expressions

$$\left.\begin{aligned} T_0(\lambda) &\sim (\tfrac{1}{8})(4\pi/\lambda)+(\tfrac{1}{2})\log(\lambda/4\pi)+(\gamma/2)- \\ &\qquad -\zeta(3)(\lambda/4\pi)^2+O(\lambda^4) \cdot \\ T_2(\lambda) &\sim (\tfrac{1}{48})(4\pi/\lambda)^2-(\tfrac{1}{8})(4\pi/\lambda)+(\tfrac{1}{4})+O(\lambda^2) \\ T_{2j}(\lambda) &\sim (B_j/8j)(4\pi/\lambda)^{2j}-(B_{j-1}/4)(4\pi/\lambda)^{2j-2}+O(\lambda^{-2j+4}) \\ &\qquad (j = 2,\ 3,\ldots) \end{aligned}\right\}, \quad (15)$$

where $\zeta(n)$ is the zeta function and the B_j are Bernoulli's numbers as before.

By making use of these results together with the expansions of $I_m(ka)$ and $K_m(ka)$ we can obtain, after tedious calculations, required expressions for the χ_{mn}. However, we shall only note here the following results:

$$\left.\begin{aligned} \chi_{2m,2n} &= O[(ka)^{-2m}], & \chi_{2m+1,2n} &= O[(ka)^{-2m}] \\ \chi_{2m,2n+1} &= O[(ka)^{-2m+1}], & \chi_{2m+1,2n+1} &= O[(ka)^{-2m-1}] \\ (m &= 0,\ 1,\ldots), & (n &= 0,\ 1,\ldots) \end{aligned}\right\}. \quad (16)$$

From this and (10) it is suggested that

$$a_{2m} = O[(ka)^{2m}], \qquad a_{2m+1} = O[(ka)^{2m+2}].$$

Therefore, to the lowest order in ka, we can determine the a_{2m} separately

from the a_{2m+1}. Thus, after some calculation, we obtain

$$\left.\begin{aligned} a_0/U &= -(2/\Lambda_0)+O[(ka)^2], \qquad a_2/U = (\Lambda_2/\Lambda_0)(ka)^2+O[(ka)^4] \\ a_4/U &= -(\Lambda_4/\Lambda_0)(ka)^4+O[(ka)^6], \quad \ldots \end{aligned}\right\}, \tag{17}$$

where

$$\left.\begin{aligned} \Lambda_0 &= 1-2\log\tau+\tfrac{1}{6}\tau^2-\tfrac{1}{144}\tau^4+\tfrac{1}{1080}\tau^6- \\ &\qquad -\tfrac{53}{345600}\tau^8+\tfrac{139}{5443200}\tau^{10}+O(\tau^{12}) \\ \Lambda_2 &= \tfrac{1}{48}(\tau^2-\tfrac{2}{15}\tau^4+\tfrac{1}{48}\tau^6-\tfrac{67}{18900}\tau^8)+O(\tau^{10}) \\ \Lambda_4 &= \tfrac{1}{46080}(\tau^4-\tfrac{4}{21}\tau^6)+O(\tau^8), \quad \ldots \\ \tau &= 2\pi a/h \end{aligned}\right\}. \tag{17a}$$

Inserting these in (12) combined with (6), we arrive at a formula

$$D/(\mu U) = RC_D = 8\pi/\Lambda_0+O(R^2), \tag{18}$$

where μ is the viscosity coefficient, Λ_0 is given by (17 a), and

$$R = 4ka = 2aU/\nu$$

as before.

4. Numerical discussion and conclusions

We are now able to calculate the drag per unit length of a cylinder in various rows with different diameter-distance ratios $2a/h$, at arbitrary Reynolds numbers R. For sufficiently small R, formula (18) is used and the formula (13) is valid when R becomes comparable with or exceeds the ratio $2a/h$. It may be remarked here that (13) diverges for some value of R which makes the denominator Z vanish. This is, however, a trivial singularity brought about by the expansion of the modified Bessel function $K_n(ka)$, and is of common occurrence in formulae of the same kind (cf. reference **1**). To avoid this difficulty it is better to use a direct method in which we start with the simultaneous equations (10), evaluate their coefficients and then solve the equations with numerical coefficients thus obtained.

Tables 1–4 and Fig. 1 show the variation of $D/\mu U$ with the Reynolds number R for various values of $2a/h$, while Table 5 gives the values of $D/\mu U$ against $2a/h$ for sufficiently small R for which $D/\mu U$ becomes independent of R. In these tables $(D/\mu U)_0$, $(D/\mu U)_1$, and $(D/\mu U)_2$ denote respectively the values calculated by (18), (13), and the direct method mentioned above.

These results may be summarized as follows:

(1) The drag acting on a cylinder in the row is, in general, greater than that on the same cylinder when alone in a uniform flow of the same velocity. Further, the drag increases as the diameter-distance ratio of the row becomes large.

(2) As the Reynolds number of the flow is reduced, the value of $D/\mu U$

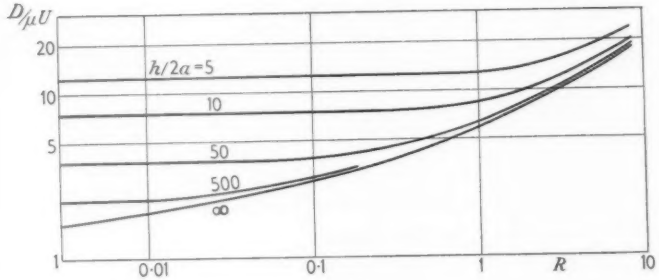

FIG. 1

TABLE 1
Values of $D/\mu U$
$(2a/h = \frac{1}{5})$

R	$(D/\mu U)_1$	$(D/\mu U)_2$
0	12·58	
0·08	12·59	
0·24	12·60	
0·4	12·66	12·67
0·8	12·87	12·86
1·6	13·73	13·39
2·4	15·05	14·77
3·2	16·22	16·00
4·0		17·29
4·8		18·59
5·6		19·85
6·4		21·05
7·2		22·21
8·0		23·30

TABLE 2
Values of $D/\mu U$
$(2a/h = \frac{1}{10})$

R	$(D/\mu U)_1$	$(D/\mu U)_2$
0	7·54	
0·12	7·56	
0·2	7·58	
0·4	7·72	7·72
0·8	8·20	8·19
1·6	9·66	9·53
2·4	11·52	10·98
3·2	13·76	12·40
4·0	15·76	13·75
4·8		15·04
5·6		16·30
6·4		17·45
7·2		18·62
8·0		19·60

TABLE 3
Values of $D/\mu U$
$(2a/h = \frac{1}{50})$

R	$(D/\mu U)_1$	$(D/\mu U)_2$
0	3·85	
0·08	3·91	
0·2	4·18	
0·4	4·76	4·76
0·8	5·84	5·82
1·6	7·75	7·61
2·4	9·70	9·19
3·2	11·96	10·62
4·0	14·44	11·96
4·8		13·23
5·6		14·42
6·4		15·56
7·2		16·62
8·0		17·62

TABLE 4
Values of $D/\mu U$
$(2a/h = \frac{1}{500})$

R	$(D/\mu U)_1$	$(D/\mu U)_2$
0	2·26	
0·08	2·87	
0·2	3·53	
0·4	4·30	4·30
0·8	5·47	5·46
1·6	7·43	7·30
2·4	9·37	8·87
3·2	11·61	10·31
4·0	14·09	11·64
4·8		12·90
5·6		14·09
6·4		15·21
7·2		16·27
8·0		17·28

TABLE 5

$2a/h$	$(D/\mu U)_0$
0·0010	2·01
0·0020	2·26
0·0025	2·35
0·004	2·58
0·005	2·70
0·010	3·17
0·020	3·85
0·025	4·13
0·04	4·88
0·05	5·34
0·1	7·54
0·2	12·60
0·4	31·73

deviates more and more from that for the case of a single cylinder. Moreover, it tends to a finite limit when $R \to 0$, whereas in the case of a single cylinder it tends to zero as $(\log R)^{-1}$.

Lastly, the following remark may be made. The flow is narrowed down as it passes through the row and the shear in the fluid near the surface of each cylinder thereby becomes greater. This brings about the increase in drag on each cylinder. In this respect, there is an essential difference between the case when the number of cylinders is infinite and that in which it is large but finite. In the latter case, the flow may pass round the system of cylinders, leaving the fluid inside the system almost at rest. Thus, in such a case the drag on a cylinder inside the system is expected to be very small.

The writers wish to express their cordial thanks to Professor S. Tomotika for his continual interest and encouragement throughout this work.

REFERENCE

1. S. Tomotika and T. Aoi, *Quart. J. Mech. App. Math.* **4** (1951) 401.

ON THE EQUILIBRIUM OF A STRATIFIED LAYER OF FLUID

By B. R. MORTON

(*Department of Mathematics, University College, London*)†

[Received 16 October 1956]

SUMMARY

This note demonstrates the equal importance of viscosity and thermal conductivity (or any equivalent process of diffusion) in determining the departure from equilibrium of continuously stratified layers of fluid. The analysis is carried out by an extension of previous variational principles, and is applied to freely bounded horizontal layers which are thermally stratified; the initial rate of growth of small disturbances is shown to depend on the Rayleigh and Prandtl numbers. The method gives the usual critical Rayleigh number for the onset of convection in unstably stratified layers with a linear density gradient, but it also indicates that this critical value of the Rayleigh number suffers little reduction when the stratification is originally non-uniform. Although the analysis is applied to a system which cannot be realized physically, the corresponding results for real systems should be qualitatively similar.

1. Introduction

If a horizontal layer of fluid is heated from below it becomes unstable to small disturbances when the temperature gradient is sufficiently large. The equilibrium of such thermally stratified layers of fluid was first studied by Rayleigh (**1**); since then notable contributions have been made by Jeffreys (**2**, **3**), and by Pellew and Southwell (**4**) who have also given a survey of the earlier work. In the theoretical treatment which has been developed it is assumed that there is a linear temperature profile in the layer, and critical conditions are determined under which a small disturbance will first be amplified. It is found that the condition for marginal stability can be described by a constant value of the Rayleigh number, the particular value depending on the nature of the surfaces bounding the layer.

Although the Rayleigh type of analysis has been used successfully to predict the critical parameter for instability of the steady state, there are problems to which it cannot be extended readily. To overcome this difficulty Chandrasekhar (**5**) has derived a variational principle and has suggested that this could be used as the basis for an approximate treatment of the equilibrium of stratified viscous fluids. Subsequently Hide (**6**) has applied this method to two problems in which layers of immiscible fluid

† Present address: Department of Mathematics, Manchester University.

are superposed, and to a third case in which a layer of viscous fluid is stratified continuously. However, Chandrasekhar developed his variational formula for immiscible viscous fluids, and consequently it takes no account of any diffusion of the property causing variations in density. It cannot, therefore, be used in considering continuously stratified fluids, whether the stratification is produced thermally, by dissolved solids, or in any other way.

The purpose of this note is to bring out the equal importance of the diffusive effects set up by gradients of velocity and of density in determining the departure from equilibrium of an unstably stratified layer. To illustrate the general nature of the equilibrium it will be sufficient to consider the stability of a freely bounded horizontal layer under various conditions of thermal stratification and with slightly simplified boundary conditions, as the effect should depend primarily on the physical properties of real fluids. Moreover, it will be shown that for this limited application it is relatively easy to extend the previous variational treatments, given by Rayleigh (**7**) for inviscid fluids and Chandrasekhar (**5**) for viscous fluids, to cover the case of real fluids possessing properties of viscosity and thermal conductivity. The results of this analysis will show that the initial growth of small disturbances in continuously stratified layers is characterized by both the Rayleigh number and the Prandtl number (i.e. the ratio of kinematic viscosity to thermometric conductivity), and not by the Grashof number alone as Hide has predicted. It will be shown also that a non-linear temperature profile can have little relative effect in modifying the critical value of the Rayleigh number for marginal stability.

2. The equations representing the motion

Consider the equilibrium of an infinite horizontal region of incompressible fluid of depth h, with its upper and lower surfaces free. The system will be referred to rectangular cartesian coordinates $(x_i) \equiv (x, y, z)$ with the origin in the mid-plane of the layer and the z-axis directed vertically upwards, and it will be assumed that the acceleration due to gravity (g) is constant throughout the layer and is directed vertically downwards. It will be assumed also that the coefficient of viscosity μ and the thermal conductivity are constants, and that local variations in temperature are always small in relation to the absolute temperature of the upper surface (and hence that variations in density are small relative to ρ_1, the density near the upper surface).

The equations representing the convective motion set up by a disturbance in the fluid can now be written in the approximate form (see, for example,

Pellew and Southwell (**4**)),

$$\left.\begin{aligned} \rho_1 \frac{\partial u_i}{\partial t} + \rho_1 u_j \frac{\partial u_i}{\partial x_j} &= -\frac{\partial (p_0+p)}{\partial x_i} - \lambda_i \rho g + \mu \nabla^2 u_i \\ \frac{\partial u_i}{\partial x_i} &= 0 \\ \frac{\partial (T+\theta)}{\partial t} + u_j \frac{\partial (T+\theta)}{\partial x_j} &= \kappa \nabla^2 (T+\theta) \\ \rho &= \rho_0 (1-\beta\theta) \end{aligned}\right\}, \tag{1}$$

where $\nabla^2 \equiv \partial^2/\partial x_i \partial x_i$, $(u_i) \equiv (u, v, w)$ is the disturbance velocity, $T = T(z)$ the undisturbed, and $T+\theta$ the disturbed, absolute temperature, p_0 the undisturbed and p the disturbance pressure, ρ_0 the undisturbed and ρ the disturbed density, $\boldsymbol{\lambda} = (\lambda_i)$ the unit vector along the z-axis, β the coefficient of cubical expansion, κ the thermometric conductivity, and t the time variable.

The previous analyses have been based on equations (1) and have been concerned with the equilibrium of a stratified layer of fluid which is initially in a steady state, and thus in each case the undisturbed temperature profile has been taken as linear. Up to the present the analysis has not been extended to determine the behaviour of layers in which the stratification of density is continuous but not uniform. According to the above assumptions, non-linear temperature profiles cannot represent equilibrium conditions and, therefore, must change steadily with time. However, it may still be possible to find the effect of small disturbances on these non-uniform layers, provided that the time scale for the decay of the temperature profile is assumed to be large in comparison with that for the initial growth of the disturbances. Some of the consequences of this condition are considered in the appendix, but it may be remarked here that this type of analysis applies only to infinitesimal disturbances, and ceases to be valid as soon as there is significant growth of the motion.

In the undisturbed state (u_i) and θ are zero, so that equations (1) reduce to

$$\left.\begin{aligned} 0 &= -\frac{\partial p_0}{\partial x_i} - \lambda_i \rho_0 g \\ \frac{\partial T}{\partial t} &= \kappa \nabla^2 T \\ \rho &= \rho_0 \end{aligned}\right\}. \tag{2}$$

In the disturbed state assume that (u_i) and θ are small quantities of the first order: their squares and products are then of the second order of smallness and may be neglected in relation to first order terms. From equations

(1) and (2) it follows that

$$\left(\frac{\partial}{\partial t}-\nu\nabla^2\right)u_i = -\frac{1}{\rho_1}\frac{\partial p}{\partial x_i}+\beta g\lambda_i\theta, \tag{3}$$

$$\frac{\partial u_i}{\partial x_i} = 0, \tag{4}$$

$$\left(\frac{\partial}{\partial t}-\kappa\nabla^2\right)\theta = -w\frac{dT}{dz}, \tag{5}$$

where ν is the kinematic viscosity, and the undisturbed temperature T is taken to vary only with height. Taking the divergence of equation (3), it follows from (4) that

$$0 = -\frac{1}{\rho_1}\nabla^2 p+\beta g\lambda_j\frac{\partial\theta}{\partial x_j};$$

and hence, operating with ∇^2 on equation (3),

$$\left(\frac{\partial}{\partial t}-\nu\nabla^2\right)\nabla^2 u_i = \beta g\left(\lambda_i\nabla^2\theta-\lambda_j\frac{\partial^2\theta}{\partial x_i\,\partial x_j}\right). \tag{6}$$

Then, from (5) and (6),

$$\left(\frac{\partial}{\partial t}-\kappa\nabla^2\right)\left(\frac{\partial}{\partial t}-\nu\nabla^2\right)\nabla^2 w = -\beta g\frac{dT}{dz}\nabla_1^2 w, \tag{7}$$

where

$$\nabla_1^2 \equiv \frac{\partial^2}{\partial x^2}+\frac{\partial^2}{\partial y^2}.$$

In order to determine the initial rate of growth of a disturbance of given wave-number, equation (7) is reduced first to an ordinary differential equation in z by separation of the vertical and horizontal variables. This can be done by assuming that

$$\nabla_1^2 w+k^2 w = 0, \tag{8}$$

and that $w(x, y, z)$ is of the form $f(x, y)\,w(z)$. Then in any pattern of motion which is such that each element of fluid moves within a restricted region, k must be real. For, from Green's theorem,

$$k^2\iint_{\mathrm{I}} w^2\,dxdy = -\iint_{\mathrm{I}} w\nabla_1^2 w\,dxdy$$

$$= \iint_{\mathrm{I}}\left[\left(\frac{\partial w}{\partial x}\right)^2+\left(\frac{\partial w}{\partial y}\right)^2\right]dxdy-\oint_{\mathrm{II}} w\frac{\partial w}{\partial n_e}\,ds,$$

where I is the whole area of the plane considered and II the perimeter of this area. If the boundary is chosen to coincide with that of a set of con-

vection cells (of any kind) the final integral will vanish, as at each point on the perimeter either the vertical velocity (w) or its normal gradient ($\partial w/\partial n_c$) will be zero: hence k^2 is positive, and k real (cf. Pellew and Southwell, (4)). Thus k may be taken as the wave-number of the (harmonic) disturbance in the horizontal plane. This method of analysis is equivalent to reducing a general disturbance into a set of normal modes, each characterized by its wave-number k, and this may be done because the equations have been linearized.

If the amplitude of the disturbance of wave-number k varies as $\exp(nt)$, equation (7) reduces to

$$[-n+\kappa(D^2-k^2)][-n+\nu(D^2-k^2)](D^2-k^2)w = \gamma k^2 w DT, \qquad (9)$$

where $D \equiv d/dz$ and $\gamma = \beta g$. If an exact solution is known for $w(z)$, equation (9) gives the corresponding values of n for each k. However, the exact form for the profile of vertical velocity is known only in the case of a linear temperature gradient, and so to obtain an approximation for n in the more general case considered here it is convenient to develop equation (9) into a variational form.

The boundary conditions which will be satisfied at the free bounding surfaces are:

(i) $w = 0$; this applies strictly for a rigid surface at which there is slip, but although the consequent small increase in constraint on the growing modes may be expected to modify the quantitative results of the analysis, the qualitative results should be unaffected;

(ii) $\partial u/\partial z$, $\partial v/\partial z = 0$ (zero viscous stress), whence from (4) $\partial^2 w/\partial z^2 = 0$;

(iii) $\theta = 0$, hence from equations (8) $\nabla_1^2 \theta = 0$, and from (6)

$$(\partial/\partial t - \nu\nabla^2)\nabla^2 w = 0.$$

Thus at a free boundary,

$$w(z) = 0, \quad D^2 w(z) = 0, \quad D^4 w(z) = 0, \quad D^6 w(z) = 0, \quad \ldots.$$

3. A variational principle for the layer with free surfaces

Equation (9) can be written

$$[-n_i+\kappa(D^2-k^2)][-n_i+\nu(D^2-k^2)](D^2-k^2)w_i = \gamma k^2 w_i DT, \qquad (10)$$

where the velocity w_i corresponds with the characteristic value n_i of the growth factor in the exponential term. Multiply (10) by w_j (corresponding with n_j) and integrate over the range $-\frac{1}{2}h \leqslant z \leqslant \frac{1}{2}h$; then, after repeated integration by parts, it follows that

$$I_{ij} = 0, \qquad (11)$$

where

$$I_{ij} \equiv n_i^2 \int_{-\frac{1}{2}h}^{\frac{1}{2}h} \{Dw_i\, Dw_j + k^2 w_i\, w_j\}\, dz +$$
$$+(\kappa+\nu) n_i \int_{-\frac{1}{2}h}^{\frac{1}{2}h} \{D^2 w_i\, D^2 w_j + 2k^2 Dw_i\, Dw_j + k^4 w_i\, w_j\}\, dz +$$
$$+\kappa\nu \int_{-\frac{1}{2}h}^{\frac{1}{2}h} \{D^3 w_i\, D^3 w_j + 3k^2 D^2 w_i\, D^2 w_j +$$
$$+3k^4 Dw_i\, Dw_j + k^6 w_i\, w_j + (\gamma k^2/\kappa\nu) DT w_i\, w_j\}\, dz.$$

Hence, subtracting I_{ji} from I_{ij}, if $n_i \neq n_j$ it follows that

$$(n_i+n_j) \int_{-\frac{1}{2}h}^{\frac{1}{2}h} \{Dw_i\, Dw_j + k^2 w_i\, w_j\}\, dz +$$
$$+(\nu+\kappa) \int_{-\frac{1}{2}h}^{\frac{1}{2}h} \{D^2 w_i\, D^2 w_j + 2k^2 Dw_i\, Dw_j + k^4 w_i\, w_j\}\, dz = 0. \quad (12)$$

A complex value of n will be associated with a complex value of w; their respective conjugates ($\bar{n}$, $\bar{w}$) will also be associated, and will satisfy the same equations and boundary conditions. Thus if n_i, w_i are taken as n, w, and n_j, w_j as $\bar{n}$, $\bar{w}$, respectively, equation (12) reduces to

$$2\,\mathrm{re}(n) \int_{-\frac{1}{2}h}^{\frac{1}{2}h} \{|Dw|^2 + k^2|w|^2\}\, dz +$$
$$+(\nu+\kappa) \int_{-\frac{1}{2}h}^{\frac{1}{2}h} \{|D^2 w|^2 + 2k^2|Dw|^2 + k^4|w|^2\}\, dz = 0. \quad (13)$$

Hence if n is complex it follows that the real part of n must be negative; that is, instability through oscillations cannot occur because of damping. Therefore $\mathrm{re}(n) > 0$ is possible for real values of n only, and imaginary values of n need not be considered in a search for unstable modes. It also follows from (11) that if n is to have real positive values (and these give rise to the only instabilities) DT must be negative over at least part of the range.

To obtain an equation which can be used as the basis for a variational determination of n put $i = j$ in (11) and suppress subscripts,

$$n^2 \int_{-\frac{1}{2}h}^{\frac{1}{2}h} \{(Dw)^2 + k^2 w^2\}\, dz + (\kappa+\nu) n \int_{-\frac{1}{2}h}^{\frac{1}{2}h} \{(D^2 w)^2 + 2k^2 (Dw)^2 + k^4 w^2\}\, dz +$$
$$+\kappa\nu \int_{-\frac{1}{2}h}^{\frac{1}{2}h} \{(D^3 w)^2 + 3k^2 (D^2 w)^2 + 3k^4 (Dw)^2 + k^6 w^2 + (\gamma k^2/\kappa\nu) DT w^2\}\, dz = 0. \quad (14)$$

Equation (14) is in suitable form, for if it is written

$$n^2 I_1 + (\kappa+\nu) n I_2 + \kappa\nu I_3 = 0, \quad (15)$$

then to the first order, if δw is an arbitrary functional variation in w (compatible with the boundary conditions on w),

$$\{2nI_1+(\kappa+\nu)I_2\}\delta n+\{n^2\delta I_1+(\kappa+\nu)n\,\delta I_2+\kappa\nu\,\delta I_3\} = 0. \tag{16}$$

On integrating by parts in each case it is found that

$$\delta I_1 = -2\int_{-\frac{1}{2}h}^{\frac{1}{2}h} \delta w(D^2-k^2)w\,dz,$$

$$\delta I_2 = 2\int_{-\frac{1}{2}h}^{\frac{1}{2}h} \delta w(D^2-k^2)^2 w\,dz,$$

$$\delta I_3 = -2\int_{-\frac{1}{2}h}^{\frac{1}{2}h} \delta w(D^2-k^2)^3 w\,dz + 2(\gamma k^2/\kappa\nu)\int_{-\frac{1}{2}h}^{\frac{1}{2}h} \delta w DTw\,dz,$$

and hence

$$n^2\delta I_1+(\kappa+\nu)n\,\delta I_2+\kappa\nu\,\delta I_3$$

$$= -2\int_{-\frac{1}{2}h}^{\frac{1}{2}h} \{\kappa\nu(D^2-k^2)^3 w-(\kappa+\nu)n(D^2-k^2)^2 w+n^2(D^2-k^2)w-\gamma k^2 DTw\}\times \times\delta w\,dz.$$

As any function w which is a solution of the problem satisfies the differential equation

$$\kappa\nu(D^2-k^2)^3 w-(\kappa+\nu)n(D^2-k^2)^2 w+n^2(D^2-k^2)w-\gamma k^2 DTw = 0,$$

it follows that if w satisfies the differential equations representing the motion together with the boundary conditions for free surfaces, then

$$\{2nI_1+(\kappa+\nu)I_2\}\delta n = 0. \tag{17}$$

But the factor $\{2nI_1+(\kappa+\nu)I_2\}$ in (17) is a positive definite function under these conditions; hence $\delta n = 0$ and n is stationary.

If the correct solution for w is inserted in equation (14) the correct value for n will be found. However, if the precise form of w is unknown it follows from the stationary property that any reasonably close approximation will give a good estimate for n from equation (14), since all small variations in w which are compatible with the boundary conditions leave n unchanged to the first order of accuracy.

It is apparent from (14) that the effects of thermal conductivity and viscosity enter symmetrically through the coefficients κ and ν, and that in general neither may be neglected in considering the equilibrium of continuously stratified fluids. Although no allowance has been made for variations in κ or ν (as in Chandrasekhar's formulation) this neglect should only introduce small errors into the numerical results which will be obtained.

4. The approximate treatment of equilibrium

Before considering the various ways in which the equilibrium of the layer may be affected, it will be convenient to change the variational equation into dimensionless form: this can be done by means of the transformation

$$z = hZ, \quad k = \frac{1}{h}K, \quad n = (\kappa\nu)^{\frac{1}{2}}\frac{N}{h^2}, \quad w(z) \equiv W(Z), \quad D \equiv \frac{d}{dz} \equiv \frac{1}{h}\frac{d}{dZ}.$$

Two non-dimensional parameters can be used to describe the equilibrium and the growth of disturbances in the layer: the Rayleigh number $A = \gamma h^3 \Delta T/\kappa\nu$ provides an 'entire' parameter, and the 'profile number' $b(z/h) = h\,DT/\Delta T$ provides a local parameter, where $\Delta T = |T_0 - T_1|$ and T_0, T_1 are the temperatures of the lower and upper surfaces respectively. A does not depend on local values in the temperature profile, while b represents the ratio of the local to the average temperature gradient. Equation (14) can now be reduced to the dimensionless form

$$N^2 \int_{-\frac{1}{2}}^{\frac{1}{2}} \{(DW)^2 + K^2W^2\}\,dZ +$$

$$+ (\sigma^{\frac{1}{2}} + \sigma^{-\frac{1}{2}})N \int_{-\frac{1}{2}}^{\frac{1}{2}} \{(D^2W)^2 + 2K^2(DW)^2 + K^4W^2\}\,dZ +$$

$$+ \int_{-\frac{1}{2}}^{\frac{1}{2}} \{(D^3W)^2 + 3K^2(D^2W)^2 + 3K^4(DW)^2 + K^6W^2 + K^2Ab\,W^2\}\,dZ = 0, \quad (18)$$

where $\sigma = \nu/\kappa$ is the Prandtl number.

In previous treatments no attempt has been made to determine the form of motion that may develop in unstably stratified layers where there is a non-uniform distribution of temperature. However, for the case of a linear profile Pellew and Southwell (**4**) have given exact solutions for free layers in which there is neutral stability (i.e. $N = 0$). They distinguish between 'even' solutions $W = C\cos(2p+1)\pi Z$, and 'odd' solutions $W = C\sin 2q\pi Z$, where C is a constant representing the initial magnitude of the disturbance and p, q are integers ($q \neq 0$): thus their general solution can be written

$$W = C\begin{matrix}\cos\\ \sin\end{matrix} MZ, \quad (19)$$

where $M = m\pi$ and m is an appropriate integer. Although there is little doubt that the pattern of convection will be different when N is not zero or when the motion grows in a layer which is not uniformly stratified, it seems reasonable to assume that these differences will be relatively small. There will still be a similar tesselation of the flow in horizontal planes, and cells will continue to occupy the whole region between the bounding surfaces.

for it seems that any other arrangement would increase the constraint on the motion. Therefore, this solution (19) may be used as the basis for an approximate investigation of the dependence of N on the dimensionless parameters A, b, and σ; if it is substituted in equation (18), then

$$(K^2+M^2)N^2+(\sigma^{\frac{1}{2}}+\sigma^{-\frac{1}{2}})(K^2+M^2)^2N+(K^2+M^2)^3+K^2AB=0, \quad (20)$$

where

$$B=2\int_{-\frac{1}{2}}^{\frac{1}{2}} b(Z)\begin{matrix}\cos^2\\ \sin^2\end{matrix} MZ\,dZ$$

is the 'entire profile number'.

A simple check can be applied to the present treatment at this point. For marginal stability $N=0$, and hence from equation (20)

$$AB=-\frac{1}{K^2}(K^2+M^2)^3. \quad (21)$$

In particular for a linear temperature profile $B=-1$, and in this case (21) reduces to the criterion for neutral stability given by Pellew and Southwell. However, for other values of B representing different profiles the critical Rayleigh number will be decreased or increased according as $|B|>$ or <1.

5. The effect of non-uniform stratification

If at time $t=0$ the lower surface of the layer is suddenly raised in temperature from T_1 to T_0, the temperature profile at any subsequent time can be expressed in the form

$$\frac{T-T_1}{\Delta T}=(\tfrac{1}{2}-Z)-\frac{2}{\pi}\sum_{r=1}^{\infty}\frac{\sin r\pi(\frac{1}{2}+Z)}{r}\exp\left(-\frac{\pi^2r^2\kappa t}{h^2}\right).$$

The corresponding value of the entire profile number is $B=-1$. Thus, to the present order of approximation, the stability of the layer is not affected by this method of initial heating, although inaccuracy in this result will arise from any considerable departure of W from the form $C\begin{matrix}\cos\\ \sin\end{matrix} MZ$.

By considering a rather wider range of physically possible profile functions, it may be shown that the entire profile number

$$B=\frac{2}{\Delta T}\int_{-\frac{1}{2}}^{\frac{1}{2}}\frac{dT}{dZ}\begin{matrix}\cos^2\\ \sin^2\end{matrix} MZ\,dZ=-1\pm\frac{1}{\Delta T}\sum_{r=-m}^{m-1}\int_{r\pi}^{(r+1)\pi}\frac{dT(u)}{du}\cos u\,du$$

lies within the range $-1\leqslant B\leqslant 0$ for all functions $T(Z)$ which are such that (i) $dT/dZ\leqslant 0$ and (ii) $d^2T/dZ^2\geqslant 0$ for $-\frac{1}{2}\leqslant Z\leqslant\frac{1}{2}$. These conditions are equivalent to stipulating that within the layer conduction is

directed from the hot to the cold surface at all intermediate points, and that there are no internal heat sources. Thus it appears that the critical Rayleigh number for marginal stability will certainly not be appreciably reduced in free layers which are non-uniformly stratified, and it may actually be increased. This result is of some interest in problems of thermal stability because it has been suggested (Sutton (**8**)) that such non-linear temperature profiles may be specially effective in the initiation of instabilities.

One of the predictions of the Rayleigh theory for marginal stability in fluids which are uniformly and unstably stratified is that very large temperature gradients will be needed to set up cellular convection in thin layers. While previous experimental work had shown excellent agreement with the general results of the Rayleigh analysis, there had been no special attention to thin layers until some experiments by Chandra (**9**). He verified the original results for Bénard cells, but he also found evidence for a new kind of convective instability which could grow in thin layers between rigid surfaces at Rayleigh numbers which, under some conditions, were far below the usual critical values. It was this new type of instability (described by Chandra as 'columnar') which Sutton suggested might grow from a thermal boundary layer near the lower surface in the fluid.

Although the present analysis has been developed for the freely bounded layer, the two types of system are sufficiently close physically for the results in each to be of similar nature. If the effects of both viscosity and thermal conductivity are taken into account, it has been shown that reductions in the critical Rayleigh number for the free layer may be expected to be relatively small: it may reasonably be inferred that the equivalent reductions for the layer with rigid boundaries will not be as large as those reported by Chandra (ranging up to a reduction of > 90 per cent. for a layer of air *c.* 5 mm thick).† Thus the effect of a thermal boundary layer on the equilibrium of stratified layers appears unlikely to represent the true source of the reported 'columnar' instability; if this is a genuine instability of the layer some new mechanism will probably have to be found.

6. The unstably stratified layer

The results of this section may conveniently be discussed in terms of a modified Rayleigh number $A^* = AB$, and for the unstably stratified layer $A^* < 0$. The behaviour of N in terms of the non-dimensional parameters A^* and σ can now be found from the solution to equation (20),

$$N = \tfrac{1}{2}(K^2+M^2)\left\{-(\sigma^{\frac{1}{2}}+\sigma^{-\frac{1}{2}})+\left[(\sigma^{\frac{1}{2}}-\sigma^{-\frac{1}{2}})^2-\frac{4K^2A^*}{(K^2+M^2)^3}\right]^{\frac{1}{2}}\right\}, \qquad (22)$$

† Moreover, there appears to be no reason for anticipating Chandra's observation that the depression of the critical Rayleigh number increased with decreasing thickness of the layer,

where the positive sign has been chosen since this corresponds with the instability. For given values of K, A^*, and σ the largest value of N corresponds with the first harmonic mode, for which $m = 1$ (i.e. $M = \pi$), and

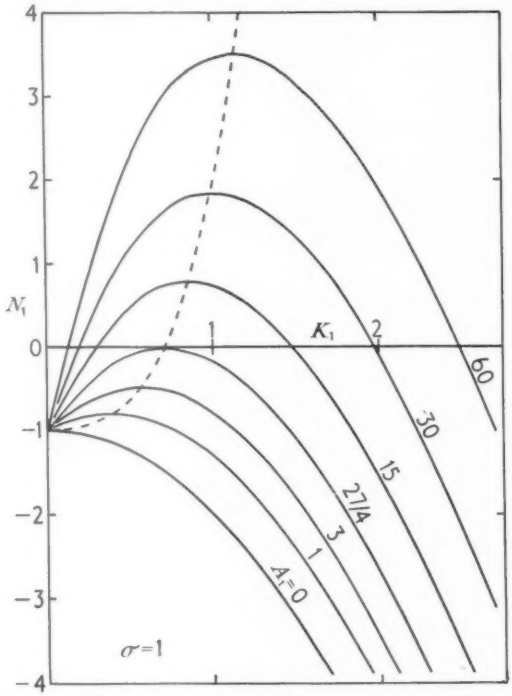

FIG. 1. The initial rates of growth (N_1) for disturbances of wave-number (K_1) in unstably stratified layers, plotted in dimensionless form for a range of values of the Rayleigh number (A_1) and for $\sigma = 1$

since this analysis applies only to the onset of convection other modes need not be considered. If relation (22) is reduced by the substitution

$$M = \pi, \qquad K_1 = K/\pi, \qquad A_1 = -A^*/\pi^4, \qquad N_1 = N/\pi^2,$$

it takes the form

$$N_1 = \tfrac{1}{2}(1+K_1^2)\left\{-(\sigma^{\frac{1}{2}}+\sigma^{-\frac{1}{2}})+\left[(\sigma^{\frac{1}{2}}-\sigma^{-\frac{1}{2}})^2+\frac{4K_1^2 A_1}{(1+K_1^2)^3}\right]^{\frac{1}{2}}\right\}. \qquad (23)$$

The variation of the rate of growth coefficient ($N_1 = \hbar^2 n/\pi^2(\kappa\nu)^{\frac{1}{3}}$) with the wave-number ($K_1 = hk/\pi$) is shown in non-dimensional form in Fig. 1 for a variety of values of the modified Rayleigh number ($A_1 = -A^*/\pi^4$) and for Prandtl number $\sigma = 1$. Although the present linearized theory

applies only to infinitesimal disturbances, the plotted curves do serve to illustrate the earliest stages of the growth or decay of disturbance modes. There is a critical Rayleigh number $A_{1c} = \frac{27}{4}$ below which all wave-numbers will be damped out, while for $A_1 > A_{1c}$ there is in each case a band of wave-numbers for which disturbances will be amplified. In such cases of instability one mode will grow more rapidly than the others, and it can be seen that

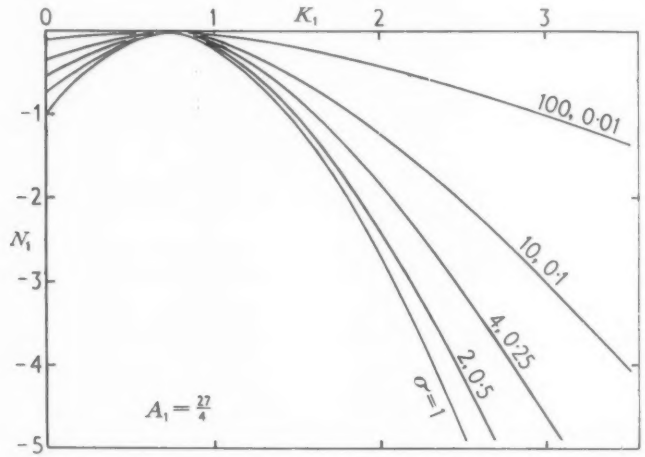

FIG. 2. The dependence of the rate of growth factor (N_1) on the wave number (K_1) for various values of the Prandtl number (σ) in the case of marginal stability (i.e. $A_1 = \frac{27}{4}$) for an unstably stratified layer

the wave-number of this dominant mode increases slightly with increasing Rayleigh number. Thus disturbances with larger wave-numbers will begin to grow in those layers of fluid in which the effects of diffusion are small. The broken line which joins the maxima of the set of curves in Fig. 1 has the equation

$$N_1 = -1 + K_1^2 + 2K_1^4.$$

These results are in broad agreement with observations, although variations in the dominant wave-number have not been (and are unlikely to be) observed because of experimental difficulties. They may be contrasted qualitatively with the equivalent results of Hide, according to which all disturbance modes are unstable.

The symmetrical way in which viscosity and thermal conductivity affect the results is further illustrated in Fig. 2 by a set of curves showing the variation of the rate of growth factor (N_1) with the wave number (K_1) for several values of σ in the case of marginal stability ($A_1 = \frac{27}{4}$). It can be seen that the critical wave number (K_1) for marginal stability is unaffected

by changes in the Prandtl number. However, this is not true generally, and for other values of A_1 the dominant wave number does depend on σ to some extent: this effect is not due to the predominance of either viscosity or thermal conductivity but only to their lack of balance, since the effect is unchanged by substituting $1/\sigma$ for σ.

7. The stably stratified layer

Attention has been concentrated so far on the equilibrium of unstably stratified layers where the neglect of thermal conduction in the fluid is likely to have the most serious effects. In order to complete the qualitative comparison with the treatment given by Hide (**6**) a brief discussion will now be given for the stability of stably stratified layers.

In this case $A^* > 0$, and if A_1 is now written for $+A^*/\pi^4$ the corresponding solution for N_1 is

$$N_1 = -\tfrac{1}{2}(1+K_1^2)\left\{(\sigma^{\frac{1}{2}}+\sigma^{-\frac{1}{2}}) \pm \left[(\sigma^{\frac{1}{2}}-\sigma^{-\frac{1}{2}})^2 - \frac{4K_1^2 A_1}{(1+K_1^2)^3}\right]^{\frac{1}{2}}\right\}; \qquad (24)$$

hence, N_1 will be real or complex according as

$$F(K_1) = \frac{(\sigma^{\frac{1}{2}}-\sigma^{-\frac{1}{2}})^2}{A_1} - \frac{4K_1^2}{(1+K_1^2)^3} \gtrless 0.$$

The equation $F(K_1) = 0$ has either two real positive roots (${}_1K_1$, ${}_2K_1$) or none at all. In the former case if K_1 lies outside the range (${}_1K_1$, ${}_2K_1$) it follows that $F(K_1) > 0$ and that N_1 is real and negative: there will consequently be aperiodic damping of the corresponding disturbance modes. If ${}_1K_1 < K_1 < {}_2K_1$ then N_1 is complex with negative real part: in this case there will be periodic decay of these disturbance modes. Finally, if $F(K_1) = 0$ has no real positive roots, N_1 will be real and negative for all values of K_1, and hence all disturbance modes will be damped aperiodically; this will be the case when $A_1 < \frac{4}{3}(\sigma^{\frac{1}{2}}-\sigma^{-\frac{1}{2}})^2$. These results differ from those of Hide in numerical detail only; such a difference is not significant as the present results are for a slightly different system and are to be regarded as of qualitative rather than quantitative value.

APPENDIX

A COMPARISON OF THE RATE OF GROWTH OF THE DISTURBANCES AND THE RATE OF DECAY OF THE TEMPERATURE PROFILE

If the form of the disturbance is represented by $w = C \begin{matrix}\cos\\ \sin\end{matrix}(m\pi z/h)\exp(nt)$ it follows that the time in which its amplitude ($|w|$) grows by an order of magnitude is approximately $t_d = 2{\cdot}3/n = 2{\cdot}3h^2/(\pi^2(\kappa\nu)^{\frac{1}{2}}N_1)$ seconds, where N_1 (> 0 here) is the dimensionless growth factor which has been plotted in the figures.

In order to find the change that will take place during this time in the non-linear profiles it is necessary to consider special profile forms. Two of these will be sufficient for the present purposes:

(i) The profile considered already, and caused in a layer which is initially at uniform temperature T_1 when the lower surface is suddenly heated to T_0 ($> T_1$) and maintained at that temperature. If the time is measured from this instant, the profile at any subsequent time is

$$\frac{T-T_1}{T_0-T_1} = (\tfrac{1}{2}-Z)-\frac{2}{\pi}\sum_{r=1}^{\infty}\frac{\sin r\pi(\tfrac{1}{2}+Z)}{r}\exp\Big(-\frac{\pi^2r^2\kappa t}{h^2}\Big).$$

(ii) The more realistic profile, which is caused in a layer initially at uniform temperature T_1, when, at $t = 0$, steady heating of the lower surface is suddenly started at the constant rate $k(T_0-T_1)/h$ units of heat per unit area per second. The ultimate temperature of the lower surface will be T_0, and the profile is

$$\frac{T-T_1}{T_0-T_1} = (\tfrac{1}{2}-Z)-\frac{8}{\pi^2}\sum_{r=1}^{\infty}\frac{(-1)^r}{(2r+1)^2}\sin\tfrac{1}{2}\pi(2r+1)(\tfrac{1}{2}-Z)\exp\Big(-\frac{\pi^2(2r+1)^2\kappa t}{4h^2}\Big).$$

In each of these cases the ultimate profile of temperature across the layer is

$$T'-T_1 = (T_0-T_1)(\tfrac{1}{2}-Z);$$

for case (i) a simple and approximate estimate of the non-linearity of the profile is given by the value of $(T'-T)/(T_0-T_1)$ at $Z = 0$. In case (ii), however, the temperature of the lower surface, ${}_tT_0$ say, increases gradually to its final value T_0; thus the corresponding measure of non-linearity must be taken as $(T'-T)/({}_tT_0-T_1)$ at $Z = 0$. The times (t_p) in which $(T'-T)/(T_0-T_1)$ and $(T'-T)/({}_tT_0-T_1)$ are reduced to one-half of their initial values are, rather approximately, $h^2/\pi^2\kappa$ and $4h^2/\pi^2\kappa$, respectively.

These times, t_p, serve as a rough time scale for the decay of the non-linear temperature profile, while t_d serves as a time scale for the initial growth of the disturbances. The ratio t_p/t_d then provides an estimate of the extent to which disturbances can grow before the temperature profile has changed significantly towards the linear profile corresponding with the steady state. Substituting the results obtained, $t_p/t_d = 0{\cdot}4\sigma^{\frac{1}{2}}N_1$ or $1{\cdot}6\sigma^{\frac{1}{2}}N_1$, respectively, so that a value can be given to this ratio for each dimensionless wave number (K_1) and Rayleigh number (A_1) from the results which are represented in Fig. 1. It can be seen that only the more unstable modes will grow markedly in the time available, and that for $A_1-\frac{27}{4}$ small, none of the unstable modes will have time to be affected greatly by the special features of the temperature distribution. Moreover, these estimates will allow for rather more growth than is likely to occur in practice, as the exponential amplification continues only while the disturbance is still small and subsequently a steady pattern of convection is realized—in this case Bénard cells. It may be noted that Thomas (**10**) has already pointed out in a discussion of Bénard cells that strongly non-linear temperature profiles cannot persist in layers of real fluid under normal experimental conditions.

REFERENCES

1. Lord Rayleigh, *Phil. Mag.* **32** (1916) 529.
2. H. Jeffreys, ibid. **2** (1926) 833.
3. —— *Proc. Roy. Soc.* A, **118** (1928) 195.
4. A. Pellew and R. V. Southwell, ibid. A, **176** (1940) 312.

5. S. Chandrasekhar, *Proc. Camb. Phil. Soc.* **51** (1955) 162.
6. R. Hide, ibid. 179 and *Quart. J. Mech. App. Math.* **9** (1955) 22, 35.
7. Lord Rayleigh, *Proc. Lond. Math. Soc.* **14** (1883) 170.
8. O. G. Sutton, *Proc. Roy. Soc.* A, **204** (1950) 297.
9. K. Chandra, ibid. **164** (1938) 231.
10. D. B. Thomas, Dissertation (unpublished), Cambridge University (1956).

THE MOVING AEROFOIL IN SHEAR FLOW IN THE NEIGHBOURHOOD OF A PLANE BOUNDARY

By D. E. EDMUNDS (130 *Stanwell Road, Ashford, Middlesex*)

[Received 25 October 1956]

SUMMARY

In a previous paper (**1**) we have discussed the problem of finding the forces acting on a two-dimensional aerofoil moving in inviscid, incompressible fluid bounded by a plane wall, the fluid being at rest at infinity. Here the theory is extended to the case where the undisturbed fluid motion is that of linear shear flow parallel to the wall. Expressions are obtained in series form for the forces and couple acting on a fairly general type of aerofoil, and the flate plate aerofoil is considered in more detail.

1. Introduction

Coombs (**2**) has dealt with the question of a stationary aerofoil in linear shear flow in the neighbourhood of a plane boundary. He uses the method of Green (**3**) which was developed for potential flow, and expresses the results in series form. James (**4**, **5**) has discussed both the problem of the stationary aerofoil and that of the moving aerofoil in shear flow, but in an unbounded region.

In this paper we consider an aerofoil moving near a plane boundary in fluid which is in linear shear flow parallel to the boundary. It is supposed that the fluid is inviscid and incompressible, and that the aerofoil is two-dimensional. This problem does not seem to have been discussed previously, and it is found that the extension of Green's method used in (**1**) may be employed. The expressions obtained for the forces on a general aerofoil are complicated, and so detailed consideration is given only to the simple case of a flat plate aerofoil.

2. Construction of the complex function Ω

Consider the two-dimensional motion due to a cylinder moving near an infinite plane boundary in fluid whose undisturbed motion is that of linear shear flow parallel to the boundary. This motion is considered in a plane defined by a normal cross-section of the cylinder.

Define two sets of moving rectangular cartesian axes, the (x, y)-axes fixed in the aerofoil and moving with it in all respects, and the (x', y')-axes whose origin is fixed inside the aerofoil section but which do not rotate with the aerofoil and so remain at all times parallel to a set of axes fixed in space. The axes fixed in space, the (x_0, y_0)-axes, are so chosen that their real axis and the boundary wall are parallel. Thus the plane boundary has

equation $y' = -b$ at any instant, and the force components parallel to the x'- and y'-axes may be written as X' and Y' respectively. Making the (x, y)- and (x', y')-axes have a common origin O inside the boundary curve C of the aerofoil, the relation $z' = ze^{i\theta}$ holds at all times. Here θ is the angle between the (x, y)- and (x', y')- axes at any time, and $z = x+iy$, $z' = x'+iy'$ in the usual complex variable notation. The various coordinate systems are shown in Fig. 1.

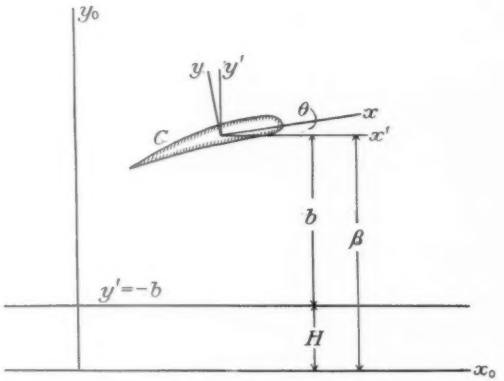

FIG. 1. The coordinate systems

Referred to the (x_0, y_0)-axes, the undisturbed shear flow considered is given by

$$U = -u_0(1+y_0 kl^{-1}), \qquad V = 0, \tag{2.1}$$

where U, V are respectively the x_0 and y_0 velocity components of the flow, u_0 and k are constants, and l is a typical length in the aerofoil (e.g. the chord).

With respect to a set of fixed axes which coincides with the instantaneous position of the (x', y')-axes, this flow has x' and y' components

$$-u_0(F+ky'l^{-1}), \quad 0 \tag{2.2}$$

respectively. Here $F = 1+\beta kl^{-1}$, (α, β) being the coordinates of O referred to the (x_0, y_0)-axes.

As usual, a stream function ψ may be defined in terms of the absolute velocity components of the fluid parallel to the x'- and y'-axes by

$$U = -\frac{\partial \psi}{\partial y'}, \qquad V = \frac{\partial \psi}{\partial x'}. \tag{2.3}$$

The Helmholtz equation for two-dimensional motion is

$$\frac{D\zeta}{D\tau} = 0,$$

$\boldsymbol{\zeta}$ being the vorticity vector, and τ the time. In terms of ψ this is

$$\left(\frac{\partial\psi}{\partial x'}\frac{\partial}{\partial y'}-\frac{\partial\psi}{\partial y'}\frac{\partial}{\partial x'}\right)\nabla^2\psi = 0. \tag{2.4}$$

Choosing the undisturbed stream function ψ_0 before the introduction of the cylinder to give $\psi_0 = 0$ on the plane boundary, we have

$$\psi_0 = u_0(y'+b)\{F+\tfrac{1}{2}k(y-b)l^{-1}\}$$

so that

$$\nabla^2\psi_0 = \frac{\partial^2\psi_0}{\partial x'^2}+\frac{\partial^2\psi_0}{\partial y'^2} = \frac{k}{l}u_0. \tag{2.5}$$

The obvious solution to (2.5) and (2.4) is that the vorticity remains constant and equal to $u_0 k/l$, i.e. ψ must satisfy

$$\nabla^2\psi = u_0 k/l. \tag{2.6}$$

The uniqueness of this solution follows from the assumption that the presence of the cylinder produces no change in the total vorticity of the fluid.

Following James (**4**) we introduce a stream function ψ' defined by

$$\psi = \psi_0+\psi', \tag{2.7}$$

where

$$\nabla^2\psi' = 0. \tag{2.8}$$

Hence ψ' defines an irrotational disturbance motion, and a complex potential function $\Omega'(z')$ may be defined which has ψ' as its imaginary part.

Define also a complex function Ω of which the complete stream function ψ is the imaginary part. The real part of Ω is not a velocity potential since the flow is not a potential flow.

If the aerofoil has a translatory motion defined by velocity components u', v' along the x'-, y'-axes respectively, and has an angular velocity ω about O, then Ω' satisfies the conditions:

(i) Ω' is a function of z' but not of $\bar{z}'$ (a bar placed above a quantity will be used to denote the complex conjugate of that quantity throughout this paper).

(ii) On the aerofoil boundary

$$\mathrm{im}\left\{\Omega'+u_0 Fz'-\tfrac{1}{4}i\frac{k}{l}u_0(z'^2-z'\bar{z}')+\bar{w}'z'-\tfrac{1}{2}i\omega z'\bar{z}'\right\} = \text{constant},$$

where $w' = u'+iv'$.

(iii) $\mathrm{im}(\Omega') = \text{constant}$ on $y' = -b$.

(iv) Ω' reduces to zero at infinity, where the effect of the aerofoil is imperceptible.

The function

$$\Omega' = iu_0 A_0\{\log z' - \log(z'+2ib)\}+u_0\sum_{n=1}^{\infty}\left\{\frac{A_n}{(z')^n}+\frac{\bar{A}_n}{(z'+2ib)^n}\right\} \quad (2.9)$$

satisfies conditions (i), (iii), (iv), and includes a circulation $K = 2\pi A_0 u_0$ around the aerofoil.

We define the aerofoil considered here by the transformation

$$z = t^{-1}\sum_{n=0}^{\infty} a_n t^n, \quad (2.10)$$

which maps the boundary of the unit circle $|t| = 1$ in the t-plane on to the boundary of the aerofoil in the z-plane. The region outside the aerofoil C transforms conformally to the region inside the unit circle γ in the t-plane.

As the method of solution is now similar to that of Green (**3**), only the essentials will be given.

In terms of t, (2.9) becomes

$$\Omega' = -iu_0 A_0 \log t+u_0\sum_{n=1}^{\infty}(C_n t^n+D_n t^{-n}), \quad (2.11)$$

where the C_n and D_n are defined in the Appendix (section 1). Hence the boundary condition (ii) leads to the relations

$$\left.\begin{aligned}
&u_0 C_n+(\bar{w}'+u_0 F)e^{i\theta}a_{n+1}\\
&\quad = u_0\bar{D}_n+i\omega b_n+\tfrac{1}{4}iku_0({}^2\gamma_n-2b_n)l^{-1} \quad (n>2)\\
&u_0 C_2+(\bar{w}'+u_0 F)e^{i\theta}a_3\\
&\quad = u_0\bar{D}_2+i\omega b_2+\tfrac{1}{4}iku_0({}^2\gamma_2+{}^2\bar{\gamma}_{-2}-2b_2)l^{-1}\\
&u_0 C_1+(\bar{w}'+u_0 F)e^{i\theta}a_2\\
&\quad = u_0\bar{D}_1+i\omega b_1+(w'+u_0 F)e^{-i\theta}\bar{a}_0+\tfrac{1}{4}iku_0({}^2\gamma_1+{}^2\bar{\gamma}_{-1}-2b_1)l^{-1}
\end{aligned}\right\} \quad (2.12)$$

where ${}^r\gamma_s$ and b_s are given in the Appendix (section 1).

The wall $y' = -b$ will have equation $y_0 = H$ referred to the (x_0, y_0)-axes fixed in space, H being a constant satisfying $\beta = b+H$, so that

$$F = 1+\beta kl^{-1} = G+bkl^{-1}, \qquad G = 1+Hkl^{-1}. \quad (2.13)$$

Thus the boundary conditions (2.12) suggest expressing A_n in the form

$$A_n = \sum_{s=-1}^{\infty} {}^nA_s b^{-s} \quad (n \geqslant 0), \quad (2.14)$$

and the C_n and D_n can then be written as power series in b (Appendix, section 1). Substituting these expansions in (2.12) and equating coefficients of corresponding powers of b gives a set of equations defining the coefficients ${}^nA_s\,(n \geqslant 1)$ in terms of the circulation coefficients ${}^0A_s$ (Appendix, section 2). This determines Ω', and hence Ω, except for the arbitrary circulation.

3. The forces and couple on the general aerofoil

The force components Y', X' and the couple Γ about the origin O are given in terms of the pressure p by the integrals

$$Y'+iX' = \int_C p\, d\bar{z}', \qquad \Gamma = \mathrm{re} \int_C pz'\, d\bar{z}', \tag{3.1}$$

taken round the boundary curve C of the aerofoil. The ordinary pressure equation cannot be used since Ω is not a potential function, but p is determined by using James's method (**5**), which is given in some detail.

He returns to the equation of motion of the fluid, i.e. to

$$\frac{D\mathbf{q}}{D\tau} = -\frac{1}{\rho}\nabla p, \tag{3.2}$$

ρ being the fluid density, and $\mathbf{q}$ the vector velocity of the fluid, referred to axes fixed in space and coincident with the instantaneous position of the (x', y')-axes. Writing (3.2) in component form and using (2.3), gives

$$\left.\begin{aligned} \frac{\partial U}{\partial \tau} &= \frac{\partial \lambda}{\partial x'}, \qquad \frac{\partial V}{\partial \tau} = \frac{\partial \lambda}{\partial y'} \\ \text{where} \qquad \lambda &= \psi\nabla^2\psi - \tfrac{1}{2}(U^2+V^2) - \frac{p}{\rho} \end{aligned}\right\}. \tag{3.3}$$

Equation (3.3) is equivalent to

$$\frac{\partial}{\partial \bar{z}'}\left(\lambda - i\frac{\partial \psi}{\partial \tau}\right) = 0, \qquad \frac{\partial}{\partial z'}\left(\lambda + i\frac{\partial \psi}{\partial \tau}\right) = 0 \tag{3.4}$$

which has obvious solutions

$$\lambda = i\frac{\partial \psi}{\partial \tau} + f_1(z'), \qquad \lambda = -i\frac{\partial \psi}{\partial \tau} + f_2(\bar{z}'), \tag{3.5}$$

$f_1(z')$, $f_2(\bar{z}')$ being two arbitrary functions of z' and $\bar{z}'$ respectively. Hence

$$2i\frac{\partial \psi}{\partial \tau} = f_2(\bar{z}') - f_1(z'). \tag{3.6}$$

Now $\psi = \psi_0 + \psi'$, where $\partial\psi_0/\partial\tau = 0$, and ψ_0 is the only term in ψ which contains products of z' and $\bar{z}'$, and which therefore cannot be split into two functions of z' and $\bar{z}'$ as in (3.6). Thus a solution of (3.6) is possible, and

$$2i\frac{\partial \psi'}{\partial \tau} = \frac{\partial}{\partial \tau}(\Omega' - \overline{\Omega}') = f_2(\bar{z}') - f_1(z').$$

Since Ω' is a potential function,

$$f_1(z') = -\frac{\partial \Omega'}{\partial \tau}, \qquad f_2(\bar{z}') = -\frac{\partial \overline{\Omega}'}{\partial \tau},$$

which gives

$$\lambda = -\frac{1}{2}\left(\frac{\partial \Omega'}{\partial \tau} + \frac{\partial \overline{\Omega}'}{\partial \tau}\right).$$

The pressure equation is then

$$\frac{p}{\rho} = \psi\nabla^2\psi - \tfrac{1}{2}(U^2+V^2) + \frac{1}{2}\left(\frac{\partial\Omega'}{\partial\tau} + \frac{\partial\overline{\Omega}'}{\partial\tau}\right) \tag{3.7}$$

with $\nabla^2\psi = u_0 k/l$. It is easily seen that

$$U^2+V^2 = -\left(\frac{\partial\Omega}{\partial z} - \frac{\partial\overline{\Omega}}{\partial z}\right)\left(\frac{\partial\Omega}{\partial\bar{z}} - \frac{\partial\overline{\Omega}}{\partial\bar{z}}\right),$$

so that by proceeding exactly as in (**1**), (3.7) can be written in terms of t as

$$\left.\begin{aligned}\frac{p}{\rho} = {} & \frac{k}{l}u_0\psi + \frac{1}{2}\left(\frac{\partial\Omega}{\partial t} - \frac{\partial\overline{\Omega}}{\partial t}\right)\left(\frac{\partial\Omega}{\partial\bar{t}} - \frac{\partial\overline{\Omega}}{\partial\bar{t}}\right)\left(\frac{dz}{dt}\frac{d\bar{z}}{d\bar{t}}\right)^{-1} - \\ & - \tfrac{1}{2}(w'e^{-i\theta} + i\omega z)\frac{\partial\Omega'}{\partial t}\left(\frac{dz}{dt}\right)^{-1} - \tfrac{1}{2}(\bar{w}'e^{i\theta} - i\omega\bar{z})\frac{\partial\overline{\Omega}'}{\partial\bar{t}}\left(\frac{d\bar{z}}{d\bar{t}}\right)^{-1} + \\ & + \frac{1}{2}\left(\omega\frac{\partial}{\partial\theta} + v'\frac{\partial}{\partial b} + \dot{w}'\frac{\partial}{\partial w'} + \dot{\bar{w}}'\frac{\partial}{\partial\bar{w}'} + \dot{\omega}\frac{\partial}{\partial\omega}\right)(\Omega'+\overline{\Omega}')\end{aligned}\right\} \tag{3.8}$$

dots denoting differentiation with respect to τ.

Using (2.11), (3.1), and the relation

$$\Omega = \Omega' + u_0 Fz' - \tfrac{1}{4}iku_0(z'^2 - z'\bar{z}')l^{-1} \tag{3.9}$$

which follows by definition of the complete complex function Ω, the forces and couple may be calculated. The various integrals are evaluated as indicated in (**1**), and it is found that

$$\left.\begin{aligned}\frac{Y'+iX'}{\rho\pi ie^{-i\theta}} = {} & \frac{iku_0}{2l}\Big[2\sum_{n=1}^{\infty} n\bar{a}_{n+1}(\bar{w}'e^{i\theta}a_{n+1} - i\omega b_n) - 2\bar{a}_0(\bar{w}'e^{i\theta}a_0 - i\omega\bar{b}_1) - \\ & - \frac{iku_0}{2l}\Big(\sum_{n=0}^{\infty}(n-1)\bar{a}_n{}^2\gamma_{n-1} + 2\Big(\bar{a}_0\bar{b}_1 - \sum_{n=1}^{\infty} nb_n\bar{a}_{n+1}\Big)\Big) + \\ & + e^{2i\theta}\Big(iA_0a_1 - \overline{D}'_1a_0 + \sum_{n=1}^{\infty} n\overline{C}'_n a_{n+1}\Big)u_0 - \\ & - \Big(iA_0\bar{a}_1 + \overline{C}'_1\bar{a}_0 - \sum_{n=1}^{\infty} n\overline{D}'_n\bar{a}_{n+1}\Big)u_0 + \\ & + \Big\{iA_0h'_1 - \sum_{n=1}^{\infty} n(C'_nh'_{n+1} - D'_nh_{n-1})\Big\}u_0 + \\ & + e^{-2i\theta}u_0\Big(-iA_0f'_3 + \sum_{n=1}^{\infty} nC'_nf'_{n+3} - \\ & - \sum_{n=3}^{\infty} nD'_nf_{n-3} - 2D'_2f'_1 - D'_1f'_2\Big)\Big] -\end{aligned}\right\} \tag{3.10}$$

$$
\begin{aligned}
&-iA_0u_0^2\sum_{n=1}^{\infty}nc_{n-1}(\bar{C}'_n+D'_n)+\\
&+u_0^2\sum_{n=1}^{\infty}c_{n-1}\Big\{\sum_{r=1}^{\infty}r(n+r)(C'_r\bar{C}'_{n+r}+\bar{D}'_rD'_{n+r})\Big\}-\\
&-u_0^2\sum_{n=2}^{\infty}c_{n-1}\Big\{\sum_{r=1}^{n-1}r(n-r)\bar{C}'_rD'_{n-r}\Big\}-i\bar{w}'e^{i\theta}A_0u_0+\\
&+w'e^{-i\theta}u_0\Big\{-iA_0d'_2-D_1d'_1+\sum_{n=1}^{\infty}nd'_{n+2}C_n-\\
&\qquad-\sum_{n=2}^{\infty}nd_{n-2}D_n\Big\}+\\
&+i\omega u_0\Big\{iA_0(\tilde{a}_1-h'_1)+\\
&\qquad+\sum_{n=1}^{\infty}n(C_nh'_{n+1}-D_nh_{n-1}-\bar{D}_n\tilde{a}_{n+1})+\bar{C}_1\tilde{a}_0\Big\}+\\
&+u_0\Big(\omega\frac{\partial}{\partial\theta}+\dot{w}'\frac{\partial}{\partial w'}+\dot{\bar{w}}'\frac{\partial}{\partial\bar{w}'}+\dot{\omega}\frac{\partial}{\partial\omega}+v'\frac{\partial}{\partial b}\Big)\times\\
&\qquad\times\Big\{2iA_0\Big(\tilde{a}_0+\sum_{n=2}^{\infty}\tilde{a}_n\Big)-\\
&\qquad\qquad-\tilde{a}_0(\bar{C}_1+D_1)+\sum_{n=1}^{\infty}n\tilde{a}_{n+1}(C_n+\bar{D}_n)\Big\}
\end{aligned}
$$

and

$$
\begin{aligned}
\frac{\Gamma}{\pi\rho}=\frac{u_0k}{2l}\mathrm{re}\Big[&2w'e^{-i\theta}\tilde{a}_0\bar{b}_1-2\bar{w}'e^{i\theta}\sum_{n=1}^{\infty}n\bar{b}_na_{n+1}-\\
&-\frac{iu_0k}{2l}\Big(\sum_{n=1}^{\infty}n\bar{b}_n{}^2\gamma_n+2\bar{b}_2{}^2\bar{\gamma}_{-2}+{}^2\bar{\gamma}_{-1}\bar{b}_1\Big)+\\
&+iA_0u_0(b_0+m'_2e^{-2i\theta}-{}^2\gamma_0-l_0)+u_0\sum_{n=1}^{\infty}n\bar{C}'_n(b_n-{}^2\gamma_n)+\\
&+u_0\sum_{n=1}^{\infty}nC'_n(l'_n-m'_{n+2}e^{-2i\theta})-u_0\sum_{n=1}^{\infty}n(\bar{D}'_n\bar{b}_n+D'_nl_n)+\\
&+u_0\sum_{n=2}^{\infty}nD'_nm_{n-2}e^{-2i\theta}+u_0(2\bar{D}'_2{}^2\gamma_{-2}+\bar{D}'_1{}^2\gamma_{-1}+D'_1m'_1e^{-2i\theta})\Big]+\\
&+\mathrm{im}\Big[u_0^2\sum_{n=2}^{\infty}g_n\Big\{\sum_{r=1}^{n-1}r(n-r)\bar{C}'_rD'_{n-r}\Big\}-\\
&-u_0^2\sum_{n=1}^{\infty}g_n\Big\{-iA_0n(\bar{C}'_n+D'_n)+\sum_{r=1}^{\infty}r(n+r)(C'_r\bar{C}'_{n+r}+\bar{D}'_rD'_{n+r})\Big\}-\\
&-u_0w'e^{-i\theta}\Big\{-iA_0h'_1+\sum_{n=1}^{\infty}n(C_nh'_{n+1}-D_nh_{n-1})\Big\}+
\end{aligned}
\tag{3.11}
$$

$$
\left.\begin{aligned}
&+u_0\bar{w}'e^{i\theta}\Big(iA_0a_1-\bar{D}_1a_0+\sum_{n=1}^{\infty}na_{n+1}\bar{C}_n\Big)-\\
&-i\omega u_0\Big\{iA_0(b_0-l_0)+\sum_{n=1}^{\infty}n(C_nl'_n-D_nl_n+\bar{C}_nb_n-\bar{D}_n\bar{b}_n)\Big\}-\\
&-u_0\Big(\omega\frac{\partial}{\partial\theta}+\dot{w}'\frac{\partial}{\partial w'}+\dot{\bar{w}}'\frac{\partial}{\partial\bar{w}'}+\dot{\omega}\frac{\partial}{\partial\omega}+v'\frac{\partial}{\partial b}\Big)\times\\
&\qquad\times\Big\{2iA_0\sum_{n=1}^{\infty}\bar{b}_n+\sum_{n=1}^{\infty}(\bar{C}_n+D_n)\Big(\sum_{r=0}^{\infty}(r-1)a_{n+r}\bar{a}_r\Big)+\\
&\qquad\qquad+\sum_{n=1}^{\infty}(C_n+\bar{D}_n)\Big(\sum_{r=0}^{\infty}(n+r-1)\bar{a}_{n+r}a_r\Big)\Big\}\Big]
\end{aligned}\right\}
$$

where

$$C'_n=C_n+Fe^{i\theta}a_{n+1},\qquad D'_1=D_1+Fe^{i\theta}a_0,\qquad D'_n=D_n\quad(n>1)$$

and the coefficients c_n, g_n, d_n, d'_n, h_n, h'_n, l_n, l'_n, f_n, f'_n, m_n, m'_n are defined in the Appendix, section 3.

The form of these expressions suggests writing

$$Y'+iX'=\sum_{s=-2}^{\infty}(Y'_s+iX'_s)b^{-s},\qquad\Gamma=\sum_{s=-2}^{\infty}\Gamma_sb^{-s},\tag{3.12}$$

and these expansions can be obtained for any particular aerofoil.

To complete the solution a definite value for the circulation must be obtained. For an aerofoil with a sharp trailing edge T, this can be done by assuming the Joukowski condition to hold, so that the fluid leaves T smoothly with finite velocity. The velocity at T due to the term ψ_0 in ψ is clearly finite, and the transformation (2.10) can always be chosen so that T corresponds to $t=-1$. Hence the condition requires that $\partial\Omega'/\partial t=0$ at $t=-1$. Proceeding as in (**1**), the circulation coefficients are found to be

$$
\left.\begin{aligned}
&{}^0A_{-1}=ik(\bar{a}_0e^{-i\theta}-a_0e^{i\theta})l^{-1}\\
&{}^0A_0u_0=\tfrac{1}{2}iu_0{}^0A_{-1}(a_0e^{i\theta}-\bar{a}_0e^{-i\theta})+\\
&\quad+i\{(w'+u_0G)e^{-i\theta}\bar{a}_0-(\bar{w}'+u_0G)e^{i\theta}a_0\}+\omega\sum_{n=1}^{\infty}(-1)^nnb_n+\\
&\quad+\tfrac{1}{2}u_0k\Big\{a_0(a_0-a_1)e^{2i\theta}+\bar{a}_0(\bar{a}_0-\bar{a}_1)e^{-2i\theta}-\sum_{n=1}^{\infty}(-1)^nnb_n\Big\}l^{-1},\\
&{}^0A_su_0=i\sum_{n=1}^{s+1}\sum_{m=n}^{s+1}(-1)^{n+1}n\,{}^0A_{s-m}({}^m\bar{\gamma}_{-n}\,{}^m\bar{\alpha}_0-{}^m\gamma_{-n}\,{}^m\alpha_0)+\\
&\quad+i\sum_{n=1}^{s}\sum_{r=n-1}^{s-1}\sum_{m=n}^{r+1}(-1)^{n+1}n({}^m\bar{\gamma}_{-n}\,{}^m\bar{\alpha}_{s-r}\,{}^{s-r}A_{r-m}-{}^m\gamma_{-n}\,{}^m\alpha_{s-r}\,{}^{s-r}\bar{A}_{r-m})\\
&\qquad\qquad(s\geqslant1).
\end{aligned}\right\}\tag{3.13}
$$

4. Discussion of the solution

The work of this paper differs from that of (**1**) in the appearance of terms involving b^{+1} and b^{+2} in the expressions (3.12) for the forces and

couple. This is because at infinite distances from the aerofoil ψ reduces to ψ_0, which contains terms of this sort. On putting $u_0 = 0$ these terms in b^{+1} and b^{+2} vanish, and the problem reduces to that treated in (1).

By replacing H by $(\beta - b)$ wherever it occurs, it may be verified that (3.12) can be expressed in a form which contains terms in β^2 and β in place of those in b^{+2}, b^{+1}, H, and H^2, i.e. as

$$Y' + iX' = \sum_{s=0}^{\infty} (Y''_s + iX''_s) b^{-s}, \qquad \Gamma = \sum_{s=0}^{\infty} \Gamma''_s b^{-s}. \tag{4.1}$$

The assumption is of course made that these rearrangements of terms are valid.

The expansions (4.1) are often more convenient than the alternative expressions (3.12), and will be used here. In particular, they give a clearer picture of what really happens in the limiting case of the aerofoil in unbounded shear flow. Using (3.12) the limit is deduced by allowing b and H to become infinite in such a manner that $(b + H)$ remains finite and equal to β. (4.1) provides the limit merely by letting b become infinite, when the forces and couple are Y''_0, X''_0, and Γ''_0 respectively.

5. The flat plate aerofoil

The plate is defined by the transformations

$$z = \tfrac{1}{4} l(t^{-1} + t), \qquad z' = ze^{i\theta}, \tag{5.1}$$

where l is the length of the plate, and θ the angle between the plate and the wall at any time. Expanding the forces and couple in the form (4.1) gives, after some reduction:

$$\left.\begin{aligned}
Y''_0/\pi\rho &= l(u' + u_0 F)\{(u' + u_0 F)\sin\theta - v'\cos\theta\} - \\
&\quad - \tfrac{1}{8} klu_0(2v' - l\omega\cos\theta)\sin 2\theta - \tfrac{1}{4} l^2(\dot{u}'\sin\theta - \dot{v}'\cos\theta + \tfrac{1}{2} l\dot{\omega})\cos\theta \\
Y''_1/\pi\rho &= -\tfrac{1}{4} l^2\{(u' + u_0 F)\sin\theta - v'\cos\theta\} \times \\
&\qquad \times \{2(u' + u_0 F)\sin\theta - v'\cos\theta + \tfrac{1}{4}\omega l(1 + \sin^2\theta)\} + \\
&\quad + \tfrac{1}{8} u_0 kl^2\{(u' + u_0 F)\sin\theta - \tfrac{1}{4}\omega l\cos^2\theta\}\sin^2\theta + \\
&\quad + (\tfrac{1}{4} l)^3\{2(\dot{u}'\sin\theta - \dot{v}'\cos\theta) + \tfrac{1}{2}\dot{\omega} l\}\sin 2\theta \\
Y''_2/\pi\rho &= \tfrac{1}{16} l^3\{(u' + u_0 F)\sin\theta - v'\cos\theta\} \times \\
&\qquad \times \{(u' + u_0 F)(1 + 3\sin^2\theta) - 2v'\sin 2\theta\} - \\
&\quad - \tfrac{1}{64}\omega l^4\{(u' + u_0 F)(1 - 9\sin^2\theta + 4\sin^4\theta) + \\
&\quad + \tfrac{1}{2} v'(9 - 4\sin^2\theta)\sin 2\theta\} + 4\omega^2(\tfrac{1}{4} l)^5(4 - 3\sin^2\theta)\sin\theta + \\
&\quad + 4(u_0^2 k^2/l^2)(\tfrac{1}{4} l)^5\sin^5\theta - (u_0 k/l)(\tfrac{1}{4} l)^4\sin\theta\{16(u' + u_0 F)\sin^3\theta + \\
&\qquad + 8v'(1 - 3\sin^2\theta)\cos\theta - \omega l(2 - 9\sin^2\theta + 5\sin^4\theta)\} - \\
&\quad - 2(\tfrac{1}{4} l)^4\{(\dot{u}'\sin\theta - \dot{v}'\cos\theta)(3 - 2\sin^2\theta) + \tfrac{1}{2}\dot{\omega} l\cos^2\theta\}\cos\theta
\end{aligned}\right\} \tag{5.2}$$

$$
\begin{aligned}
X_0''/\pi\rho &= -lv'\{(u'+u_0F)\sin\theta - v'\cos\theta\} + \\
&\quad + \tfrac{1}{4}u_0kl(2v'-\omega l\cos\theta)\sin^2\theta + \tfrac{1}{8}l^2\{2(\dot u'\sin\theta - \dot v'\cos\theta) + l\dot\omega\}\sin\theta \\
X_1''/\pi\rho &= \tfrac{1}{4}l^2\{(u'+u_0F)\sin\theta - v'\cos\theta - \tfrac{1}{2}u_0k\sin^2\theta\}\times \\
&\qquad \times(v' - \tfrac{1}{4}\omega l\cos\theta)\sin\theta - \\
&\qquad - \tfrac{1}{16}l^3(\dot u'\sin\theta - \dot v'\cos\theta + \tfrac{1}{4}l\dot\omega)\sin^2\theta \\
X_2''/\pi\rho &= -\tfrac{1}{16}l^3v'\{(u'+u_0F)\sin\theta - v'\cos\theta\}\cos^2\theta - \\
&\quad - 6\omega^2(\tfrac{1}{4}l)^5\sin\theta\sin 2\theta + 4\omega(\tfrac{1}{4}l)^4\{(u'+u_0F)(1-4\sin^2\theta)\cos\theta + \\
&\qquad + v'(5-4\sin^2\theta)\sin\theta\}\sin\theta + \\
&\quad + \tfrac{1}{2}(u_0k/l)(\tfrac{1}{4}l)^4\{8v'\cos\theta - \omega l(2-5\sin^2\theta)\}\sin\theta\sin 2\theta + \\
&\quad + 2\dot\omega(\tfrac{1}{4}l)^5\cos\theta\sin 2\theta + \\
&\quad + 2(\tfrac{1}{4}l)^4(\dot u'\sin\theta - \dot v'\cos\theta)(3-2\sin^2\theta)\sin\theta
\end{aligned}
\tag{5.3}
$$

and

$$
\begin{aligned}
\Gamma_0''/\pi\rho &= \tfrac{1}{4}l^2\{(u'+u_0F)\cos\theta + v'\sin\theta\}\times \\
&\qquad \times\{(u'+u_0F)\sin\theta - v'\cos\theta - \tfrac{1}{4}\omega l\} + \\
&\quad + \tfrac{1}{16}u_0kl^2\sin\theta\{(u'+u_0F)\sin 2\theta - v'(3-2\sin^2\theta) + \\
&\qquad + \omega l\cos\theta - \tfrac{1}{8}u_0k\sin\theta\sin 2\theta\} - \\
&\quad - \tfrac{1}{16}l^3(\dot u'\sin\theta - \dot v'\cos\theta) - 6\dot\omega(\tfrac{1}{4}l)^4 \\
\Gamma_1''/\pi\rho &= -\tfrac{1}{16}l^3\{(u'+u_0F)\sin\theta - v'\cos\theta\}\times \\
&\qquad \times\{(u'+u_0F)\sin 2\theta - v'\cos 2\theta\} + \\
&\quad + \tfrac{1}{64}u_0kl^3\sin^2\theta(2v' - \tfrac{5}{4}\omega l\cos\theta + \tfrac{1}{4}u_0k\sin\theta\sin 2\theta) + \\
&\quad + 4\omega^2(\tfrac{1}{4}l)^5\cos\theta + 4(\tfrac{1}{4}l)^4\{(\dot u'\sin\theta - \dot v'\cos\theta) + \tfrac{1}{4}\dot\omega l\}\sin\theta \\
\Gamma_2''/\pi\rho &= 2(\tfrac{1}{4}l)^4\{(u'+u_0F)\sin\theta - v'\cos\theta\}\times \\
&\quad \times\{(u'+u_0F)(1+10\sin^2\theta)\cos\theta - v'(9-10\sin^2\theta)\sin\theta\} - \\
&\quad - \omega(\tfrac{1}{4}l)^5\{(u'+u_0F)(5-34\sin^2\theta)\cos\theta + \\
&\qquad + v'(37-34\sin^2\theta)\sin\theta\} + \\
&\quad + (u_0k/l)(\tfrac{1}{4}l)^5\sin\theta\{3(u'+u_0F)(1-4\sin^2\theta)\sin 2\theta - \\
&\quad - v'(11-32\sin^2\theta+24\sin^4\theta) + \omega l(2-5\sin^2\theta)\cos\theta - \\
&\qquad - \tfrac{1}{8}u_0k\sin\theta\sin 4\theta\} + \\
&\quad + 6\omega^2(\tfrac{1}{4}l)^6\sin 2\theta - \\
&\quad - (\tfrac{1}{4}l)^5\{(\dot u'\sin\theta - \dot v'\cos\theta)(5-2\sin^2\theta) + \tfrac{1}{4}\dot\omega l(3-2\sin^2\theta)\}
\end{aligned}
\tag{5.4}
$$

with $F = 1+\beta kl^{-1}$. The restrictions $l/b < 1$, $k < 1$ are made so that the expansions will be more likely to be convergent. Further terms of these expansions can be found if desired, but the reduction tends to become involved and tedious.

On putting $u_0 = 0$ these results reduce to those obtained in (**1**) for the plate moving in fluid at rest at infinity. Agreement with the force expressions given by Coombs is reached on writing $u' = 0$, $v' = 0$, $\omega = 0$, $F = 1$ in (5.2) and (5.3). He does not give the couple, but (5.4) shows that this is given by

$$\left.\begin{aligned}\frac{8\Gamma}{\pi\rho l^2 u_0^2 \sin 2\theta} = {} & (1+\tfrac{1}{2}k\sin\theta-\tfrac{1}{16}k^2\sin^2\theta)-\tfrac{1}{2}(l/b)(1-\tfrac{1}{16}k^2\sin^2\theta)\sin\theta+\\ & +\tfrac{1}{32}(l/b)^2\{(1+10\sin^2\theta)+\tfrac{3}{4}k(1-4\sin^2\theta)\sin\theta-\\ & -\tfrac{1}{16}k^2\sin^2\theta\cos 2\theta\}+O(b^{-3})\end{aligned}\right\}. \quad (5.5)$$

For small θ,

$$\Gamma/\Gamma_0'' = 1-\tfrac{1}{2}(l/b)(1-\tfrac{1}{2}k\sin\theta+\tfrac{1}{4}k^2\sin^2\theta)\sin\theta+$$
$$+\tfrac{1}{32}(l/b)^2\{(1+10\sin^2\theta)+\tfrac{1}{4}k(1-32\sin^2\theta)\sin\theta-\tfrac{1}{8}k^2(1-38\sin^2\theta)\sin^2\theta\}+\ldots$$

neglecting powers of $(k\sin\theta)$ higher than the second. Hence Γ/Γ_0'' increases with k, for positive θ. Thus for $\theta = 10°$,

$$\left.\begin{aligned}\Gamma/\Gamma_0'' &= 1-0{\cdot}1158(l/b)+0{\cdot}0519(l/b)^2+\ldots,\\ \Gamma/\Gamma_0'' &= 1-0{\cdot}0868(l/b)+0{\cdot}0407(l/b)^2+\ldots,\\ \Gamma/\Gamma_0'' &= 1-0{\cdot}0695(l/b)+0{\cdot}0340(l/b)^2+\ldots,\end{aligned}\right\}$$

for $k = -0{\cdot}5$, 0, and 0·5, respectively.

In this case the shear flow is associated with the aerofoil in that the condition $\beta = 0$ is imposed. Removing this restriction the results take the more general form

$$\left.\begin{aligned}Y'/Y_0'' &= 1-\tfrac{1}{2}(l/b)\{1-(k/4F)\sin\theta\}\sin\theta+\\ &\quad +\tfrac{1}{16}(l/b)^2\{(1+3\sin^2\theta)-(k/F)\sin^3\theta+(k^2/16F^2)\sin^4\theta\}+\ldots\\ Y_0'' &= \pi\rho l u_0^2 F^2\sin\theta\\ X' &= 0\\ \frac{8\Gamma}{\pi\rho l^2 u_0^2\sin 2\theta} &= (F^2+\tfrac{1}{2}Fk\sin\theta-\tfrac{1}{16}k^2\sin^2\theta)-\\ &\quad -\tfrac{1}{2}(l/b)(F^2-\tfrac{1}{16}k^2\sin^2\theta)\sin\theta+\tfrac{1}{32}(l/b)^2\{F^2(1+10\sin^2\theta)+\\ &\quad +\tfrac{3}{4}Fk(1-4\sin^2\theta)\sin\theta-\tfrac{1}{16}k^2\sin^2\theta\cos 2\theta\}+\ldots\end{aligned}\right\}. \quad (5.6)$$

By giving β different values, it is now possible to determine the variation in Y' and Γ as the plate is placed at different points in the field of flow.

Returning to the general expressions (5.2)–(5.4) and writing $v' = 0$, $\omega = 0$, $u' = -u_0 F$, gives

$$\left.\begin{aligned}Y' &= \tfrac{1}{256}\pi\rho u_0^2 k^2 l(l/b)^2\sin^5\theta+O(b^{-3})\\ X' &= 0\\ \Gamma/\pi\rho &= -\tfrac{1}{128}u_0^2 k^2 l^2\sin^2\theta\sin 2\theta\{1-\tfrac{1}{2}(l/b)\sin\theta+\tfrac{1}{32}(l/b)^2\cos 2\theta+\ldots\}\end{aligned}\right\}. \quad (5.7)$$

Here the plate is in motion parallel to the wall with velocity exactly equa to the undisturbed ctream velocity at the centre of the plate. In an unbounded fluid the forces acting would reduce to zero, but the presence of the wall means that the small force Y' acts on the plate in a direction perpendicular to the wall. The shear nature of the undisturbed flow ensures that a couple acts even in the limiting case when b is infinite, and we notice that for small positive θ, the magnitude of the couple first decreases and then tends to increase as l/b increases.

Finally, consider the case when the plate executes translational oscillations in the direction of the y'-axis. This is obtained on setting

$$u' = 0, \qquad \omega = 0, \qquad v' = v_0 \sin n\tau,$$

v_0 and n being constant. It follows that

$$b = h\Big(1 - \frac{v_0}{nh}\cos n\tau\Big), \qquad \beta = \beta_0\Big(1 - \frac{v_0}{n\beta_0}\cos n\tau\Big)$$

where the constants h and β_0 are the mean values of b and β respectively, and $\beta_0 = h + H$. Writing $F_0 = 1 + k\beta_0 l^{-1}$ the forces and couple become

$$\frac{Y'}{\pi\rho l} = u_0^2 \sin\theta\Big[\Big(F_0^2 + \frac{k^2 v_0^2}{2n^2 l^2}\Big) - \frac{1}{2}\Big(F_0^2 - \tfrac{1}{4}kF_0 \sin\theta + \frac{k^2 v_0^2}{2l^2 n^2}\Big)\Big(\frac{l}{h}\Big)\sin\theta +$$

$$+ \frac{1}{16}\Big(\frac{l}{h}\Big)^2\Big\{F_0^2(1 + 3\sin^2\theta) + \frac{kv_0^2}{2l^2 n^2}(k + 16F_0\sin\theta + k\sin^2\theta) +$$

$$+ \tfrac{1}{16}(k\sin\theta - 16F_0)k\sin^3\theta\Big\}\Big] -$$

$$- \tfrac{1}{8}v_0^2\Big(\frac{l}{h}\Big)\Big(1 - \frac{3l}{4h}\sin\theta\Big)\cos^2\theta -$$

$$- u_0 v_0 \cos\theta \sin n\tau\Big[(F_0 + \tfrac{1}{2}k\sin\theta) - \frac{3}{4}\Big(\frac{l}{h}\Big)F_0\sin\theta +$$

$$+ \frac{1}{16}\Big(\frac{l}{h}\Big)^2\Big\{F_0(1 + 7\sin^2\theta) + \tfrac{1}{2}k(1 - 3\sin^2\theta)\sin\theta + \frac{3kv_0^2}{n^2 l^2}\sin\theta\Big\}\Big] +$$

$$+ \tfrac{1}{4}lnv_0 \cos n\tau\Big[\Big(\cos^2\theta - \frac{8ku_0^2}{l^2 n^2}F_0\sin\theta\Big) -$$

$$- \frac{1}{4}\Big(\frac{l}{h}\Big)\Big\{\cos^2\theta - \frac{2u_0^2 k}{l^2 n^2}(8F_0 - k\sin\theta)\sin\theta\Big\}\sin\theta - \frac{v_0^2}{4n^2 h^2}\cos^2\theta +$$

$$+ \frac{1}{32}\Big(\frac{l}{h}\Big)^2(3 - 2\sin^2\theta)\cos^2\theta -$$

$$- \frac{u_0^2 \sin\theta}{2n^2 h^2}\Big\{4F_0^2\sin\theta + kF_0(1 + 2\sin^2\theta) - \tfrac{1}{2}k^2\sin^3\theta + \frac{3k^2 v_0^2}{l^2 n^2}\sin\theta\Big\}\Big] +$$

$$+\frac{u_0 v_0^2}{8nl}\cos\theta\sin 2n\tau\left[4k-3\left(\frac{l}{h}\right)k\sin\theta+\left(\frac{l}{h}\right)^2\{3F_0\sin\theta+\tfrac{1}{4}k(1+7\sin^2\theta)\}\right]+$$

$$+\tfrac{1}{8}v_0^2\cos 2n\tau\left[\frac{4k^2u_0^2}{l^2n^2}\sin\theta+\left(\cos^2\theta-\frac{2u_0^2k^2}{l^2n^2}\sin^2\theta\right)\left(\frac{l}{h}\right)-\right.$$

$$\left.-\frac{1}{4}\left(\frac{l}{h}\right)^2\sin\theta\left\{5\cos^2\theta-\frac{16u_0^2}{l^2n^2}kF_0\sin\theta-\frac{k^2u_0^2}{l^2n^2}(1+\sin^2\theta)\right\}\right]+$$

$$+\frac{v_0^3}{32n^2h^2}\left\{2ln\left(\cos^2\theta-\frac{2k^2u_0^2}{l^2n^2}\sin^2\theta\right)\cos 3n\tau-3u_0k\sin 2\theta\sin 3n\tau\right\}+O(h^{-3})$$

$$\frac{X'}{\pi\rho l}=\tfrac{1}{2}v_0^2\cos\theta\left\{1-\frac{1}{4}\left(\frac{l}{h}\right)\sin\theta+\frac{1}{16}\left(\frac{l}{h}\right)^2\right\}-$$

$$-u_0v_0\sin\theta\sin n\tau\left[(F_0-\tfrac{1}{2}k\sin\theta)\left\{1-\frac{1}{4}\left(\frac{l}{h}\right)\sin\theta+\right.\right.$$

$$\left.\left.+\frac{1}{16}\left(\frac{l}{h}\right)^2\cos^2\theta\right\}+\frac{kv_0^2}{16n^2h^2}\sin\theta\right]-$$

$$-\frac{l}{8}nv_0\sin 2\theta\cos n\tau\left\{1-\frac{1}{4}\left(\frac{l}{h}\right)\sin\theta+\frac{1}{32}\left(\frac{l}{h}\right)^2(3-2\sin^2\theta)+\frac{v_0^2}{4n^2h^2}\right\}+$$

$$+\frac{u_0v_0^2}{2nl}\sin\theta\sin 2n\tau\left[k-\frac{1}{4}\left(\frac{l}{h}\right)k\sin\theta+\right.$$

$$\left.+\frac{1}{16}\left(\frac{l}{h}\right)^2\{4F_0\sin\theta+k(1-3\sin^2\theta)\}\right]-$$

$$-\tfrac{1}{2}v_0^2\cos\theta\cos 2n\tau\left\{1-\frac{1}{4}\left(\frac{l}{h}\right)\sin\theta+\frac{1}{16}\left(\frac{l}{h}\right)^2\cos 2\theta\right\}+$$

$$+\frac{v_0^3}{16n^2h^2}\sin\theta(ln\cos\theta\cos 3n\tau-ku_0\sin\theta\sin 3n\tau)+O(h^{-3})$$

and

$$\frac{\Gamma}{\pi\rho l^2}=\tfrac{1}{8}u_0^2\sin 2\theta\left[\left\{F_0^2+\tfrac{1}{2}k(F_0-\tfrac{1}{8}k\sin\theta)\sin\theta+\frac{k^2v_0^2}{2n^2l^2}\right\}-\right.$$

$$-\frac{1}{2}\left(\frac{l}{h}\right)\left(F_0^2-\tfrac{1}{16}k^2\sin^2\theta+\frac{k^2v_0^2}{2l^2n^2}\right)\sin\theta+$$

$$+\frac{1}{32}\left(\frac{l}{h}\right)^2\left\{(1+10\sin^2\theta)\left(F_0^2+\frac{k^2v_0^2}{2l^2n^2}\right)+\right.$$

$$\left.\left.+\tfrac{3}{4}kF_0(1-4\sin^2\theta)\sin\theta+\frac{16k}{l^2n^2}F_0v_0^2\sin\theta-\tfrac{1}{16}k^2\sin^2\theta\cos 2\theta\right\}\right]-$$

$$-\tfrac{1}{8}v_0^2\cos\theta\left(\sin\theta+\frac{1}{4}\left(\frac{l}{h}\right)\cos 2\theta-\frac{1}{32}\left(\frac{l}{h}\right)^2(7-10\sin^2\theta)\sin\theta\right)-$$

$$-\tfrac{1}{4}u_0v_0\sin n\tau\left[\{F_0\cos 2\theta+\tfrac{1}{4}k(3-2\sin^2\theta)\sin\theta\}-\right.$$

$$-\tfrac{1}{4}(F_0\sin 3\theta+\tfrac{1}{2}k\sin^2\theta)\left(\frac{l}{h}\right)+\frac{1}{32}\left(\frac{l}{h}\right)^2\{F_0(1+18\sin^2\theta-20\sin^4\theta)+$$

$$\left.+\tfrac{1}{8}k(11-32\sin^2\theta+24\sin^4\theta)\sin\theta\}+\frac{kv_0^2}{16n^2h^2}\sin 3\theta\right]+$$

$$+\frac{l}{16}nv_0\cos\theta\cos n\tau\left[\left(1-\frac{2ku_0^2}{l^2n^2}(4F_0+k\sin\theta)\sin\theta\right)-\right.$$

$$-\frac{1}{4}\left(1-\frac{16u_0^2}{l^2n^2}kF_0\sin\theta\right)\left(\frac{l}{h}\right)\sin\theta+\frac{1}{64}\left(\frac{l}{h}\right)^2(5-2\sin^2\theta)-\frac{v_0^2}{4n^2h^2}\cos 2\theta-$$

$$-\frac{u_0^2}{n^2h^2}\sin\theta\left(2\left(F_0^2+\frac{3k^2v_0^2}{4l^2n^2}\right)\sin\theta+\tfrac{1}{4}kF_0(1+10\sin^2\theta)+\right.$$

$$\left.\left.+\tfrac{1}{32}k^2(3-16\sin^2\theta)\sin\theta\right)\right]+$$

$$+\frac{u_0v_0^2}{8ln}\sin 2n\tau\left[k\cos 2\theta-\tfrac{1}{4}k\left(\frac{l}{h}\right)\sin 3\theta+\right.$$

$$\left.+\frac{1}{4}\left(\frac{l}{h}\right)^2\{F_0\sin 3\theta+\tfrac{1}{8}k(1+22\sin^2\theta-20\sin^4\theta)\}\right]+$$

$$+\tfrac{1}{8}v_0^2\cos\theta\cos 2n\tau\left[\left(1+\frac{k^2u_0^2}{l^2n^2}\right)\sin\theta+\frac{1}{4}\left(\frac{l}{h}\right)\left(\cos 2\theta-\frac{2k^2u_0^2}{l^2n^2}\sin^2\theta\right)-\right.$$

$$-\frac{1}{32}\left(\frac{l}{h}\right)^2(11-10\sin^2\theta)\sin\theta+\frac{ku_0^2}{32n^2h^2}\{32F_0\sin\theta+k(1+10\sin^2\theta)\}\sin\theta\Big]+$$

$$+\frac{v_0^3}{64n^2h^2}\left\{ln\left(\cos\theta\cos 2\theta-\frac{k^2u_0^2}{l^2n^2}\sin\theta\sin 2\theta\right)\cos 3n\tau-\right.$$

$$\left.-ku_0\sin 3\theta\sin 3n\tau\right\}+O(h^{-3}).$$

It is seen that, as in the corresponding case in (1), terms occur in these expressions which have frequencies of twice and three times the frequency of the motion of the plate; also from X' a thrust can be obtained on the plate. The mean values of the forces and couple over an interval of time

$2\pi/n$ follow at once, and denoting these mean values by the left-hand subscript m, we have

$$\left.\begin{aligned}\frac{{}_mY'}{\pi\rho l} = u_0^2\sin\theta\Big[\Big(F_0^2+\frac{k^2v_0^2}{2n^2l^2}\Big)-\frac{1}{2}\Big(F_0^2-\tfrac{1}{4}kF_0\sin\theta+\frac{k^2v_0^2}{2l^2n^2}\Big)\Big(\frac{l}{h}\Big)\sin\theta+\\ +\frac{1}{16}\Big(\frac{l}{h}\Big)^2\Big\{F_0^2(1+3\sin^2\theta)+\frac{kv_0^2}{2l^2n^2}(k+16F_0\sin\theta+k\sin^2\theta)+\\ +\tfrac{1}{16}(k\sin\theta-16F_0)k\sin^3\theta\Big\}\Big]-\\ -\tfrac{1}{8}v_0^2\Big(\frac{l}{h}\Big)\Big(1-\frac{3l}{4h}\sin\theta\Big)\cos^2\theta+O(h^{-3})\end{aligned}\right\} \quad (5.8)$$

$$\frac{{}_mX'}{\pi\rho l} = \tfrac{1}{2}v_0^2\cos\theta\Big\{1-\frac{1}{4}\Big(\frac{l}{h}\Big)\sin\theta+\frac{1}{16}\Big(\frac{l}{h}\Big)^2+\ldots\Big\} \quad (5.9)$$

$$\left.\begin{aligned}\frac{{}_m\Gamma}{\pi\rho l^2} = \tfrac{1}{8}u_0^2\sin 2\theta\Big[\Big\{F_0^2+\tfrac{1}{2}k(F_0-\tfrac{1}{8}k\sin\theta)\sin\theta+\frac{k^2v_0^2}{2n^2l^2}\Big\}-\\ -\frac{1}{2}\Big(\frac{l}{h}\Big)\Big(F_0^2-\tfrac{1}{16}k^2\sin^2\theta+\frac{k^2v_0^2}{2l^2n^2}\Big)\sin\theta+\\ +\frac{1}{32}\Big(\frac{l}{h}\Big)^2\Big\{(1+10\sin^2\theta)\Big(F_0^2+\frac{k^2v_0^2}{2l^2n^2}\Big)+\tfrac{3}{4}kF_0(1-4\sin^2\theta)\sin\theta+\\ +\frac{16k^2}{l^2n^2}F_0v_0^2\sin\theta-\tfrac{1}{16}k^2\sin^2\theta\cos 2\theta\Big\}\Big]-\\ -\tfrac{1}{8}v_0^2\cos\theta\Big\{\sin\theta+\frac{1}{4}\Big(\frac{l}{h}\Big)\cos 2\theta-\frac{1}{32}\Big(\frac{l}{h}\Big)^2(7-10\sin^2\theta)\sin\theta\Big\}+\\ +O(h^{-3})\end{aligned}\right\} \quad (5.10)$$

The mean forces and couple can now be determined for any specified plate motion of this sort.

Acknowledgement

In conclusion, I wish to thank Dr. R. M. Morris for her kind advice throughout the work, which was done while I was in receipt of a grant from the Department of Scientific and Industrial Research.

APPENDIX

1. The coefficients C_n and D_n are defined by

$$C_n = i^0\beta_n A_0+\sum_{r=1}^{n}{}^r\beta_n A_r+\sum_{r=1}^{\infty}{}^r\gamma_n B_r, \qquad D_n=\sum_{r=n}^{\infty}{}^r\gamma_{-n}B_r,$$

where
$$B_n = {}^n\alpha_0 A_0 b^{-n}+\sum_{r=1}^{\infty}{}^n\alpha_r\bar{A}_r b^{-(n+r)}$$

and
$${}^n\alpha_0=\frac{i^{n+1}}{n\,.\,2^n}, \qquad {}^n\alpha_r=\binom{n+r-1}{n}\frac{i^{n-r}}{2^{n+r}} \quad (n,r\geqslant 1).$$

The remaining coefficients ${}^0\beta_n, {}^r\beta_n, {}^r\gamma_n$ are expressible in terms of the a_s by the relations

$$(z')^{-r} = \sum_{n=r}^{\infty} {}^r\beta_n t^n, \qquad \log z' = -\log t + \sum_{n=0}^{\infty} {}^0\beta_n t^n, \qquad (z')^r = \sum_{n=-r}^{\infty} {}^r\gamma_n t^n$$

which follow from (2.10) on omitting terms independent of t. Finally,

$$b_r = \sum_{n=r}^{\infty} \bar{a}_{n-r} a_n.$$

Using the expansion (2.14), and assuming interchangeability of summations, the C_n and D_n become

(5.8)
$$C_n = \sum_{s=-1}^{\infty} \Big\{ i\,{}^0\beta_n\,{}^0A_s + \sum_{r=1}^{n} {}^r\beta_n\,{}^rA_s \Big\} b^{-s} + \sum_{s=0}^{\infty} \sum_{m=1}^{s+1} {}^m\gamma_n\,{}^m\alpha_0\,{}^0A_{s-m}\, b^{-s} + \\ + \sum_{s=1}^{\infty} \sum_{r=0}^{s-1} \sum_{m=1}^{r+1} {}^m\gamma_n\,{}^m\alpha_{s-r}\,{}^{s-r}\bar{A}_{r-m}\, b^{-s},$$

(5.9)
$$D_n = \sum_{s=n-1}^{\infty} \sum_{m=n}^{s+1} {}^m\gamma_{-n}\,{}^m\alpha_0\,{}^0A_{s-m}\, b^{-s} + \sum_{s=n}^{\infty} \sum_{r=n-1}^{s-1} \sum_{m=n}^{r+1} {}^m\gamma_{-n}\,{}^m\alpha_{s-r}\,{}^{s-r}\bar{A}_{r-m}\, b^{-s}.$$

2. The set of equations defining the ${}^nA_s$ $(n \geqslant 1)$ in terms of the ${}^0A_s$ is:

$$i\,{}^0\beta_1\,{}^0A_{-1} + {}^1\beta_1\,{}^1A_{-1} + e^{i\theta}a_2\, kl^{-1} = e^{-i\theta}\bar{a}_0\, kl^{-1},$$

$$i\,{}^0\beta_n\,{}^0A_{-1} + \sum_{r=1}^{n} {}^r\beta_n\,{}^rA_{-1} + e^{i\theta}a_{n+1}\, kl^{-1} = 0 \quad (n > 1),$$

(5.10)
$$u_0(i\,{}^0\beta_1\,{}^0A_0 + {}^1\beta_1\,{}^1A_0 + {}^1\gamma_1\,{}^1\alpha_0\,{}^0A_{-1}) + (\bar{w}' + u_0 G)e^{i\theta}a_2 \\ = u_0\,{}^1\bar{\gamma}_{-1}\,{}^1\bar{\alpha}_0\,{}^0A_{-1} + i\omega b_1 + (w' + u_0 G)e^{-i\theta}\bar{a}_0 + \tfrac{1}{4}iu_0({}^2\gamma_1 + {}^2\bar{\gamma}_{-1} - 2b_1)kl^{-1},$$

$$u_0\Big(i\,{}^0\beta_2\,{}^0A_0 + \sum_{r=1}^{2} {}^r\beta_2\,{}^rA_0 + {}^1\gamma_2\,{}^1\alpha_0\,{}^0A_{-1}\Big) + (\bar{w}' + u_0 G)e^{i\theta}a_3 \\ = i\omega b_2 + \tfrac{1}{4}iu_0({}^2\gamma_2 + {}^2\bar{\gamma}_{-2} - 2b_2)kl^{-1},$$

$$u_0\Big(i\,{}^0\beta_n\,{}^0A_0 + \sum_{r=1}^{n} {}^r\beta_n\,{}^rA_0 + {}^1\gamma_n\,{}^1\alpha_0\,{}^0A_{-1}\Big) + (\bar{w}' + u_0 G)e^{i\theta}a_{n+1} \\ = i\omega b_n + \tfrac{1}{4}iu_0({}^2\gamma_n - 2b_n)kl^{-1} \quad (n > 2)$$

$$i\,{}^0\beta_n\,{}^0A_s + \sum_{r=1}^{n} {}^r\beta_n\,{}^rA_s + \sum_{m=1}^{s+1} {}^m\gamma_n\,{}^m\alpha_0\,{}^0A_{s-m} + \sum_{r=0}^{s-1} \sum_{m=1}^{r+1} {}^m\gamma_n\,{}^m\alpha_{s-r}\,{}^{s-r}\bar{A}_{r-m} \\ = \begin{cases} \sum_{m=n}^{s+1} {}^m\bar{\gamma}_{-n}\,{}^m\bar{\alpha}_0\,{}^0A_{s-m} + \sum_{r=n-1}^{s-1} \sum_{m=n}^{r+1} {}^m\bar{\gamma}_{-n}\,{}^m\bar{\alpha}_{s-r}\,{}^{s-r}A_{r-m} & (s \geqslant 1,\ s \geqslant n) \\ {}^{s+1}\bar{\gamma}_{-s-1}\,{}^{s+1}\bar{\alpha}_0\,{}^0A_{-1} & (s \geqslant 1,\ n = s+1) \\ 0 & (n > s+1 \geqslant 2) \end{cases}$$

3. The coefficients c_n, g_n, d_n, d'_n, h_n, h'_n, l_n, l'_n were used in (**1**), and are given by

$$\Big(\frac{dz}{dt}\Big)^{-1} = -t^2 \sum_{n=0}^{\infty} c_n t^n, \qquad g_n = \sum_{r=0}^{n} a_r c_{n-r},$$

$$d_n = \sum_{r=0}^{\infty} (r-1)c_{n+r}\bar{a}_r, \qquad d'_n = \sum_{r=0}^{\infty} (n+r-1)\bar{a}_{n+r}c_r,$$

$$h_n = \sum_{r=0}^{\infty} (r-1)g_{n+r}\bar{a}_r, \qquad h'_n = \sum_{r=0}^{\infty} (n+r-1)g_r\bar{a}_{n+r},$$

$$l_n = \sum_{r=0}^{n} h_{n-r}a_r + \sum_{r=1}^{\infty} h'_r a_{n+r}, \qquad l'_n = \sum_{r=0}^{\infty} h'_{n+r}a_r.$$

Lastly, the following expansions hold on γ:

$$\bar{z}\left(\frac{dz}{dt}\right)^{-1}\frac{d\bar{z}}{dt} = -t^5\Big(\sum_{n=0}^{\infty} f_n t^n + \sum_{n=1}^{\infty} f'_n t^{-n}\Big),$$

where $$f_n = \sum_{r=0}^{\infty} \bar{a}_r d_{n+r}, \qquad f'_n = \sum_{r=0}^{\infty} \bar{a}_{n+r} d_r + \sum_{r=1}^{n} \bar{a}_{n-r} d'_r;$$

and

$$z\bar{z}\left(\frac{dz}{dt}\right)^{-1}\frac{d\bar{z}}{dt} = -t^4\Big(\sum_{n=0}^{\infty} m_n t^n + \sum_{n=1}^{\infty} m'_n t^{-n}\Big),$$

where $$m_n = \sum_{r=0}^{\infty} \bar{a}_r h_{n+r}, \qquad m'_n = \sum_{r=0}^{\infty} \bar{a}_{n+r} h_r + \sum_{r=1}^{n} \bar{a}_{n-r} h'_r.$$

These define f_n, f'_n, m_n, m'_n.

REFERENCES

1. D. E. Edmunds, *Quart. J. Mech. App. Math.* **9** (1956) 400.
2. A. Coombs, *Proc. Cambridge Phil. Soc.* **45** (1949) 612.
3. A. E. Green, *Quart. J. Math.* (Oxford), **18** (1947) 167.
4. D. G. James, *Quart. J. Mech. App. Math.* **4** (1951) 407.
5. —— Ph. D. Thesis, University of Wales (1950).

CYLINDRICAL STRESS WAVES IN FLAT SLABS†

By NORMAN DAVIDS‡ *and* SUDHIR KUMAR§ (*University Park, Pa.*)

[Received 28 August 1956]

SUMMARY

After developing Goodman's solution for radially symmetric modes of stress wave propagation in infinite slabs, this paper gives first a detailed analysis of the determination of the various modes. Then, curves of both the non-dimensional phase and group velocities are given for Poisson's ratio from zero to half. The form of excitation at the centre is discussed as well as the limiting cases for thin slabs and surface waves. The theoretical curves are compared with some recent experimental data from Bell Telephone Laboratories and fairly good agreement was found. Some experimental work at Frankford Arsenal is also discussed from the point of view of the present theory.

Nomenclature

r, θ, z = cylindrical coordinates.
u_r, u_θ, u_z = displacements along r, θ, and z-axes.
$\omega_r, \omega_\theta, \omega_z$ = rotations about r, θ, and z-axes.
Δ = dilation.
λ, μ = Lamé's constants.
σ = stresses.
a = thickness of the slab.
ρ = density.
$\zeta = z/a$, the non-dimensional axial distance.
$c, \bar{c}, \bar{c}_2, c_1, c_s$ = velocities.
$v, \bar{v}, v_1, v_g$ = non-dimensional velocities.
p = frequency $\times 2\pi$.
Λ = wavelength.
γ = wave number.
ν = Poisson's ratio.
α = a function of Poisson's ratio.
A, B = arbitrary constants.
t = time.
J_n = Bessel functions of order n.
$f(r,z,t)$, $g(r,z,t)$ = functions.

† This work has been sponsored by the Office of Ordnance Research, U.S. Army.
‡ Professor of Engineering Mechanics, Pennsylvania State University.
§ Research Assistant, Department of Engineering Mechanics, Pennsylvania State University.

h = a parameter $= \sqrt{\left(\frac{\rho p^2}{\lambda+2\mu} - \gamma^2\right)}$.

k = a parameter $= \sqrt{\left(\frac{\rho p^2}{\mu} - \gamma^2\right)}$.

$s = \gamma a$.

$\tau = pa$.

$u = x/s = ha/\gamma a$.

$v = y/s = ka/\gamma a$.

1. Introduction

THIS paper presents an elastic analysis of stress-wave propagation in an infinite slab of arbitrary thickness for the radially-symmetric modes under suitable line-source excitations. It then presents appropriate numerical data and discusses the results in terms of some recent experimental data. The treatment of cylindrical stress waves was first applied to rods by Pochhammer (**1**). Among later workers on this problem have been Love (**2**), Bancroft (**3**), and Davies (**4**, **5**). The corresponding problem of stress waves in a plate shows more recent activity, notably by Goodman (**6**), Kane and Mindlin (**7**), and Feder (**8**). Correlation between theory and experiment is difficult because of the complexity introduced into the problem by the numerous boundaries of actual specimens and uncertainties regarding the exact form of the excitation. Also experiments on scabbing which necessitate the use of explosives to initiate stress waves, involve important non-linearities in the modes of propagation. This, however, does not invalidate the need for extending the 'exact' linear analysis, nor does it even reduce its importance, since it is necessary to ascertain the limits of its applicability.

Goodman, in (**6**), has worked out the boundary-value problem for infinite plates and obtained the 'frequency equation', that is, the transcendental relation between frequency of vibration and wavelength. Kane and Mindlin's paper gives an approximate solution for the high-frequency extensional vibrations of plates by use of energy methods. The still more general case of arbitrary line-source excitation can be dealt with by Fourier integral synthesis techniques based on the results of this paper, which should be of aid in experimental investigation of pulse propagation caused by explosives, such as were made by Feder and her group.

2. The boundary-value problem

Fig. 1 shows an infinite slab of thickness $2a$ excited along a line coinciding with the axis of z together with the appropriate cylindrical coordinate system. Details regarding the excitation will be discussed later. In this

section, however, we shall restrict ourselves to a radially-symmetric sinusoidal excitation.

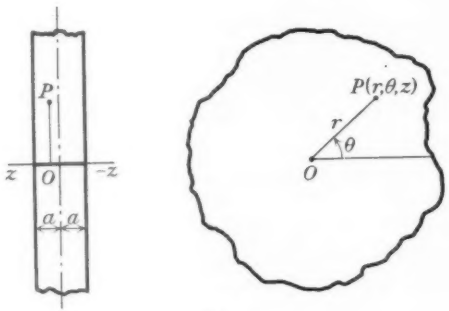

FIG. 1

The displacements u_r, u_θ, u_z satisfy the Pochhammer equations in the form given by Love (**2**), as follows:

$$\rho\frac{\partial^2 u_r}{\partial t^2} = (\lambda+2\mu)\frac{\partial\Delta}{\partial r} - \frac{2\mu}{r}\frac{\partial\omega_z}{\partial\theta} + 2\mu\frac{\partial\omega_\theta}{\partial z}, \tag{1}$$

$$\rho\frac{\partial^2 u_\theta}{\partial t^2} = (\lambda+2\mu)\frac{1}{r}\frac{\partial\Delta}{\partial\theta} - 2\mu\frac{\partial\omega_r}{\partial z} + 2\mu\frac{\partial\omega_z}{\partial r}, \tag{2}$$

$$\rho\frac{\partial^2 u_z}{\partial t^2} = (\lambda+2\mu)\frac{\partial\Delta}{\partial z} - \frac{2\mu}{r}\frac{\partial}{\partial r}(r\omega_\theta) + \frac{2\mu}{r}\frac{\partial\omega_r}{\partial\theta}, \tag{3}$$

in which λ and μ are Lamé's constants for the material, ρ is the density, and Δ is the dilation, given by

$$\Delta = \frac{1}{r}\frac{\partial(ru_r)}{\partial r} + \frac{1}{r}\frac{\partial u_\theta}{\partial\theta} + \frac{\partial u_z}{\partial z}, \tag{4}$$

and the components of rotation ω_r, ω_θ, ω_z by

$$\omega_r = \frac{1}{2}\left(\frac{1}{r}\frac{\partial u_z}{\partial\theta} - \frac{\partial u_\theta}{\partial z}\right), \tag{5}$$

$$\omega_\theta = \frac{1}{2}\left(\frac{\partial u_r}{\partial z} - \frac{\partial u_z}{\partial r}\right), \tag{6}$$

$$\omega_z = \frac{1}{2r}\left(\frac{\partial(ru_\theta)}{\partial r} - \frac{\partial u_r}{\partial\theta}\right). \tag{7}$$

At this point the statement of the problem is mathematically similar to that for the cylindrical rod—indeed, both are constructed from the same basic solution. For an angular frequency p and wavelength Λ, the only product-type solutions to Pochhammer's equations are of the form

$$u_r = A_r e^{i\alpha_1 z} J_1(\alpha_2 r), \qquad u_z = A_z e^{i\alpha_1 z} J_0(\alpha_2 r), \tag{8}$$

with $$\alpha_1^2+\alpha_2^2=\frac{\rho p^2}{\lambda+2\mu}, \tag{9a}$$

or $$\alpha_1^2+\alpha_2^2=\frac{\rho p^2}{\mu}. \tag{9b}$$

For the rod problem we obtain the required two linearly-independent solutions by putting

$$\alpha_1=\gamma=2\pi/\Lambda,$$

$$\alpha_2=h,\ k \quad \text{according as (9 a) or (9 b) holds.}$$

For the present problem of the slab, on the other hand, where the boundaries go with the coordinate z instead of r, we obtain an appropriate pair of linearly-independent solutions by interchanging the roles of α_1 and α_2, i.e. putting $\alpha_2=\gamma=2\pi/\Lambda$, and in one solution

$$\alpha_1=h=\sqrt{\left(\frac{\rho p^2}{\lambda+2\mu}-\gamma^2\right)}, \tag{10a}$$

while in the other $$\alpha_1=k=\sqrt{\left(\frac{\rho p^2}{\mu}-\gamma^2\right)}. \tag{10b}$$

With α_1 and α_2 understood as above, and keeping in mind that (8) is a solution, the general solution may be written as

$$u_r=(A\cos hz+B\cos kz)J_1(\gamma r)e^{ipt}, \tag{11}$$

$$u_z=\left(\frac{Ah}{\gamma}\sin hz-\frac{B\gamma}{k}\sin kz\right)J_0(\gamma r)e^{ipt}, \tag{12}$$

which can be verified by direct substitution in (1), (2), and (3).

The boundary conditions that the front and back surfaces $z=a$ and $z=-a$ be free of stress are

$$\sigma_{zz}=\lambda\Delta+2\mu\frac{\partial u_z}{\partial z}=\lambda\frac{\partial u_r}{\partial r}+\lambda\frac{u_r}{r}+(\lambda+2\mu)\frac{\partial u_z}{\partial z}=0, \tag{12a}$$

$$\sigma_{z\theta}=\mu\left(\frac{\partial u_\theta}{\partial z}+\frac{1}{r}\frac{\partial u_z}{\partial\theta}\right)=0, \tag{12b}$$

$$\sigma_{zr}=\mu\left(\frac{\partial u_r}{\partial z}+\frac{\partial u_z}{\partial r}\right)=0. \tag{12c}$$

When these are worked out and the common radial factors cancelled, we obtain, for $r\neq 0$,

$$A\cos ha\left(\lambda\gamma+(\lambda+2\mu)\frac{h^2}{\gamma}\right)-B\cos ka\,2\mu\gamma=0, \tag{13}$$

$$A\sin ha(-2h)+B\sin ka\left(-k+\frac{\gamma^2}{k}\right)=0. \tag{14}$$

For these equations to be satisfied by non-identically-zero values for A and B requires that the determinant formed by the coefficients of A and B be zero:

$$\cos ha \sin ka\left(\lambda\gamma+(\lambda+2\mu)\frac{h^2}{\gamma}\right)\left(-k+\frac{\gamma^2}{k}\right)+\sin ha \cos ka(-2h)(2\mu\gamma)=0. \quad (15)$$

This relationship between p and γ, or alternatively between the propagation velocity and wavelength, is referred to as the *frequency equation*. Another form of the above equation was first obtained by Goodman (**6**).

3. Thin slabs

As the thickness a of the slab tends to zero we can determine directly the limiting wave velocity of propagation. Given that the frequency p is constant, two distinct states may occur: (i) either the velocity $c = p/\gamma$ becomes infinite, corresponding to $\gamma \to 0$, or (ii) the velocity is finite for all γ. The first corresponds to the second and higher modes and the latter corresponds to the lowest, i.e. the first mode of propagation. This mode can only be propagated in the limit $a \to 0$ provided γ does not tend to infinity, so that h and k also remain finite. We then have

$$\cos ha \sim 1, \qquad \cos ka \sim 1,$$
$$\sin ha \sim ha, \qquad \sin ka \sim ka,$$

and the frequency equation (15) becomes

$$ka\left(\lambda\gamma+(\lambda+2\mu)\frac{h^2}{\gamma}\right)\left(-k+\frac{\gamma^2}{k}\right)-4ah^2\mu\gamma=0. \quad (16)$$

Since $\gamma \neq 0$ we may divide by it, then solve the resulting equation for the ratio p/γ, which gives, for the limiting velocity,

$$\frac{p}{\gamma}=\bar{c}=2\sqrt{\left(\frac{\mu}{\rho}\right)}\sqrt{\left(\frac{\lambda+\mu}{\lambda+2\mu}\right)}. \quad (17)$$

For steel we have $\bar{c} = 1{\cdot}68c_2$, where $c_2 = \sqrt{(\mu/\rho)}$ is the velocity of distortional waves. This value for $\bar{c}$ can also be obtained by considering the propagation in a thin slab to be a plane stress problem. In plane strain the velocity of plane dilatational waves is $\sqrt{(\lambda+2\mu/\rho)}$, and so to obtain the corresponding velocity in a plane stress problem, replacing λ by $2\lambda\mu/(\lambda+2\mu)$ (see Love (**2**), p. 208) we can get (17).

4. Determination of the lowest mode

By suitable transformation the frequency equation (15) can be put into a form which contains three variables only, thus facilitating the numerical computation procedure:

$$\left[\lambda+(\lambda+2\mu)\frac{h^2}{\gamma^2}\right]\left[-1+\frac{\gamma^2}{k^2}\right]-4\frac{h}{k}\mu\frac{\tan ha}{\tan ka}=0.$$

This may be written further as

$$\left(\frac{c^2}{c_2^2}-2\right)^2+4\frac{h}{\gamma}\frac{k}{\gamma}\tan ha\tan ka=0, \tag{18}$$

where c = wave velocity p/γ,

c_2 = distortional wave velocity $\sqrt{(\mu/\rho)}$.

We also have $$\frac{h}{\gamma}=\sqrt{\left(\frac{c^2}{c_1^2}-1\right)},\qquad \frac{k}{\gamma}=\sqrt{\left(\frac{c^2}{c_2^2}-1\right)}, \tag{19}$$

where c_1 is the dilatational wave velocity given by

$$c_1^2=\frac{\lambda+2\mu}{\rho}=\frac{2\mu(1-\nu)}{(1-2\nu)\rho}=\frac{c_2^2}{\alpha^2} \tag{20}$$

and $$\alpha^2=\frac{1-2\nu}{2(1-\nu)}.$$

Substituting this in (19), we have

$$\frac{h}{\gamma}=\sqrt{\left(\frac{c^2}{c_2^2}\alpha^2-1\right)}. \tag{21}$$

Now, substituting for h and k in (18) from (21) and (19), and putting

$$c/c_2=V, \tag{22}$$

we have

$$(V^2-2)^2+4\sqrt{(V^2\alpha^2-1)}\sqrt{(V^2-1)}\frac{\tan a\gamma\sqrt{(V^2\alpha^2-1)}}{\tan a\gamma\sqrt{(V^2-1)}}=0. \tag{23}$$

When $$1<V^2<1/\alpha^2,$$

equation (23) may be written as

$$(V^2-2)^2-4\sqrt{(1-V^2\alpha^2)}\sqrt{(V^2-1)}\frac{\tanh a\gamma\sqrt{(1-V^2\alpha^2)}}{\tan a\gamma\sqrt{(V^2-1)}}=0. \tag{24}$$

This equation is to be used for the calculation of the first mode. Now, from (17),

$$\bar{c}=2\sqrt{\left(\frac{\mu}{\rho}\right)}\sqrt{\left(\frac{\lambda+\mu}{\lambda+2\mu}\right)}=c_2\sqrt{\left(\frac{2}{1-\nu}\right)},$$

so that $$V^2=\bar{V}^2\{2/(1-\nu)\}, \tag{25}$$

where $$\bar{V}=c/\bar{c}. \tag{26}$$

By giving various values to Poisson's ratio ν and solving for $a\gamma$ from (24) by giving various values to V, we locate the points on the curve of the first mode as given in Table 1 and shown in Fig. 2. In Table 1 the values have been computed so that the maximum error in the third decimal place does not exceed ± 3 units. For Poisson's ratio $\nu=0$ the point where $\bar{V}$ becomes unity is $a\gamma=1{\cdot}5708$. Since the curve for $\nu=0$ is to be understood only

in the limiting sense $\nu \to 0$, we have chosen that branch which remains identically equal to unity for all $a\gamma$ less than the above value.

TABLE 1

Values of $\overline{V}$ as a function of $a\gamma$ and Poisson's ratio, for the lowest mode

	$\overline{V}$					
$a\gamma$ \ ν	0·0	0·1	0·2	0·3	0·4	0·5
0·0	1·000	1·000	1·000	1·000	1·000	1·000
0·5	1·000	1·000	0·997	0·993	0·981	0·960
1·0	1·000	0·997	0·984	0·955	0·911	0·854
1·5	1·000	0·966	0·912	0·855	0·793	0·723
2·0	0·832	0·810	0·777	0·734	0·683	0·626
2·5	0·732	0·714	0·688	0·654	0·614	0·566
3·0	0·682	0·665	0·639	0·610	0·573	0·530
	0·707	0·671	0·632	0·592	0·548	0·500

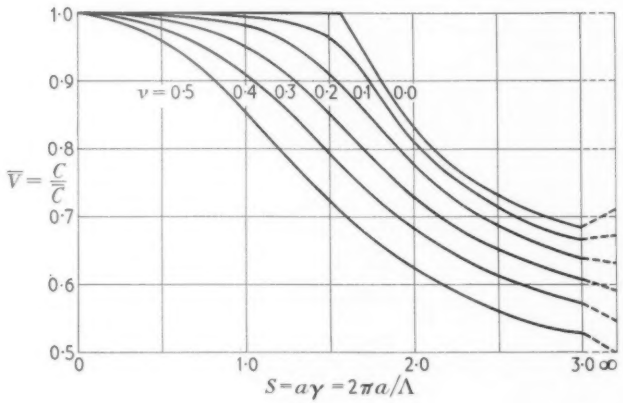

FIG. 2

The short-wave limit, that is $a\gamma \to \infty$, can only be obtained from (23) or (24) if V^2 becomes less than unity. For then the tangent functions in both the numerator and denominator of (23) become hyperbolic and we have

$$\tan a\gamma\sqrt{(V^2\alpha^2-1)} = i\tanh a\gamma\sqrt{(1-V^2\alpha^2)} \to i,$$

$$\tan a\gamma\sqrt{(V^2-1)} = i\tanh a\gamma\sqrt{(1-V^2)} \to i,$$

and the frequency equation reduces to

$$(V^2-2)^2-4\sqrt{(1-V^2\alpha^2)}\sqrt{(1-V^2)} = 0,$$

or, putting $V^2 = y$,

$$y^3-8y^2+8(3-2\alpha^2)y+16(\alpha^2-1) = 0.$$

This equation is the same as that deduced by Rayleigh for the velocity of surface waves (Rayleigh waves) on a semi-infinite isotropic solid. This equation has always just one real positive root, which gives us the asymptotic value for the curves, i.e. the surface velocity:

$$C_s = 2980 \text{ m/sec} \quad \text{(steel)}.$$

For the second and higher modes, (23) can be used, but the arguments of the tangents become very large so that the location of the roots becomes quite cumbersome to calculate. For the determination of these modes a method described in the next section has been used.

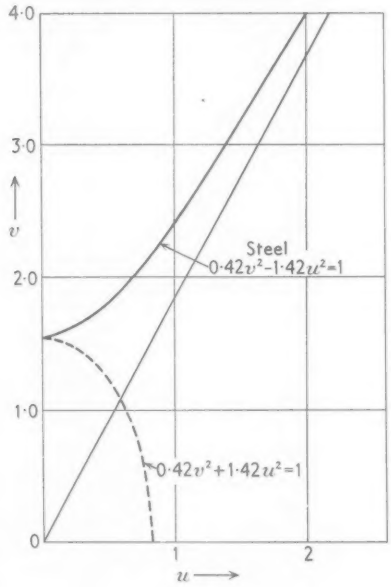

FIG. 3

5. Determination of the higher modes

The higher modes become of importance as the frequency of the excitation increases, or if the distribution of the exciting forces along the axis of the slab changes rapidly. The method described here was used to calculate the second and third modes explicitly, and can easily be extended to modes of higher order.

If, in (15), we introduce the variables

$$x = ha, \qquad s = \gamma a,$$
$$y = ka, \qquad \tau = pa,$$

the frequency equation, now independent of the thickness a, becomes

$$\left[\lambda+(\lambda+2\mu)\frac{x^2}{s^2}\right]\left(\frac{s^2}{y^2}-1\right)\cos x\sin y-4\mu\frac{x}{y}\sin x\cos y=0, \tag{28}$$

with

$$x^2=\frac{\rho\tau^2}{\lambda+2\mu}-s^2; \qquad y^2=\frac{\rho\tau^2}{\mu}-s^2. \tag{29}$$

Equations (28), (29) form a system of simultaneous equations for the variables x, y, s, and τ. We seek p/γ $(=\tau/s)$.

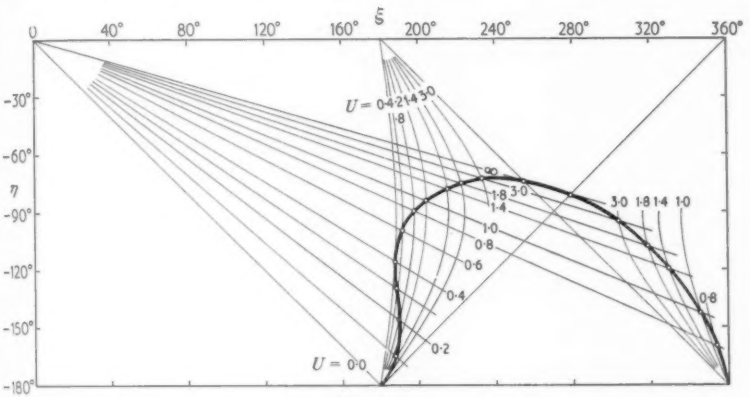

FIG. 4

A direct substitution of the relations (29) into (28) would lead to a formidable equation to solve. Instead, if we eliminate τ^2 from (29), we obtain

$$(\lambda+2\mu)x^2-\mu y^2+(\lambda+\mu)s^2=0.$$

Dividing by s^2 and letting

$$x/s=u, \qquad y/s=v,$$

we obtain a relation which is fixed for a given material

$$(\lambda+2\mu)u^2-\mu v^2=-(\lambda+\mu). \tag{30}$$

This relation is shown in Fig. 3 for steel. The dotted branch corresponds to imaginary values of u. The frequency equation (28) now reduces to

$$(v^2-1)^2\cos x\sin y+4uv\sin x\cos y=0.$$

The final changes of variable

$$(x+y)=\xi, \qquad (x-y)=\eta$$

reduce this further to

$$\beta/\alpha=\sin\xi/\sin\eta, \tag{31}$$

where

$$\alpha=\tfrac{1}{2}[(v^2-1)^2+4uv],$$

$$\beta=\tfrac{1}{2}[(v^2-1)^2-4uv].$$

Since v is a known function of u, as given by (30), these are also functions of u. In this analysis it is convenient to take u as the independent variable.

We finally have (31) and the relation

$$x/y = u/v = q(u), \tag{32}$$

which is now in a form suitable for fairly rapid graphical solution.

Fig. 4 shows some of the loci $\beta/\alpha = \text{const}$, as given by equation (31), in the (ξ, η) plane, but labelled by the corresponding value of u. It also shows the straight lines $u/v = \text{const}$, labelled in terms of the same values of u. The intersection of the two sets gives the common solution (u, ξ, η), from which we go back and determine x, y, s, and τ, then p and γ for a given a, and hence finally the velocity c.

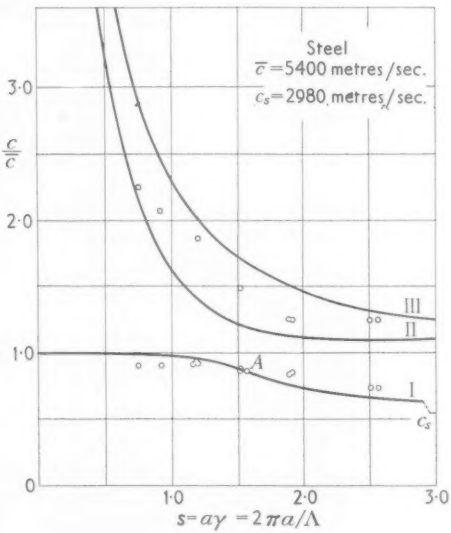

FIG. 5

The main numerical results are shown in Fig. 5, which plots the ratio of c to $\bar{c}$ in terms of $s = a\gamma$ for the first three modes. This manner of plotting was chosen to be similar to the curves which Bancroft (3) obtained for the cylindrical rod, to afford easy comparison.

While the method of this section does not lend itself easily to the lowest mode, there is one point on that curve which is easily obtained. If we make $v = 1$ then (30) also gives for steel $u = 0{\cdot}640i$ from which $x = 1{\cdot}048i$, $y = \frac{1}{2}\pi$, $s = \frac{1}{2}\pi$, $c = 4580$ m/sec, or $c/\bar{c} = 0{\cdot}85$. This corresponds to the point marked A in Fig. 5 which coincides with the value obtained from formula (24).

6. The excitation

In this section will be discussed the conditions under which a wave represented by the solution (11), (12) can be generated. Since the boundaries have been made free, there can be no excitation from the faces of the slab. The only remaining source for the wave, which must be radially symmetrical, can be a line corresponding to the axis of the cylindrical coordinate system or on a cylinder concentric with this axis.

We have, from (11), (12), (12 c),

$$\sigma_{rz} = [-2hA \sin hz + B(-k+\gamma^2/k)\sin kz]J_1(\gamma r)e^{ipt} \tag{33}$$

and

$$\sigma_{rr} = \lambda\Delta + 2\mu\frac{\partial u_r}{\partial r}$$

$$= (A\cos hz + B\cos kz)\left[(\lambda+2\mu)\frac{\partial J_1(\gamma r)}{\partial r} + \frac{\lambda}{r}J_1(\gamma r)\right]e^{ipt} \tag{34}$$

$$\sigma_{r\theta} = 0$$

for the values of the stress components on a cylinder of radius r. In these expressions the constants A and B are no longer both arbitrary, but must be connected by the boundary relations (13) or, equivalently, (14).

We have, from (13),

$$\frac{A}{B} = \frac{2\mu\gamma\cos ka}{\cos ha[\lambda\gamma+(\lambda+2\mu)h^2/\gamma]}$$

$$= \frac{\cos ka}{\cos ha}\frac{2\mu\gamma}{\rho\gamma(c^2-2c_2^2)} = \frac{\cos ka}{\cos ha}\frac{2}{V^2-2}. \tag{35}$$

The case of axial excitation can be dealt with by letting $r \to 0$ in these expressions.

From (33) $\sigma_{rz} = 0$ so that only the radial normal stress of the above is present in this case. Its value then is

$$(\sigma_{rr})_{r=0} = \frac{C}{\gamma}\left[\frac{\cos ka\cos hz}{\cos ha}\frac{2}{V^2-2} + \cos kz\right]e^{ipt}, \tag{36}$$

where C is an arbitrary constant replacing $2B(\lambda+2\mu+1)$. In terms of new variables this can be re-written as

$$(\sigma_{rr})_{r=0} = \phi(\zeta) = \frac{C}{\gamma}\left[\frac{\cos y}{\cos x}\frac{2}{V^2-2}\cos x\zeta + \cos y\zeta\right]e^{i\tau(t/a)}$$

$$= (C/\gamma)\,F\,e^{i\tau(t/a)}, \text{ say,}$$

where $\zeta = z/a$ varies from 0 to ± 1 as z varies to $\pm a$. Fig. 6 shows how the normal stress varies along the axis in the case of steel, for some differing values of the parameter s or τ, for the lowest mode, I.

From a physical point of view, that curve of the figure (and with it the

corresponding value of the parameters) has to be chosen which most nearly corresponds to the excitation. If we imagine this to be caused by an explosive packed into a very thin hole, then the curves of normal stresses shown in the figure, together with the fact that $\sigma_{rz} = 0$, fits in with the picture of

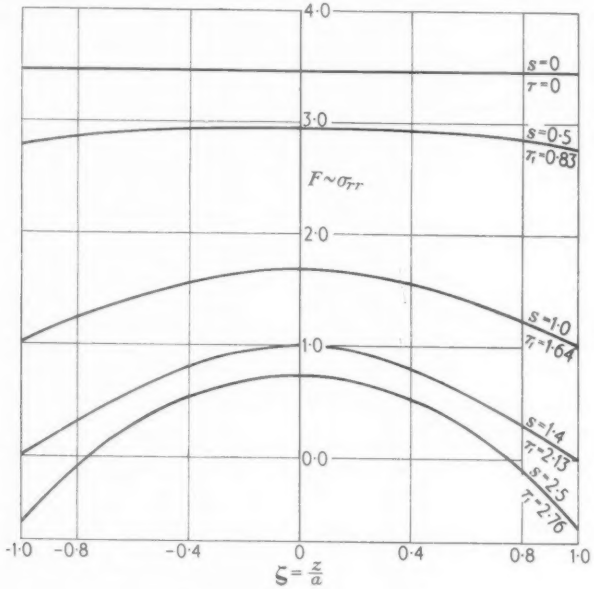

FIG. 6

an expanding gas at high pressure. It must be borne in mind, however, that our present analysis only applies strictly to a periodic disturbance. Because of the Fourier Integral Theorem, it is possible to extend our inference to pulse propagation.

Although little is actually known at present concerning how the above pressure varies along the hole, we can reasonably imagine that due to some pressure relief it will be expected to fall off towards the ends somewhat. The one limiting case of complete confinement (pressure constant) is that for $s = 0$. The other is that for complete release at the ends, corresponding to the value $s = 1{\cdot}4$ (approximately). It is interesting to note that beyond this value there is a change in sign of the stress to tension over part of the range. This, of course, could not be excited by means of expanding gases.

The conditions of continuity of the medium in the case of a radially symmetrical disturbance necessitate that the radial displacements at the

line of symmetry must be zero. This is evidently satisfied in (12) above, since $u_r = 0$ at $r = 0$.

7. Experimental results and their comparison with theory

Having completed the general theoretical analysis of the infinite plate we wish to discuss here from its standpoint two recently obtained experimental data. Since the data must of necessity be limited to finite plates, it can be expected to be an approximation to the results of the theory for infinite plates at best. However, it affords some indication which can serve to illuminate both approaches.

Some work was done at Bell Telephone Laboratories on the propagation of longitudinal stress waves in circular disks of barium titanate with various diameters, thicknesses, and their ratios, i.e. $d/2h = R/h$, where d is diameter and R is the radius of the disk. The resonant frequencies of the disk for the first two modes were determined with the help of a tuneable oscillator and a frequency counter. The results of the above work were first used by Kane and Mindlin (**7**) and the same have been used here for calculations in Table 2.

As also indicated by Kane and Mindlin the frequencies of the first mode of vibration were comparatively easy to determine but the measurements for the second mode were difficult because in addition to locating resonances, their relative strengths had also to be determined. Thus the frequencies of the second mode are less reliable than the first.

In the simplest way that resonant radial vibrations of a disk may be excited, the disk has a node at the centre and the next antinode at the free periphery. This is also the easiest vibration to excite in experiments. Thus, taking

$$\Lambda = d = 2R, \tag{37}$$

the velocity of propagation c becomes

$$c = \Lambda f = d\omega/2\pi. \tag{38}$$

Also
$$a\gamma = 2\pi(a/\Lambda) = 2\pi(a/2R) = \pi/(R/a). \tag{39}$$

The elastic constants of the barium titanate used for the disk are

$$\nu = 0{\cdot}3,$$
$$\mu = 49{\cdot}3 \times 10^{10} \text{ dynes/cm}^2,$$
$$\rho = 5{\cdot}33 \text{ g/cm}^3.$$

Hence the thin plate velocity is

$$\bar{c} = \sqrt{(\mu/\rho)}\sqrt{\{2/(1-\nu)\}} = 3635 \text{ m/sec}. \tag{40}$$

With the help of (37), (38), (39), and (40) values of $c/\bar{c}$ and $a\gamma$ were calculated

and are given in Table 2. The dimensions of the disk and corresponding resonant frequencies are taken directly from Table 2 of Kane and Mindlin's paper (7).

TABLE 2

Velocities calculated from experimental data for barium titanate disks ($\nu = 0{\cdot}3$)

Diameter (*cm*)	*Thickness* (*cm*)	1*st mode*	2*nd mode*	$a\gamma = \frac{\pi}{R/a}$
$2R$	$2a$	$c/\bar{c}$	$c/\bar{c}$	
2·68	0·648	0·8927	2·2228	0·7588
2·63	0·640	0·8927	2·2176	0·7644
2·16	0·564	0·8938	2·1607	0·8181
2·16	0·637	0·8919	2·0525	0·9267
2·17	0·638	0·8935	2·0644	0·9267
1·58	0·596	0·9054	1·9037	1·1810
1·59	0·612	0·9120	1·8459	1·2083
1·58	0·604	0·9070	1·8977	1·1991
1·31	0·639	0·8564	1·4795	1·5325
1·05	0·636	0·8245	1·2421	1·9040
1·05	0·637	0·8349	1·2336	1·9156
0·783	0·629	0·7194	1·2322	2·5133
0·777	0·636	0·7238	1·2377	2·5751

The experimental points of Table 2 are shown in Fig. 5. The theoretical curves drawn there are for steel ($\nu = 0{\cdot}29$) but the experimental points are for barium titanate ($\nu = 0{\cdot}3$). Part of the discrepancy in the two is due to the different Poisson's ratios. Bearing in mind the fact that the experimental points were obtained for finite disks and the curves for the infinite plates, the agreement between the two is fairly good, especially for the first mode.

It is worth while to discuss here two bases used for doing the above calculations:

(i) The velocity of propagation of the cylindrical stress waves in infinite flat slabs can be determined from experiments with circular disks of finite radius, only as an approximation.

(ii) It is assumed in the above calculations of both the first and second modes, that under resonance the centre of the disk is a node and the periphery an antinode, there being no node or antinode in between (cf. (37)). This is evidently true for the first mode but is also true for the second or higher modes. Otherwise the velocities for the second mode would be lower than the velocities for the first mode, which does not make much sense and hence the above assumption can be justified. Actually, the first mode differs from the second in the number of nodal planes of the lateral displacements u_z. The first mode has one nodal plane, the second has two, and so on.

In a second group of experiments made at Frankford Arsenal by Feder

et al. (8), a stress wave was initiated in a transparent plastic (Columbia Resin CR–39) by dynamic loading methods. In order to ensure a wavelength sufficiently short compared with the specimen and for other reasons a blasting cap was exploded at a point on the specimen and photographed photoelastically with a high-speed framing camera. Among the variously-shaped specimens one of them was a circular model as shown in Fig. 7.

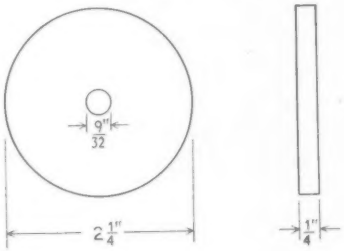

FIG. 7

A comparison of the relevant velocities is given in the following table:

1. Measured fringe velocity (in./microsec)	= 0·104
2. Calculated velocity of dilatation waves (compression)	= 0·077
3. Long thin bar velocity	= 0·0414
4. Thin plate velocity	= 0·051
5. 'Thick' plate velocity	= 0·027–0·051

In the reference it is noted that the measured velocity is greater than the longitudinal velocity c_1, by a factor of 25 per cent. The non-linearity of the stress-strain relation at high stress would not be able to account for this. Actually it would be more accurate to compare the measured velocity with the 'thick-plate' value, i.e. that given by the analysis of this paper. It can be seen that this would furnish at most the upper limit $\bar{c} = 0{\cdot}051$ in./microsec. The pulse length, although not accurately known, is sufficiently short to make the assumption of infinite plates reasonably accurate. This can be determined from the photographs which were taken in connexion with these experiments. It is not possible at the present moment to determine the velocity more exactly because of this uncertainty, and because, as pointed out by Davies (5), the detonation phenomena at the interface between a solid and a gas are too complex.

Nevertheless, the higher observed velocities depart even more by comparing with the plate velocity instead of the dilatation velocity. It may be due to the presence of shock waves generated by the high degree of loading used. Another possibility may be that second or higher modes are being observed.

8. Group velocities for the first mode of propagation

The relation between the group velocity c_g and the phase velocity c is

$$c_g = c - \Lambda\,(dc/d\Lambda),$$

which on dividing by the thin plate velocity $\bar{c}$ can be written as

$$V_g = \overline{V} - \Lambda\,(d\overline{V}/d\Lambda),$$

or, putting Λ in terms of s,

$$V_g = \overline{V} + s\,(d\overline{V}/ds). \tag{41}$$

TABLE 3

Group velocities V_g against $a\gamma$ for various Poisson's ratio

	V_g					
$a\gamma$ \ ν	0·0	0·1	0·2	0·3	0·4	0·5
0·0	1·000	1·000	1·000	1·000	1·000	1·000
0·5	1·000	0·999	0·991	0·973	0·939	0·883
1·0	1·000	0·986	0·932	0·839	0·723	0·592
1·5	1·000	0·734	0·568	0·477	0·406	0·375
1·6	0·233	0·434	0·471	0·423	0·373	0·352
1·7	0·184	0·314	0·387	0·373	0·354	0·336
1·8	0·201	0·265	0·321	0·340	0·338	0·324
2·0	0·284	0·291	0·299	0·305	0·312	0·319
2·2	0·324	0·324	0·324	0·324	0·324	0·324
2·5	0·388	0·383	0·375	0·365	0·350	0·333
3·0	0·457	0·436	0·415	0·393	0·367	0·341
∞	0·707	0·671	0·632	0·592	0·548	0·500

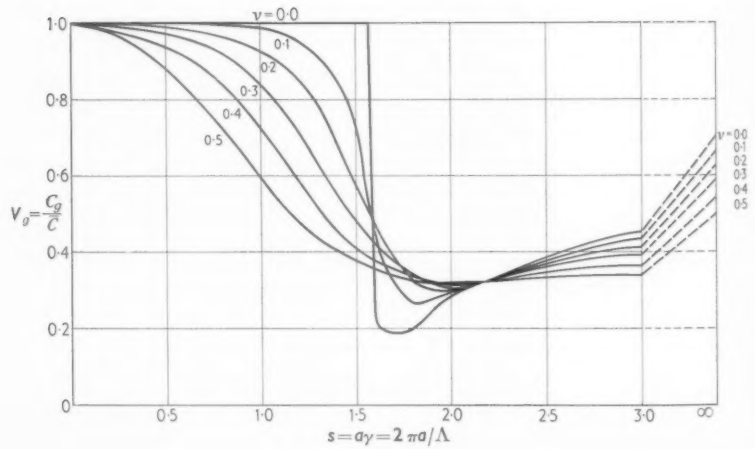

FIG. 8

This formula is used for determining the group velocity curves of $\overline{V}_g$ against s, graphically, from the phase velocity curves of $\overline{V}$ against s. The phase velocity curves were plotted accurately on a large scale and the values of tangents read. This gave $d\overline{V}/ds$ and consequently V_g against s. The error introduced due to inaccurate reading of the tangents was reduced by plotting curves of V_g against Poisson's ratio, ν, for various $a\gamma$ and smoothing them. These curves were quite flat and so minor errors in points could easily be detected. The results thus obtained are given in Table 3 for various Poisson's ratios and plotted in Fig. 8. Due to the graphical procedure, the third decimal place in Table 3 may not be accurate. It is interesting to note that all the curves appear to pass through $a\gamma = 2{\cdot}2$, $V_g = 0{\cdot}325$. As in the case of rods, the group velocity V_g approaches the surface velocity for very small wavelength.

9. Acknowledgement

The authors appreciate the financial assistance and sponsorship by the Office of Ordnance Research in making possible this investigation, which is a part of a research project on 'Scabbing on Materials'. Acknowledgement is also due to Mrs. Josephine Feder for making available helpful material and to Mr. Amnon Foux for assistance in calculations and graphical work.

REFERENCES

1. L. Pochhammer, 'Über die Fortpflanzungsgeschwindigkeiten kleiner Schwingungen in einem unbegrenzten isotropen Kreiscylinder', *J. reine angew. Math.* **81** (1876) 324.
2. A. E. H. Love, *The Mathematical Theory of Elasticity*, 4th edition (Cambridge, 1927), p. 288.
3. D. Bancroft, 'The velocity of longitudinal waves in cylindrical bars', *Phys. Rev.* **59** (1941) 588.
4. R. M. Davies, 'A critical study of the Hopkinson pressure bar', *Phil. Trans.* A, **240** (1948) 375.
5. R. M. Davies, *Stress-waves in solids*, Surveys in Mechanics, the G. I. Taylor 70th Anniversary Volume, ed. G. K. Batchelor and R. M. Davies (Cambridge, 1956).
6. L. E. Goodman, 'Circular-crested vibrations of an elastic solid bounded by two parallel planes', *Proc. First U.S. National Congress of App. Mech.* (1951) 65–73.
7. T. R. Kane and R. D. Mindlin, 'High-frequency extensional vibrations of plates', *J. App. Mech.* **23** (1956) 277–83.
8. J. C. Feder, R. A. Gibbons, J. T. Gilbert, and E. L. Offenbacher, 'The study of the propagation of stress-waves by photoelasticity', *Proc. Soc. Exper. Stress Analysis* **14** (1956) 109–118.

SOME CONDUCTION PROBLEMS IN THE HEATING OF SMALL AREAS ON LARGE SOLIDS

By P. H. THOMAS (*D.S.I.R. and Fire Offices' Committee, Fire Research Station*)

[Received 19 September 1957]

SUMMARY

This paper discusses a number of problems the common feature of which is the heating by a constant flux of small areas, generally circular, on the surface of a semi-infinite solid or on an infinite thin sheet. In addition to a number of analytic results, the variation with time of the surface temperature of the centre of the heated area on a semi-infinite solid has been computed for various sizes of area and degrees of cooling.

1. Notation

x, y, z	cartesian coordinates.
r, x	cylindrical coordinates.
θ	temperature above ambient.
t	time of heating.
K	thermal conductivity.
ρ	density.
c	specific heat.
k	thermal diffusivity ($K/\rho c$).
Q	incident heat flux per unit area.
R	radius of heated circular area.
$2L$	width of heated infinite strip.
D	perpendicular distance between point source and surface of solid.
Δ	thickness of thin sheet.
H	heat transfer coefficient at the surface.
h	H/K.
∇^2	Laplacian operator.

2. Introduction

WHEN a small area on the surface of a large solid is heated, the temperature at first rises in substantially the same manner as does that of a much larger area. Eventually, however, the cooling effect of heat flowing laterally away from the heated area becomes important and it is necessary in experimental work which employs small areas to simulate larger ones to be able to assess the time before this occurs. For example it is desirable to know the time after which the temperature of the centre of the heated area is no longer within, say, 10 or 20 per cent of what it would have been had the heated

area extended over the whole surface, i.e. had been a plane source producing one-dimensional flow. An approximate assessment can often be made from the magnitude of certain dimensionless parameters.

Consider a small circular area of radius R on the surface of a semi-infinite solid, and suppose that only this area is directly heated. The rate of heat loss from unit area of surface may be taken to be of the form $H\theta$ whilst the rate of heat loss by conduction into the solid is $K\theta/R$. The ratio of these two losses is HR/K and if this is very much larger than unity, the surface loss predominates and the size of the area is unimportant. Similarly kt/R^2 represents the ratio of the rate of lateral loss of heat $K\theta/R$ by conduction over the cylindrical surface of a region of unit depth to the rate of retention of heat $R\rho c\theta/t$ by that region. It follows that if the ratio kt/R^2 (the Fourier number) is markedly different from unity then one or other factor is of negligible consequence and an approximate but simpler conduction model may be substituted. Where $kt/R^2 \sim 1$ and $HR/K \sim 1$ analysis of some kind is required, if it is desired to use an experimental system to the limit of its accuracy in representing large areas.

It is the purpose of this paper to give a number of results for the heating of small parts of large solids or thin sheets. In section 3 some results are given for the transient and steady-state temperature at the centre of a circular area on the surface of a semi-infinite solid subject to surface cooling when the area is heated by uniform constant heat flux. The steady-state temperature on the surface of a large solid due to an external point source is also discussed. Section 4 deals with the problem of a heated circular area or infinite strip on a thin sheet. Finally, in section 5, a brief discussion is given on the results obtained in sections 3 and 4. Note that all physical constants of the heated material are taken to be independent of temperature variation.

3. Local heating on semi-infinite solid

Two conditions are considered. The first is the heating of a circular area of radius R on the surface of a semi-infinite solid by a constant flux uniform over that area and zero elsewhere. The second is the heating of the surface of a semi-infinite solid by a point source external to it. In this latter problem only the steady state is considered. The transient heat conduction equation is

$$k\nabla^2\theta = \frac{\partial\theta}{\partial t}. \tag{1}$$

The initial condition is $\theta = 0, \quad t = 0$

and one boundary condition is

$$\theta \to 0, \quad x \to \infty.$$

When the heat flux is incident on a circular area, the second boundary condition is that at $x = 0$

$$H\theta - K\frac{\partial\theta}{\partial x} = \begin{cases} Q & (r < R \quad \text{and} \quad t > 0), \\ 0 & (r > R \quad \text{and} \quad t > 0). \end{cases} \tag{2a, 2b}$$

For the point source external to the solid it is

$$H\theta - K\frac{\partial\theta}{\partial x} = Q(r) \quad (t > 0),$$

where $Q(r)$ can be determined as a function of r.

In practical problems, the primary interest is in the temperature of the centre of the heated area.

(i) *Transient temperature at the centre for constant heat flux*

The transient temperature at the centre of the heated area may be found by making use of Green's function u for a point source of unit strength at (x', y', z') in a semi-infinite solid having surface loss of heat at the boundary $x = 0$ (see Carslaw and Jaeger (**1**)). The point source is considered to be situated at the surface $x' = 0$ so that the transient temperature at the centre of the heated area ($x = y = z = 0$) is

$$u_0 = \frac{1}{4(\pi kt)^{\frac{3}{2}}} e^{-(y'^2+z'^2)/4kt} - \frac{h}{4\pi kt}\operatorname{erfc} h\sqrt{(kt)}\exp\left(h^2kt - \frac{y'^2+z'^2}{4kt}\right). \tag{3}$$

Hence for a continuous source of strength $Q/\rho c$, over the region $r < R$, where $r = \sqrt{(z'^2+y'^2)}$ the temperature is

$$\theta_0 = \frac{Q}{2\rho c}\int_0^t d\lambda \int_0^R \left\{\frac{1}{\pi^{\frac{1}{2}}(k\lambda)^{\frac{3}{2}}} - \frac{h}{k\lambda}e^{h^2k\lambda}\operatorname{erfc} h\sqrt{(k\lambda)}\right\} e^{-r^2/4k\lambda} r\, dr. \tag{4}$$

Integrating first with respect to r, writing θ_{NC} for the temperature with no surface cooling and substituting $\lambda = \omega^2/h^2k$ we have from equation (4)

$$\theta_0 = \theta_{NC} - \frac{2Q}{H}\int_0^{h\sqrt{(kt)}} (1 - e^{-h^2R^2/4\omega^2})\omega e^{\omega^2}\operatorname{erfc}\omega\, d\omega \tag{5}$$

and

$$\theta_{NC} = \frac{QR}{K}\left[\frac{2}{\sqrt{\pi}}\left(\frac{kt}{R^2}\right)^{\frac{1}{2}}(1 - e^{-R^2/4kt}) + \operatorname{erfc}\frac{R}{2\sqrt{(kt)}}\right],$$

a result obtained by Blok (**2**).

The integral in equation (5) has been numerically evaluated and the resulting values of θ_0 are shown in Fig. 1, for various values of hR and kt/R^2. It is possible to find the values of kt/R^2 at which the temperature at the centre of the disk is, say, 10 or 20 per cent less than it would be for a source extending over the whole surface $x = 0$, i.e. a plane source. These values of kt/R^2 are given in Fig. 2 as a function of hR, while in Fig. 3 the

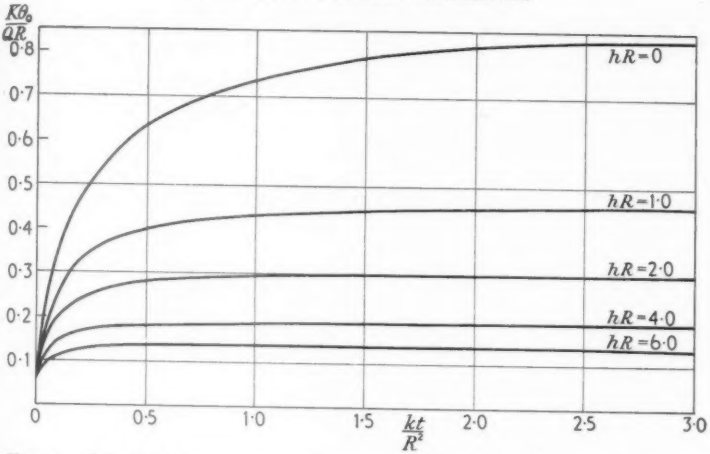

FIG. 1. Transient temperature at centre of heated circular area on semi-infinite solid

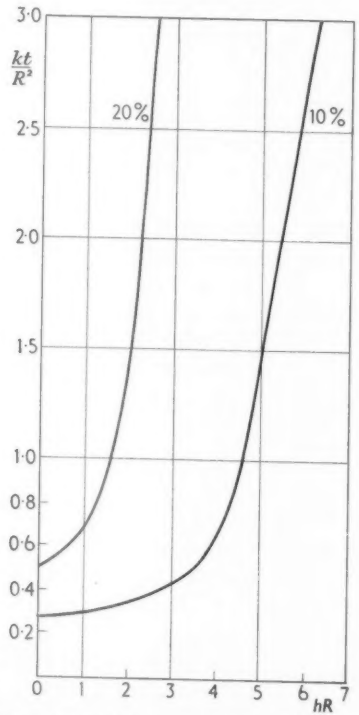

FIG. 2. Values of kt/R^2 at which temperature of centre of circular area is 10% and 20% below that of heated extended plane source

corresponding values of h^2kt are given as a function of hR. For any h, R, and k it is thus possible to find the maximum duration of heating for which the temperature of a small area is sensibly the same as a large one when heated by a constant uniform flux.

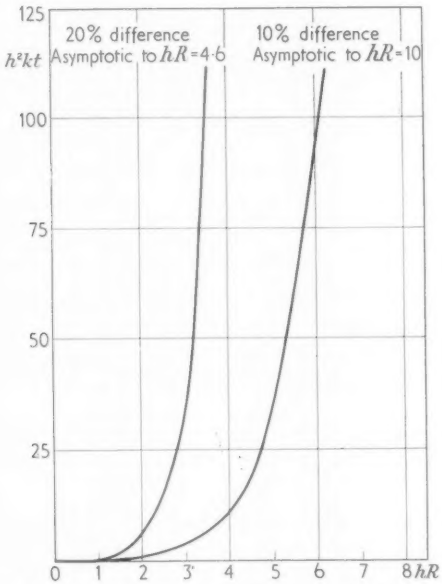

FIG. 3. Values of h^2kt as a function of hR for 10% and 20% difference between centre of circular area and extended plane

(ii) *Steady-state temperature at centre for constant heat flux*

For this problem a solution in terms of tabulated functions is possible. A solution to equations (1) and (2) for the steady state is

$$\theta = \frac{QR}{K}\int_0^\infty \frac{e^{-\alpha x}J_0(\alpha r)J_1(\alpha R)}{h+\alpha}\,d\alpha, \tag{6}$$

where J_0 and J_1 are the Bessel functions of the first kind of zero and first order respectively.

This integral can be evaluated at $r = 0$ and $x = 0$ by means of an integral given by Watson (**3a**) to give

$$\theta_0 = \frac{QR}{K}\left[1+\frac{1}{hR}+\tfrac{1}{2}\pi\{Y_1(hR)-H_1(hR)\}\right], \tag{7}$$

where Y_1 is Weber's Bessel function of the second kind of first order and H_1 is Struve's function of first order. The variation of $K\theta_0/QR$ with hR is shown in Fig. 4. As $hR \to \infty$, $\theta_0 \to (QR/K)(1/hR)$, i.e. Q/H, which is the steady-state temperature for an infinite plane source—as should be the case. Furthermore, when h is zero, i.e. there is no surface cooling, it can

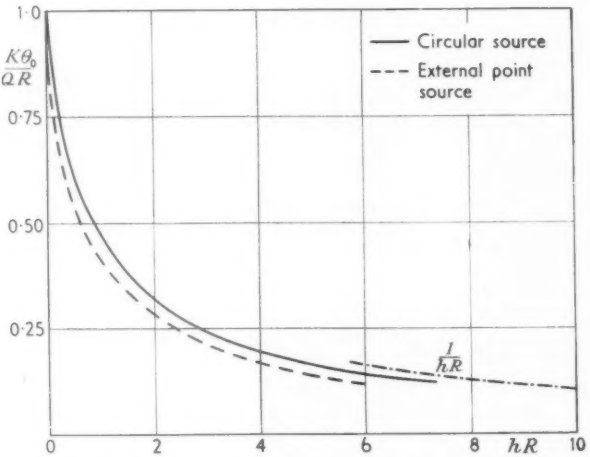

FIG. 4. The steady temperature of the centre of a heated circular area on a semi-infinite solid or below a point source

be shown from equation (7) that θ_0 is equal to QR/K. This case, however, is of special interest since θ for all values of r may be obtained in terms of tabulated functions.

By considering sources of strength $r_1\,dr_1\,d\phi_1\,Q/\rho c$ over the region

$$r_1 < R, \qquad 0 < \phi < 2\pi, \qquad x = 0,$$

the steady-state temperature distribution at any point on the surface $x = 0$ can be obtained as

$$\theta = \frac{Q}{4\rho c}\int_0^{\infty} d\lambda \int_0^{2\pi} d\phi \int_0^{R} r_1 \exp\left(-\frac{r_1^2+r^2-2rr_1\cos\phi}{4k\lambda}\right)(\pi k\lambda)^{-\frac{1}{2}}\,dr_1. \qquad (8)$$

We make use of a particular case of Weber's second exponential integral (**3b**), namely,

$$\frac{1}{4\pi k\lambda}\int_0^{2\pi} \exp\left(-\frac{r_1^2+r^2-2rr_1\cos\phi}{4k\lambda}\right) d\phi = \int_0^{\infty} e^{-\alpha^2 k\lambda} J_0(\alpha r_1) J_0(\alpha r)\alpha\,d\alpha.$$

After integrating with respect to λ and r_1 we obtain

$$\theta = \frac{QR}{K} \int_0^\infty \frac{J_1(\alpha R) J_0(\alpha r)}{\alpha} \, d\alpha.$$

It may be shown (**3c**) that this reduces to

$$\theta = \frac{2}{\pi} \frac{QR}{K} E(r/R) \quad (r < R), \tag{9}$$

$$= \frac{2}{\pi} \frac{Qr}{K} \left[E\left(\frac{R}{r}\right) - \left(1 - \frac{R^2}{r^2}\right) K\left(\frac{R}{r}\right) \right] \quad (r > R), \tag{10}$$

where K and E are the complete elliptic integrals of the first and second kinds respectively.

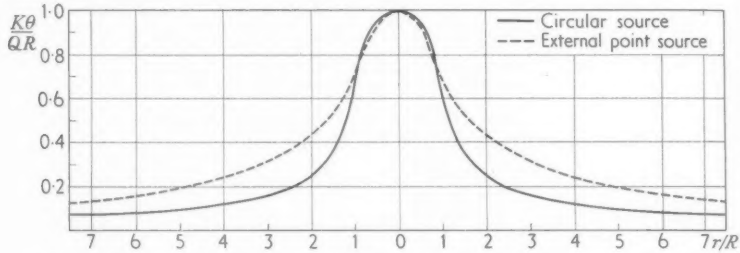

FIG. 5. Surface temperature distribution due to uniform circular area over $0 < r < R$ and to an external point source

This distribution of temperatures is shown in Fig. 5. In particular the maximum temperature at the centre ($r = 0$) is QR/K and the mean temperature over the area $r < R$ is $8QR/3\pi K$.

(iii) *Steady-state temperature due to an external point source*

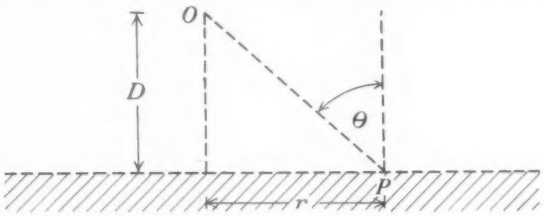

FIG. 6. Point source external to semi-infinite solid

If W is the heat radiated per second at O a distance D from a non-reflecting semi-infinite solid, the heat flux at P normal to the surface of the solid is (see Fig. 6)

$$Q(r) = \frac{W \cos\theta}{4\pi(D^2+r^2)} = \frac{WD}{4\pi(D^2+r^2)^{\frac{3}{2}}}.$$

Therefore, at $x = 0$,
$$h\theta - \frac{d\theta}{dx} = \frac{WD}{4\pi K(D^2+r^2)^{\frac{1}{2}}} \tag{11 a}$$

and at $x = \infty$,
$$\theta = 0. \tag{11 b}$$

Applying the Hankel transformation

$$\bar{\theta}(p) = \int_0^\infty \theta(r) r J_0(pr)\, dr, \tag{12 a}$$

$$\theta(r) = \int_0^\infty \bar{\theta}(p) p J_0(pr)\, dp \tag{12 b}$$

we have for the steady-state from equations (11 a), (11 b), and (12 a) that $\theta = Ae^{-px}$ and at $x = 0$

$$(h+p)\bar{\theta} = \frac{WD}{4\pi K}\int_0^\infty \frac{rJ_0(pr)\, dr}{(D^2+r^2)^{\frac{1}{2}}} = \frac{W}{4\pi K}e^{-pD} \tag{13}$$

from an integral given by Watson (**3d**). At the centre $r = 0$, from equations (12 b) and (13),

$$\theta_0 = \frac{W}{4\pi KD}\left[1 - hDe^{hD}\int_{hD}^\infty \frac{e^{-u}\, du}{u}\right]. \tag{14}$$

The integral in equation (14) is the exponential integral and is a tabulated function. The value of θ_0 for various values of hD is shown in Fig. 4, D being denoted by R and $W/4\pi D^2$ by Q for comparison with equation (7). For no cooling, equations (12 b) and (13) give

$$\theta = \frac{W}{4\pi K}\int_0^\infty J_0(pr)e^{-pD}\, dp = \frac{W}{4\pi K\sqrt{(D^2+r^2)}} \tag{15}$$

using an integral given by Watson (**3e**).

The central temperature without cooling is seen to equal that due to a disk on the surface of radius D and intensity equal to the maximum $W/4\pi D^2$. Because the total heat falling on the surface $x = 0$ is $2\pi D^2$ times the maximum intensity, and for a uniform disk on the surface it is only πD^2 times the maximum, there is a factor of 2 between the respective temperatures at large radial distances.

4. The heating of thin sheets

In these problems the thickness Δ of the thin sheet is assumed small enough for thermal gradients across the sheet to be neglected. The validity of this assumption depends on the conditions

$$h\Delta \ll 1, \qquad \Delta \ll R, \quad \text{or} \quad \Delta \ll L.$$

In transient problems the equations will only be valid for

$$t \gg \Delta^2/k.$$

The systems considered are the heating by a constant flux of a small circular area and an infinite strip as shown in Fig. 7.

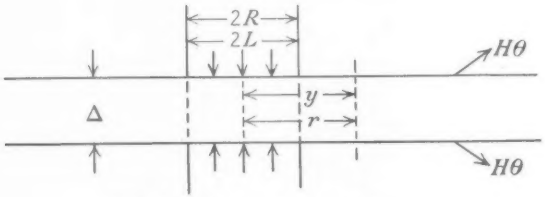

FIG. 7. Heating of thin sheet

(i) *Circular area*

For the condition shown in Fig. 7 we have

$$\frac{\partial^2\theta}{\partial r^2}+\frac{1}{r}\frac{\partial\theta}{\partial r}=\frac{1}{k}\frac{\partial\theta}{\partial t}+\frac{2h\theta}{\Delta}-\frac{Q(r)}{K\Delta}, \tag{16}$$

where

$$Q(r)=\begin{cases}Q & r<R\\ 0 & r>R\end{cases}, \tag{16a}$$

$$\theta=0 \quad \text{at } t=0.$$

Applying the Hankel transformation to equations (16) and (16 a) we obtain

$$-p^2\bar{\theta}=\frac{1}{k}\frac{d\bar{\theta}}{dt}-\frac{QRJ_1(pR)}{K\Delta p}+\frac{2h\bar{\theta}}{\Delta},$$

whence

$$\theta=\frac{QR}{K\Delta}\int_0^\infty \frac{J_1(pR)J_0(pr)}{(p^2+2h/\Delta)}[1-\exp\{-(p^2+2h/\Delta)kt\}]\,dp. \tag{17}$$

For no cooling the transient central temperature is, from equations (12 b) and (17),

$$\theta_0=\frac{Qt}{\rho c\Delta}\left(1-e^{-X^2}+X^2\int_{X^2}^\infty \frac{e^{-u}\,du}{u}\right), \tag{18}$$

where

$$X=\frac{R}{2\sqrt{(kt)}}.$$

The relation between θ_0 and X is shown in Fig. 8. The steady-state central temperature with surface cooling is, from equation (17),

$$\theta_0=\frac{QR}{K\Delta}\int_0^\infty \frac{J_1(pR)}{(p^2+2h/\Delta)}\,dp,$$

which, from an integral given by Watson (**3d**), may be shown to be

$$\theta_0 = \frac{Q}{2H}\left\{1 - R\sqrt{\left(\frac{2h}{\Delta}\right)}\,K_1\left[R\sqrt{\left(\frac{2h}{\Delta}\right)}\right]\right\}, \tag{19}$$

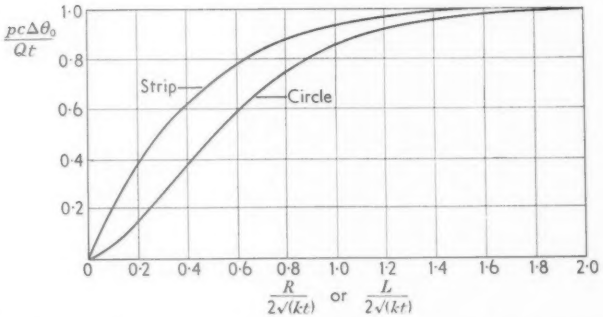

FIG. 8. The effect of size and heating time on the maximum temperature of irradiated areas on thin strips and sheets (no surface cooling)

where K_1 is the modified Bessel function of the second kind of first order. The relation between θ_0 and $2hR^2/\Delta$ is shown in Fig. 9.

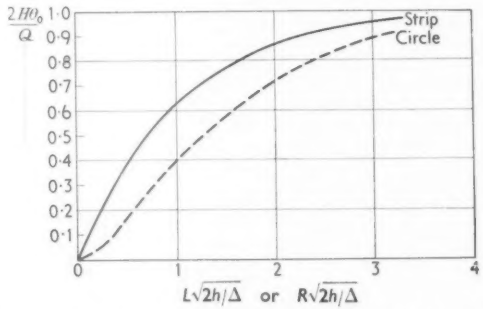

FIG. 9. Steady-state temperature at centre of heated sheet for different degrees of cooling

(ii) *Infinite strip*

We have

$$\frac{\partial^2\theta}{\partial y^2} = \frac{1}{k}\frac{\partial\theta}{\partial t} + \frac{2h\theta}{\Delta} - \frac{Q(y)}{K\Delta}, \tag{20a}$$

where

$$Q(y) = \begin{cases} Q & |y| < L \\ 0 & |y| > L \end{cases}, \tag{20b}$$

$$\theta = 0 \quad \text{at } t = 0.$$

Applying the cosine transformation

$$\bar{\theta}(p) = \int_0^\infty \theta(y) \cos py \, dy, \tag{21a}$$

$$\theta(y) = \frac{2}{\pi} \int_0^\infty \bar{\theta}(p) \cos py \, dp \tag{21b}$$

we obtain from equations (20a), (20b), and (21a)

$$-p^2\bar{\theta} = \frac{1}{k}\frac{d\bar{\theta}}{dt} + \frac{2h\bar{\theta}}{\Delta} - \frac{Q \sin pL}{K\Delta p},$$

and eventually

$$\theta = \frac{2}{\pi}\frac{Q}{K\Delta} \int_0^\infty \frac{\sin pL}{p(p^2+2h/\Delta)} [1 - \exp\{-(p^2+2h/\Delta)kt\}] \cos py \, dp. \tag{22}$$

If there is no surface cooling the temperature along the axis of the strip is, from equation (22),

$$\theta_0 = \frac{Qt}{\rho c \Delta} \left(\operatorname{erf} Y - 2Y^2 \operatorname{erfc} Y + \frac{2}{\sqrt{\pi}} Y e^{-Y^2} \right), \tag{23}$$

where

$$Y = \frac{L}{2\sqrt{(kt)}}.$$

The variation of θ_0 with Y is shown in Fig. 8. The transient axial temperature with cooling is given by

$$\theta_0 = \frac{Q}{\rho c \Delta} \int_0^t e^{-2hk\lambda/\Delta} \operatorname{erf}\left(\frac{L}{2\sqrt{(k\lambda)}} \right) d\lambda, \tag{24}$$

so the effect of cooling may be estimated from the magnitude of $2Ht/\rho c\Delta$.

The steady-state temperature with cooling is obtained from equation (22) with $t \to \infty$ and $y = 0$. Thus

$$\theta_0 = \frac{Q}{2H}(1 - e^{-L\sqrt{(2h/\Delta)}}), \tag{25}$$

which is shown in Fig. 9.

5. Discussion

A number of results are listed in Table 1. If, when comparing the disk source on a thin sheet and on a semi-infinite solid, the semi-infinite solid is regarded as approximating to a 'thin' sheet of thickness $2R$, the conditions for a 10 per cent difference between a small and large area are the same. By analogy with the transient behaviour of a disk on a semi-infinite solid we should expect the permitted value of kt/R^2 (for a 10 per cent difference) to increase with hR^2/Δ and the shape of the curve relating hR^2/Δ to kt/R^2 (for a 10 per cent difference) to be similar to that

given in Fig. 2, hR being replaced by $2hR^2/\Delta$. The minimum value of kt/R^2 for a thin sheet is, however, 25 per cent less (0·21 instead of 0·28) than for a semi-infinite solid.

TABLE 1. *Values of size parameters at which size has less than 10 and 20 per cent effect*

Problem	*Conditions*	*Condition for less than 10 per cent difference from plane at centre*	*Condition for less than 20 per cent difference from plane at centre*
Point source near semi-infinite solid	*Steady-state* with surface cooling, uniform steady flux	$hD > 17$	$hD > 7{\cdot}5$
Disk on semi-infinite solid	*Steady-state* with surface cooling, uniform steady flux	$hR > 10$	$hR > 4{\cdot}5$
Disk on thin sheet	*Steady-state* with surface cooling, uniform steady flux	$hR^2/\Delta > 5{\cdot}0$	$hR^2/\Delta > 2{\cdot}9$
Strip on thin sheet	*Steady-state* with surface cooling, uniform steady flux	$hL^2/\Delta > 2{\cdot}6$	$hL^2/\Delta > 1{\cdot}3$
Disk on semi-infinite solid	*Transient* with surface cooling, uniform steady flux	$hR = 0$ $kt/R^2 < 0{\cdot}28$ $= 2$ $< 0{\cdot}35$ $= 4$ $< 0{\cdot}65$	$hR = 0$, $kt/R^2 < 0{\cdot}52$ $= 2$, $kt/R^2 < 1{\cdot}4$
Disk on thin sheet	*Transient*, no cooling	$kt/R^2 < 0{\cdot}21$	$kt/R^2 < 0{\cdot}32$
Strip on thin sheet	*Transient*, no cooling	$kt/L^2 < 0{\cdot}36$	$kt/L^2 < 0{\cdot}65$

Acknowledgement

The work described in this paper forms part of the programme of the Joint Fire Research Organization of the Department of Scientific and Industrial Research and Fire Offices' Committee; publication is by permission of the Director of Fire Research.

REFERENCES

1. H. S. CARSLAW and J. C. JAEGER, *Conduction of Heat in Solids* (Oxford, 1947), p. 308.
2. H. BLOK, 'General discussion on lubrication and lubricants', *Proc. Inst. Mech. Engrs.* **2** (1937), 222.
3a. G. N. WATSON, *Treatise on the Theory of Bessel Functions* (Cambridge, 1944), p. 436.
3b. Ibid., p. 395.
3c. Ibid., p. 401.
3d. Ibid., p. 434.
3e. Ibid., p. 386.
4. C. J. TRANTER, *Integral Transforms in Mathematical Physics* (London, 1951).

ON FREE MOTION IN THE GRAVITATIONAL FIELD OF THE EARTH

By G. C. SCORGIE (*Calcot, Nr. Reading*)

[Received 27 September 1956]

SUMMARY

A literal approximate solution is given for the motion of a particle in the earth's gravitational field as modified by ellipticity of the figure of the earth. In particular, the resulting torsion of the path is calculated.

1. Introduction

In connexion with the launching of artificial earth satellites during the International Geophysical Year, and of intercontinental ballistic missiles, it is of interest to investigate the motion of a particle in the earth's gravitational field. In both cases a body is to be rapidly propelled into an orbit which is then traversed under the action of gravity and disturbing influences of various kinds, air resistance accounting, presumably, for most of the disturbance. The present note is concerned with the solution of the basic problem of the free motion of a particle in the earth's gravitational field when account is taken of the ellipticity of the figure of the earth, that is, of the departure of the external field of gravity from a force varying inversely as the square of the distance from a fixed centre. The departure being small, the most suitable method of dealing with it is likely to be by a numerical perturbation of the ordinary Kepler motion. However, for the discussion of general characteristics of the motion, some interest attaches to an approximate literal treatment described here.

2. Approximate solution

Being interested in the purely gravitational field, excluding centrifugal effects caused by the rotation of the earth, we take a non-rotating reference frame with origin at the centre of the earth, and choose spherical polar coordinates q^n $(n = 1, 2, 3)$; q^1 is the radius, q^2 is the angle measured from the earth's polar axis drawn towards the north pole, and q^3 is the angle measured about that axis. Since, in discussing the geometry of the path, we wish to use tensor notation, it is used throughout, with indices running from 1 to 3.

The purely gravitational potential, the negative of the potential energy of unit mass, at a point outside the earth is (**1**)

$$V = V_0 + v_0,$$

where

$$V_0 = \frac{a}{q^1},$$

$$v_0 = \frac{ab(1-3\cos^2 q^2)}{(q^1)^3}, \text{ approximately,}$$

$$a = 3{\cdot}986 \times 10^{20} \text{ cm}^3 \text{ sec}^{-2},$$

and

$$b = 2{\cdot}225 \times 10^{14} \text{ cm}^2.$$

v_0 may be regarded as perturbing the Kepler motion corresponding to V_0. Alternatively we can write

$$V = V_1 + v_1,$$

where

$$V_1 = \frac{a}{q^1} + \frac{ab(1-3\cos^2 q^2)}{R(q^1)^2},$$

$$v_1 = \frac{(1-q^1/R)ab(1-3\cos^2 q^2)}{(q^1)^3},$$

and R is a constant length comparable with the mean value of q^1 over an orbit. This procedure is useful because v_1 is a smaller perturbation than v_0, and the motion in the field V_1 can be found by quadratures. It follows that

$$\left|\frac{\partial v_1}{\partial q^1}\right| \Big/ \left|\frac{\partial v_0}{\partial q^1}\right| = |1-2q^1/3R| \quad \text{and} \quad \left|\frac{\partial v_1}{\partial q^2}\right| \Big/ \left|\frac{\partial v_0}{\partial q^2}\right| = |1-q^1/R|.$$

Thus, for example, provided that q^1 does not differ from R by more than 5 per cent of R, the field V_1 contains at least 95 per cent of the perturbing transverse acceleration caused by ellipticity of the earth's figure, and at least 63 per cent of the perturbing radial acceleration.

The problem of motion in the field V_1 can be reduced to quadratures by standard methods (**2**). Since q^3 is an ignorable coordinate the conjugate momentum p_3 is a constant m, say, and we have a system of the fourth order, the Hamiltonian for unit mass being

$$H = \frac{1}{2}\left[(p_1)^2 + \frac{(p_2)^2}{(q^1)^2} + (q^1)^{-2}\left\{\frac{m^2}{\sin^2 q^2} - \frac{2ab(1-3\cos^2 q^2)}{R}\right\}\right] - \frac{a}{q^1}. \qquad (1)$$

Since the Hamilton–Jacobi equation is separable, it is possible to find a contact transformation to new variables in which the coordinates and momenta are constants. Alternatively we can make an extended contact transformation, transforming the time while preserving invariant the Pfaffian

$$\Delta = p_1\,dq^1 + p_2\,dq^2 - H\,dt, \qquad (2)$$

and solve the canonical equations in the transformed variables. Adopting

the latter course, we regard the negative of the Hamiltonian as the momentum canonically conjugate to the time, noting that, since time does not appear explicitly in the Hamiltonian, its value must be a constant: and, since the coordinate system is inertial, this constant is the total energy E, say, of unit mass. Hence we have

$$H - E = 0, \tag{3}$$

where H is given by (1).

Choosing q^1 as the transformed time we can write

$$\Delta = -E\,dt + p_2\,dq^2 - J\,dq^1, \tag{4}$$

where the transformed Hamiltonian J is the value of $-p_1$ found from (3). Thus

$$J = -\left[2E - \frac{(p_2)^2}{(q^2)^2} - (q^1)^{-2}\left\{\frac{m^2}{\sin^2 q^2} - \frac{2ab(1-3\cos^2 q^2)}{R}\right\} + \frac{2a}{q^1}\right]^{\frac{1}{2}}.$$

From the canonical equations

$$\frac{\partial J}{\partial E} = -\frac{dt}{dq^1}, \qquad \frac{\partial J}{\partial p_2} = \frac{dq^2}{dq^1}, \qquad \frac{\partial J}{\partial t} = \frac{dE}{dq^1}, \qquad \frac{\partial J}{\partial q^2} = -\frac{dp_2}{dq^1},$$

we obtain t and q^2 in terms of q^1, and q^3 in terms of q^2, as follows.

From
$$\frac{dq^2}{dq^1} = -\frac{p_2}{J(q^1)^2}$$

and
$$\frac{dp_2}{dq^1} = -\frac{\cos q^2}{J(q^1)^2}\left\{\frac{m^2}{\sin^3 q^2} + \frac{6ab\sin q^2}{R}\right\}$$

we obtain
$$\frac{dp_2}{dq^2} = \frac{\cos q^2}{p_2}\left\{\frac{m^2}{\sin^3 q^2} + \frac{6ab\sin q^2}{R}\right\}$$

which can be integrated to

$$p_2 = \left\{-\frac{m^2}{\sin^2 q^2} + \frac{6ab\sin^2 q^2}{R} + n\right\}^{\frac{1}{2}}, \tag{5}$$

where n is a constant.

Hence
$$\frac{dt}{dq^1} = q^1\{2E(q^1)^2 + 2aq^1 - (n + 4ab/R)\}^{-\frac{1}{2}} \tag{6}$$

and
$$\frac{dq^2}{dq^1} = \frac{\{n - (m/\sin q^2)^2 + 6(ab/R)\sin^2 q^2\}^{\frac{1}{2}}}{q^1\{2E(q^1)^2 + 2aq^1 - (n + 4ab/R)\}^{\frac{1}{2}}}. \tag{7}$$

By definition,
$$m = p_3 = (q^1 \sin q^2)^2 \frac{dq^3}{dt};$$

hence
$$\frac{dq^3}{dq^2} = \frac{m}{\sin^2 q^2}\left\{n - \frac{m^2}{\sin^2 q^2} + \frac{6ab\sin^2 q^2}{R}\right\}^{-\frac{1}{2}}. \tag{8}$$

The solution by quadratures is expressed by (6), (7), and (8).

From (6), $$t-t_a = a(-2E)^{-\frac{1}{2}}(\psi+e\sin\psi),$$

where $$e = \{1-(-2E/a^2)(n+4ab/R)\}^{\frac{1}{2}},$$

$$q^1 = (-a/2E)(1+e\cos\psi),$$

and t_a is a constant. From (7),

$$\frac{2}{a}\left(-\frac{2E}{1-e^2}\right)^{\frac{1}{2}}\tan^{-1}\left[\left(\frac{1-e}{1+e}\right)^{\frac{1}{2}}\tan\tfrac{1}{2}\psi\right]$$

$$= -\frac{\beta}{A^{\frac{1}{2}}}[F\{\beta/\alpha, \sin^{-1}(\alpha\cos q^2)\} - F\{\beta/\alpha, \sin^{-1}(\alpha\cos Q^2)\}],$$

where

$$\alpha = 2^{\frac{1}{2}}\{-B/A-(B^2/A^2-4C/A)^{\frac{1}{2}}\}^{-\frac{1}{2}},$$

$$\beta = 2^{\frac{1}{2}}\{-B/A+(B^2/A^2-4C/A)^{\frac{1}{2}}\}^{-\frac{1}{2}},$$

$$A = 6ab/R,$$

$$B = -(n+12ab/R),$$

$$C = n-m^2+6ab/R,$$

and $F(\mu,\phi)$ denotes the incomplete elliptic integral of the first kind, viz.

$$F(\mu,\phi) = \int_0^{\phi} \frac{dx}{(1-\mu^2\sin^2 x)^{\frac{1}{2}}}.$$

The integral of (8), viz.

$$q^3 = \int_{Q_0^2}^{q^2} \frac{dx}{\{n-(m/\sin x)^2+6(ab/R)\sin^2 x\}^{\frac{1}{2}}\sin^2 x},$$

where Q_0^2 is a constant, can be expressed in terms of incomplete elliptic integrals of the third kind: these need not be given here as they are not required.

Thus the motion is expressed in terms of six constants, viz.

E, the total energy of unit mass,

m, the angular momentum of unit mass about the earth's axis,

t_a, the time of passage through apogee,

Q^2, the apogee distance,

Q_0^2, the value of q^2 for which q^3 vanishes, and

n, which has in general no unique readily identified physical meaning but which enters most directly through (5).

Naturally, some of these equations closely resemble the corresponding relations for Kepler motion. Thus e corresponds to the eccentricity of the Kepler ellipse, the apogee and perigee distances being $(-a/2E)(1+e)$ and $(-a/2E)(1-e)$ respectively. In particular, the orbit will have constant radius if $(-2E/a^2)(n+4ab/R) = 1$, although such an orbit may not be confined to a plane.

3. The torsion

Perhaps the most obvious effect caused by ellipticity of the figure of the earth is departure of the path of a freely falling body from a plane curve, although, of course, for certain obvious initial conditions the path will be plane. Turning aside from the special problem, it is a ready deduction from the Frenet relations that the torsion of a free path in a field of acceleration f^n is

$$\sigma = \frac{\epsilon^{ijk}\tau_i f_j f_{k;m}\tau^m}{(g^{mn}-\tau^m\tau^n)f_m f_n}, \tag{9}$$

where g^{mn} is the (contravariant) metric tensor, τ^m is unit tangent to the path, ϵ^{ijk} is the skew-symmetric (absolute) tensor whose non-vanishing elements have magnitude $g^{-\frac{1}{2}}$, g being the determinant $|g_{mn}|$, and $f_{k;m}$ is the covariant derivative

$$f_{k;m} = \frac{\partial f_k}{\partial q^m} - \left\{ \begin{matrix} n \\ k\ m \end{matrix} \right\} f_n.$$

For motion in a field of potential V, (9) is particularly convenient since $f_n = \partial V/\partial q^n$. If the field is symmetric about the axis of spherical polar coordinates, then

$$\begin{aligned}\epsilon^{ijk}\tau_i f_j f_{k;m}\tau^m &= [\{(f_1 f_{2;1}-f_2 f_{1;1})\sin q^2+(q^1)^{-2}f_2(f_1 q^1\sin q^2+f_2\cos q^2)\}\tau^1+ \\ &\quad +\{(f_{2;2}-f_1 q^1)f_1\sin q^2-(f_{1;2}\sin q^2+f_1\cos q^2)f_2\}\tau^2]\tau^3. \end{aligned}\tag{10}$$

An immediate consequence of (9) and (10) is that the torsion is zero if $\tau^3 = 0$ or if $\tau^1 = \tau^2 = 0$, i.e. if the instantaneous velocity is entirely in or normal to a plane containing the axis of symmetry.

Applying (9) to the case of motion in the field of potential V_1, and retaining only the first power of b, we find

$$\sigma = \frac{6b\sin^2 q^2}{R(q^1)^2}\left\{\frac{x_2 x_3}{(x_2)^2+(x_3)^2}\right\}, \tag{11}$$

where x_n denote the physical components of the tensor τ^n. Hence $|\sigma|$ is a maximum when $x_3 = x_2$: in geographical terms, the projection of the path on the tangent plane to the earth's surface (at the point having the same values of q^2 and q^3 as the particle) bisects the angle between adjacent pairs of cardinal directions on the compass. A similar application of (9) to the case of motion in the original field of potential V gives the result

$$\sigma = \frac{6b\sin^2 q^2}{(q^1)^3}\left\{\frac{x_2 x_3 + x_1 x_3\cot q^2}{(x_2)^2+(x_3)^2}\right\}. \tag{12}$$

4. Numerical estimates

Finally, we may illustrate the influence of ellipticity of the earth's figure by quoting some numerical values deduced from the relations given here.

Thus, suppose that a particle is set moving at right angles to the radius and in a meridian plane, with such speed that, in the Kepler field V_0, a circular orbit would result. In the field V_1 it is found that

$$e = (2b/DR)|1-3\cos^2\Theta|,$$

where D and Θ are, respectively, the values of q^1 and q^2 at the initial point. In particular, a circular orbit results if $\Theta = \cos^{-1}(\pm 1/\sqrt{3})$, which corresponds to a geocentric latitude of 35° 20′ north or south. Although this orbit is circular it is not traversed at constant speed: it is found that the speed is $(a/D)^{\frac{1}{2}}\{1+(3b/DR)\sin^2 q^2\}$ and, if D and R are both of the order of the earth's radius, the fluctuation in speed amounts to 0·16 per cent. On the other hand, the greatest value of e is found when Θ is 0 or π, and this value is about 0·0022 if R and D are of the order of the earth's radius. Hence the total fluctuation in the distance of the particle from the centre of the earth amounts to about 28 km. This is, of course, much less than the expected variation in distance of an artificial satellite, due to the inaccuracy in controlling its initial velocity.

For motion in the field of potential V_1, and assuming the path to have the curvature of a terrestrial great circle, the ratio of the maximum magnitude of torsion to curvature is about 1/600. This may be otherwise expressed by giving the displacement that the particle undergoes in a direction normal to the osculating plane. If κ is the curvature, the displacement parallel to the binormal is $\kappa\sigma s^3/6$, when the small displacement along the path is s. For s = 1,000 km (roughly one-sixth of the earth's radius) the displacement normal to the osculating plane is only 8 m. In calculating the effect of torsion in the path of a ballistic missile it is convenient to take the osculating plane at apogee as a reference; the displacements of the initial and final points of the path are equal in magnitude but oppositely directed normal to this plane. As an example we may consider a total path length of 4,000 km, i.e. 2,000 km each side of apogee; the range on the surface of the earth will, of course, be somewhat less than 4,000 km. The curvature of the path at apogee is several times, perhaps four times, that of a terrestrial great circle, and it is found that the maximum displacements of the initial and final points of the path, normal to the reference plane, have magnitude about 250 m; hence the relative displacement between those two points is about 500 m. Thus, even in the most pronounced case, departure of the path from a plane curve is likely to be a matter of some refinement.

REFERENCES

1. G. Bomford, *Geodesy* (Oxford, 1952).
2. E. T. Whittaker, *Analytical Dynamics* (Cambridge, 1937).

ON THE ZEROS OF BESSEL FUNCTIONS OF PURE IMAGINARY ORDER

By ENOK PALM

(*Institute for Weather and Climate Research, Blindern, Norway*)

[Received 1 November 1956]

SUMMARY

It is proved that Bessel functions of pure imaginary order (defined as a solution of equation (1) below) cannot have two zeros on a line parallel to the real axis. A consequence of this result is that Couette flow with static stability does not possess exponential unstable waves. It also follows from the proof that the Bessel function $G_\nu(z)$ defined by $G_\nu(z) = \frac{1}{2}\pi i e^{-\frac{1}{2}\nu\pi} H^{(1)}_{i\nu}(iz)$ can only have real zeros for finite values of the argument.

1. Introduction

BESSEL functions of pure imaginary order play an important role in the study of some hydrodynamical models. An example is the following: the basic velocity is independent of the horizontal coordinates and a linear function of the vertical coordinate (Couette flow). The static stability is assumed constant, and the motion is limited by two horizontal planes. A discussion of the stability of this model has been given by Taylor (**1**) and recently by Eliassen, Höiland, and Riis (**2**). A result of their investigations is that in the case of positive static stability the problem of the existence of exponential unstable waves is reduced to the question of whether there exists a linear combination of two Bessel functions of pure imaginary order with two zeros on a line parallel to the real axis. The aim of this paper is to prove that such a combination does not exist, and the physical conclusion is that the model just described has no exponential unstable waves.

If the uppermost plane (the vertical coordinate is positive upwards) is displaced so that the distance between the planes tends to infinity, the stability question depends on whether the Bessel function, of pure imaginary argument which vanishes for positive *real* arguments, has any *complex* zeros for finite values of the argument. It is shown below that this Bessel function has no such zeros, a result which has been published previously by Pólya (**3**) (only the result, not the proof, is published), in connexion with a discussion of the form of $F(t)$ necessary to make $\int_0^\infty F(t)\cos zt\, dt$ a function of z with only real zeros.

2. Proof of the statement

The equation for Bessel functions of pure imaginary order may be written

$$\frac{d^2u}{dz^2}+\frac{1}{z}\frac{du}{dz}+\left(\frac{\nu^2}{z^2}-1\right)u=0, \tag{1}$$

where ν is a real constant. A real value of z corresponds to Bessel functions of pure imaginary argument. As mentioned above we will prove that no solution of (1) can have two zeros on a line parallel to the real axis. To prove this we will make use of Green's transform of a second-order differential equation. Consider a self-adjoint, linear differential equation of the second order, viz.,

$$\frac{d}{dz}\left(K(z)\frac{dw}{dz}\right)+G(z)w=0, \tag{2}$$

where $K(z)$ and $G(z)$ are assumed to be analytical functions in a domain D throughout which $K(z)$ does not vanish. If

$$w_1=w, \qquad w_2=K(z)\frac{dw}{dz},$$

the Green's transform of equation (1) is (see (**4**)):

$$[\bar{w}_1 w_2]_{z_1}^{z_2}-\int_{z_1}^{z_2}|w_2|^2L(z)\,d\bar{z}+\int_{z_1}^{z_2}|w_1|^2G(z)\,dz=0, \tag{3}$$

assuming that every point of the path of integration lies in D. Here a bar denotes the complex conjugate of the quantity, and $L(z)$ is defined by

$$L(z)=1/\{\overline{K(z)}\}.$$

Separating the real and imaginary parts, we have

$$\mathrm{re}[\bar{w}_1 w_2]_{z_1}^{z_2}-\mathrm{re}\int_{z_1}^{z_2}|w_2|^2L(z)\,d\bar{z}+\mathrm{re}\int_{z_1}^{z_2}|w_1|^2G(z)\,dz=0, \tag{4}$$

$$\mathrm{im}[\bar{w}_1 w_2]_{z_1}^{z_2}-\mathrm{im}\int_{z_1}^{z_2}|w_2|^2L(z)\,d\bar{z}+\mathrm{im}\int_{z_1}^{z_2}|w_1|^2G(z)\,dz=0. \tag{5}$$

We first prove that, if a solution of (1) with two zeros on a line parallel to the real axis exists, then the two zeros must lie on opposite sides of the imaginary axis (it will be assumed throughout the paper that the two zeros can be combined with a path which does not enclose the origin). To prove this statement we assume for the moment that the two zeros are on the same side of the imaginary axis. By introducing

$$u=z^{\frac{1}{2}}v$$

equation (1) takes the self adjoint form

$$\frac{d}{dz}\left(z^2\frac{dv}{dz}\right)+(\mu^2-z^2)v=0, \tag{7}$$

where $$\mu^2=\nu^2+\tfrac{1}{4}.$$

Comparing (7) with (2) we notice that in our case

$$\frac{1}{K(z)}=\frac{1}{z^2}=\frac{x^2-y^2-2xyi}{(x^2+y^2)^2}, \tag{8}$$

$$G(z)=\mu^2-z^2=\mu^2-x^2+y^2-2xyi,$$

since $$z=x+iy.$$

Let z_1 and z_2 represent the two zeros. In (5) the first term vanishes. As the path of integration we choose the straight line connecting z_1 and z_2. It is then seen that the two integrals in (5) have opposite signs, and thus (5) cannot be satisfied.

To complete the proof we return to (1) and now introduce

$$u=z^{-\frac{1}{2}}w. \tag{9}$$

Equation (1) takes the form

$$\frac{d^2w}{dz^2}+\left(\frac{\mu^2}{z^2}-1\right)w=0. \tag{10}$$

This equation is self adjoint with

$$K(z)=1$$

and $$G(z)=\frac{\mu^2}{z^2}-1=\mu^2\frac{x^2-y^2-2xyi}{(x^2+y^2)^2}-1. \tag{11}$$

We assume again that a solution with two zeros on a line parallel to the real axis exists. From the above result these two zeros must lie on opposite sides of the imaginary axis. Choosing z_1 and z_2 to represent the zeros, the first term in (4) vanishes. There are two possibilities for the path of integration: (i) if the imaginary parts of the zeros are positive, we integrate along a line parallel to the imaginary axis in a positive direction to a point A, then along the line parallel to the real axis to a point B, and finally along a line parallel to the imaginary axis to the other zero point; (ii) if the imaginary parts of the zeros are negative, the path of the integration will be the corresponding path in the half-plane of $y<0$. Let z_1 represent the zero with negative real part. It is then readily seen that the second term in (4), namely, $-\mathrm{re}\int_{z_1}^{z_2}|w_2|^2L(z)\,d\bar{z}$, will be either zero or negative on the path of integration. The third term, $\mathrm{re}\int_{z_1}^{z_2}|w_1|^2G(z)\,dz$, is negative on the lines parallel to the imaginary axis. By choosing the distance between the line

through the zeros and the line AB large enough, it can be seen that the contribution from the path AB is also negative. Equation (4) cannot be satisfied, and we conclude that two such zeros cannot exist.

The arguments given above are also valid if one of the zeros tends to infinity. We therefore see that the function which is often denoted by $G_\nu(z)$ and defined by

$$G_\nu(z) = \tfrac{1}{2}\pi i e^{-\frac{1}{2}\nu\pi} H^{(1)}_{i\nu}(iz), \tag{12}$$

where $H^{(1)}_{i\nu}$ is a Bessel function of third order, has no complex (or pure imaginary) zeros for finite values of the argument since this function tends to zero when $z \to \infty$ and $|\arg z| < \frac{1}{2}\pi$. A similar result is true for the solution of (1) which tends towards zero when $z \to \infty$ and $\frac{1}{2}\pi < \arg z < \frac{3}{2}\pi$.

It should perhaps be mentioned that these functions have an infinite number of *real* zeros.

By applying a similar method to that used above it follows also that no solution of (1) can have two zeros which lie on a line parallel to the imaginary axis and on the same side of the real axis. To obtain the results above we have made use of the fact that

$$\mu^2 = \nu^2 + \tfrac{1}{4}$$

is a positive quantity. The results derived are also valid for pure imaginary values of ν, provided that

$$|\nu^2| < \tfrac{1}{4}.$$

REFERENCES

1. G. I. Taylor, 'Effect of variation in density on the stability of superposed streams of fluid', *Proc. Roy. Soc.* A, **132** (1931) 499.
2. A. Eliassen, E. Höiland, and E. Riis, *Two-dimensional Perturbation of a Flow with Constant Shear of a Stratified Fluid*, Publ. No. 1, Inst. Weather and Climate Research (Oslo, 1953).
3. G. Pólya, 'On the zeros of certain trigonometric integrals', *J. Lond. Math. Soc.* **1** (1926) 98.
4. E. L. Ince, *Ordinary Differential Equations* (Longmans, Green & Co., London, 1927. Dover, New York, 1944)

DETERMINATION OF THE OPTIMUM RESPONSE OF LINEAR SYSTEMS (ZERO DISPLACEMENT ERROR SYSTEMS)†

By A. W. BABISTER (*The University, Glasgow*)

[Received 4 September 1956]

SUMMARY

In (1) two response functions L and L_1 were defined by the equations

$$L = \int_0^\infty e^2\, d\tau \quad \text{and} \quad L_1 = \int_0^\infty \left(\frac{de}{d\tau}\right)^2 d\tau,$$

where e is the error at time τ. These relations are applied to a linear system having one degree of freedom. By considering the response to a step-function disturbance it is found that systems making L a minimum have a lightly damped oscillatory response. The smaller L_1 is, the 'smoother' is the response.

Values are obtained for the coefficients of the characteristic equation of any order making L a minimum. An approximate method is given for correcting these coefficients to enable the response to be improved to give equal damping in the least damped modes of oscillation.

1. Introduction

In (1) two response functions L and L_1 were defined by the equations

$$L = \int_0^\infty e^2\, d\tau \tag{1}$$

and

$$L_1 = \int_0^\infty \left(\frac{de}{d\tau}\right)^2 d\tau, \tag{2}$$

where e is the error at time τ. Formulae were given for L and L_1 in terms of (i) the coefficients of the characteristic equation, and (ii) the frequency response spectrum. We shall now show how L and L_1 can be used to obtain the optimum response. As stated in (1) a system based on minimizing L often has an undesirable overshoot. We shall consider the performance of systems for which L is near its minimum value while L_1 is considerably lower than its value when L is a minimum. We shall obtain the relation between the transient response, the frequency response, and the roots of the characteristic equation for systems having no static error.

We consider a system for which the equation of motion is

$$a_n \frac{d^n x}{d\tau^n} + a_{n-1} \frac{d^{n-1} x}{d\tau^{n-1}} + a_{n-2} \frac{d^{n-2} x}{d\tau^{n-2}} + \ldots + a_1 \frac{dx}{d\tau} + a_0 x = f(\tau), \tag{3}$$

† The material in this paper is taken from a Ph.D. thesis for the University of Glasgow.

where $a_0, a_1, a_2, \ldots, a_n$ are constants and $a_n \neq 0$, and x is the response of the system with input f.

2. Response of zero displacement error systems to step function disturbance (constant displacement input)

In this case

$$f = 0 \quad \text{for } \tau \leqslant 0; \qquad f = f_0 \quad \text{for } \tau > 0, \tag{4}$$

where f_0 is a constant.

As in (**2**) we shall find it convenient to normalize (3).

Let
$$a_0 = \omega_0^n a_n, \tag{5}$$

and define a new time scale by the relation

$$u = \omega_0 \tau. \tag{6}$$

From (3) to (6) the normalized equation of motion is

$$\frac{d^n x}{du^n} + q_{n-1}\frac{d^{n-1}x}{du^{n-1}} + q_{n-2}\frac{d^{n-2}x}{du^{n-2}} + \ldots + q_1\frac{dx}{du} + x = \frac{f_0}{a_0} \quad (\tau > 0), \tag{7}$$

where
$$q_r = a_r/(a_n \omega_0^{n-r}) \quad (r = 0 \text{ to } n). \tag{8}$$

Now the magnitude of the response x is proportional to f_0, but the nature of the response (per cent overshoot, damping time) is independent of f_0. We shall take

$$f_0 = a_0. \tag{9}$$

Thus we shall determine the response of the system given by (7) to a unit step function disturbance. We shall only consider stable systems; then the static error ultimately vanishes since $x \to 1$. Such systems are sometimes called 'zero displacement error systems' (see (**2**)). As shown in (**1**) the response is identical in form with that in a free motion with $x_0 = -1$ and Dx_0, $D^2x_0, \ldots, D^{n-1}x_0$ zero, where the suffix 0 denotes the values at time $\tau = 0$, and D is the differential operator.

3. Second-order zero displacement error system

From (**1**), with $x_0 = -1$, $Dx_0 = 0$,

$$2La_0a_1 = \begin{vmatrix} a_1 & a_2 \\ -a_0 & a_1 \end{vmatrix} = a_1^2 + a_0a_2 \tag{10}$$

or, in terms of the normalized coefficient q_1 given by (8),

$$2L\omega_0 = \frac{q_1^2+1}{q_1}. \tag{11}$$

Similarly,
$$\frac{2L_1}{\omega_0} = \frac{1}{q_1}. \tag{12}$$

Now for stability with $a_2 > 0$, both a_1 and a_0 must be positive, i.e. $q_1 > 0$.

We see that for a system with a given undamped natural frequency ω_0, L and L_1 are both functions of q_1 (which for a mechanical system is proportional to the damping). The minimum value of L occurs for $q_1 = 1$, i.e.

$$a_1^2 = a_0 a_2.$$

Then
$$L_{\min} = 1/\omega_0, \tag{13}$$

and for this value of q_1
$$L_1 = \tfrac{1}{2}\omega_0. \tag{14}$$

This corresponds to an oscillatory motion with overswing of 16 per cent (see Fig. 1). We shall see that this tendency for the oscillatory motion to

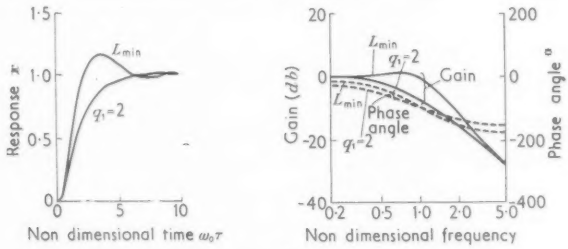

FIG. 1. Second-order zero displacement error system

be rather lightly damped is a characteristic of systems based on $L_{\min}$. This overswing is lessened by selecting a higher value of q_1 (or a_1) as is seen from the following table.

TABLE 1

Variation of response functions and overshoot with the damping coefficient for a second-order zero displacement error system

$q_1 = \frac{a_1}{\sqrt{(a_0 a_2)}}$	$L\omega_0$	L_1/ω_0	% *overshoot*
0·6	1·13	0·83	38
0·8	1·03	0·63	26
1·0	1·00	0·50	16
1·2	1·02	0·42	9
1·4	1·06	0·36	5
1·6	1·11	0·31	2
1·8	1·18	0·28	0
2·0	1·25	0·25	0

The minimum of L is seen to be fairly flat; the value of L is not more than 10 per cent greater than the minimum for values of q_1 from 0·7 to 1·5. We see that there is good correlation between the per cent overshoot and the value of L_1, as would be expected from the definition of L_1. The smaller L_1 is, the 'smoother' is the response, which becomes less oscillatory in nature. Precisely what value of q_1 is chosen for the most satisfactory system

is a matter for individual choice, depending upon the acceptable per cent overshoot. From the above table we see that to keep both L and L_1 as small as possible, q_1 should be greater than 1. Now if q_1 is greater than 2, the roots of the characteristic equation will both be real and negative, one root decreasing, the other increasing, as q_1 increases; the motion will then be composed of two monotonic functions (subsidences) and, in the terminology of servomechanism analysis, would be considered to be overdamped. We are therefore led to the criterion

$$1{\cdot}0 \leqslant q_1 \leqslant 2{\cdot}0 \tag{15}$$

for satisfactory performance for a second-order zero displacement error system. This is in good agreement with current practice with servomechanisms.

The choice of ω_0 will depend on the desired speed of response of the system; the higher the value of ω_0 the sooner will the system reach its steady state. Changing ω_0 merely alters the time scale of the damping but does not affect the per cent overshoot or the general form of the response.

The other diagram in Fig. 1 shows the gain (in decibels) plotted on a logarithmic scale against the non-dimensional frequency ω/ω_0 for the two cases $q_1 = 1$ and $q_1 = 2$. If M is the dynamic magnification (**1**), the gain $= 20 \log_{10} M$ decibels.

For the range of q_1 given by (15), $M_{\max}$ does not exceed 1·15, which is well within current practice with servomechanisms.

4. Higher-order zero displacement error systems

The above analysis can easily be extended to higher-order systems. From (1), with $x_0 = -1$,

$$Dx_0 = D^2x_0 = \ldots = D^{n-1}x_0 = 0,$$

$$2La_0 \begin{vmatrix} a_1 & a_3 & a_5 & a_7 & \cdot & \cdot & \cdot \\ a_0 & a_2 & a_4 & a_6 & \cdot & \cdot & \cdot \\ 0 & a_1 & a_3 & a_5 & \cdot & \cdot & \cdot \\ 0 & a_0 & a_2 & a_4 & \cdot & \cdot & \cdot \\ \cdot & \cdot & \cdot & \cdot & \cdot & \cdot & \cdot \end{vmatrix} = \begin{vmatrix} a_1 & a_2 & a_4 & a_6 & \cdot & \cdot & \cdot \\ -a_0 & a_1 & a_3 & a_5 & \cdot & \cdot & \cdot \\ 0 & a_0 & a_2 & a_4 & \cdot & \cdot & \cdot \\ 0 & 0 & a_1 & a_3 & \cdot & \cdot & \cdot \\ \cdot & \cdot & \cdot & \cdot & \cdot & \cdot & \cdot \end{vmatrix} \tag{16}$$

or, in terms of the normalized coefficients $q_1, q_2, \ldots, q_{n-1}$ given above,

$$2L\omega_0 \begin{vmatrix} q_1 & q_3 & q_5 & q_7 & \cdot & \cdot & \cdot \\ 1 & q_2 & q_4 & q_6 & \cdot & \cdot & \cdot \\ 0 & q_1 & q_3 & q_5 & \cdot & \cdot & \cdot \\ 0 & 1 & q_2 & q_4 & \cdot & \cdot & \cdot \\ \cdot & \cdot & \cdot & \cdot & \cdot & \cdot & \cdot \end{vmatrix} = \begin{vmatrix} q_1 & q_2 & q_4 & q_6 & \cdot & \cdot & \cdot \\ -1 & q_1 & q_3 & q_5 & \cdot & \cdot & \cdot \\ 0 & 1 & q_2 & q_4 & \cdot & \cdot & \cdot \\ 0 & 0 & q_1 & q_3 & \cdot & \cdot & \cdot \\ \cdot & \cdot & \cdot & \cdot & \cdot & \cdot & \cdot \end{vmatrix} \tag{17}$$

where the determinants on the left-hand sides of (16) and (17) are of order

$n-1$ and those on the right-hand sides are of order n. Also $q_n = 1$. Similarly,

$$\begin{vmatrix} \frac{2L_1}{\omega_0} & q_1 & q_3 & q_5 & q_7 & \cdot & \cdot & \cdot \\ 1 & q_2 & q_4 & q_6 & \cdot & \cdot & \cdot \\ 0 & q_1 & q_3 & q_5 & \cdot & \cdot & \cdot \\ 0 & 1 & q_2 & q_4 & \cdot & \cdot & \cdot \\ \cdot & \cdot & \cdot & \cdot & \cdot & \cdot & \cdot \end{vmatrix} = \begin{vmatrix} q_2 & q_4 & q_6 & q_8 & \cdot & \cdot & \cdot \\ q_1 & q_3 & q_5 & q_7 & \cdot & \cdot & \cdot \\ 1 & q_2 & q_4 & q_6 & \cdot & \cdot & \cdot \\ 0 & q_1 & q_3 & q_5 & \cdot & \cdot & \cdot \\ \cdot & \cdot & \cdot & \cdot & \cdot & \cdot & \cdot \end{vmatrix} \quad (18)$$

the final determinant on the right-hand side of (18) being of order $n-2$. Equation (18) can be written in a simple form in terms of the test functions of the characteristic equation. We find

$$L_1 = \frac{a_0 T_{n-2}}{2T_{n-1}}, \quad (19)$$

where T_r is the rth test function of the characteristic equation corresponding to (3) (see (**3**) and (**4**)). For stability when $a_n > 0$, all the test functions must be positive.

The minimum values of L and the corresponding values of $q_0, q_1, q_2, \ldots, q_n$ are given in the following table.

TABLE 2

Values of $L_{\min}$ and the normalized coefficients q_m for zero displacement error systems of order n

n	$2L_{\min}\omega_0$	q_0	q_1	q_2	q_3	q_4	q_5	q_6	q_7	q_8
1	1	1	1							
2	2	1	1	1						
3	3	1	2	1	1					
4	4	1	2	3	1	1				
5	5	1	3	3	4	1	1			
6	6	1	3	6	4	5	1	1		
7	7	1	4	6	10	5	6	1	1	
8	8	1	4	10	10	15	6	7	1	1

From the above table we see that

$$L_{\min} = \frac{n}{2\omega_0} \quad (20)$$

and that the coefficient q_m for an nth order system is equal to ${}_pC_m$, the binomial coefficient, namely

$${}_pC_m = p!/\{m!\,(p-m)!\}$$

and

$$p = \begin{cases} \dfrac{m+n}{2} & \text{if } m+n \text{ is even} \\ \dfrac{m+n-1}{2} & \text{if } m+n \text{ is odd} \end{cases}. \quad (21)$$

Thus the above table can easily be extended to any order n.

We find also that when the test functions are written in terms of the q's with the above coefficients at $L_{\min}$,

$$T_r = \omega_0^{\frac{1}{2}r(r+1)} a_n^r \quad (r = 1,..., n). \tag{22}$$

From (19) and (22) we find that when L is a minimum

$$L_1 = \frac{a_0}{2\omega_0^{n-1} a_n} = \frac{\omega_0}{2}. \tag{23}$$

Thus $L_{\min}$ is proportional to the order n of the system, but the corresponding value of L_1 is independent of the order of the system.

The motion for this system is composed of a number of damped oscillations (and possibly a monotonic function if n is odd), as shown in the following table.

TABLE 3

Roots of the characteristic equation for a zero displacement error $L_{\min}$ system of order n

n	*Roots*
2	$-0{\cdot}5 \pm 0{\cdot}87i$
3	$-0{\cdot}57,\ -0{\cdot}215 \pm 1{\cdot}31i$
4	$-0{\cdot}395 \pm 0{\cdot}505i,\ -0{\cdot}105 \pm 1{\cdot}57i$
5	$-0{\cdot}41,\ -0{\cdot}235 \pm 0{\cdot}88i,\ -0{\cdot}06 \pm 1{\cdot}70i$
6	$-0{\cdot}315 \pm 0{\cdot}362i,\ -0{\cdot}155 \pm 1{\cdot}50i$ $-0{\cdot}03 \pm 1{\cdot}78i$
7	$-0{\cdot}33,\ -0{\cdot}22 \pm 0{\cdot}665i,\ -0{\cdot}09 \pm 1{\cdot}35i$ $-0{\cdot}025 \pm 1{\cdot}83i$
8	$-0{\cdot}27 \pm 0{\cdot}283i,\ -0{\cdot}15 \pm 0{\cdot}91i,$ $-0{\cdot}068 \pm 1{\cdot}50i,\ -0{\cdot}013 \pm 1{\cdot}86i$

For a system of given order the modes of low frequencies are the more highly damped. As n increases, the damping in all the modes decreases and the corresponding frequencies increase. The mode with the least damping is an oscillatory mode of relatively short period. As would be expected, this gives a system with rather a wavy response, due to the terms of high frequency, with a certain amount of hunting (usually of small amplitude compared with the input motion). This is shown in Fig. 2 for systems of fourth and fifth order, the first overswing for a unit step disturbance being 9 per cent for the fourth-order system and 10 per cent for the fifth-order one. The amplitudes of the corresponding motions at, say, $\omega_0 \tau = 10$ are 6 and 11 per cent respectively.

As with the second-order system it is possible to find a more satisfactory response than that for $L_{\min}$ by choosing the q's so that L_1 is decreased considerably while L is only increased slightly. This could be done by determining the locus at which the surfaces $L = \text{const.}$ and $L_1 = \text{const.}$ touch one another. However, we shall be mainly interested in points close to $L_{\min}$ and the following approximate procedure can be adopted.

For values of the q's which make L a minimum we find that

$$\left.\begin{aligned} \frac{\partial L_1}{\partial q_r} &= 0 \qquad (r = 1,\ldots, n-3) \\ \frac{\partial L_1}{\partial q_r} &= -\tfrac{1}{2}\omega_0 \quad (r = n-2, n-1) \end{aligned}\right\}. \tag{24}$$

Thus for points in the neighbourhood of $L_{\min}$, L_1 can be most effectively reduced by increasing q_{n-1} and q_{n-2} by some quantity, θ say, i.e. by choosing values of the q's which are on the normal to the surface $L_1 = 0{\cdot}5\omega_0$ at the point corresponding to $L_{\min}$.

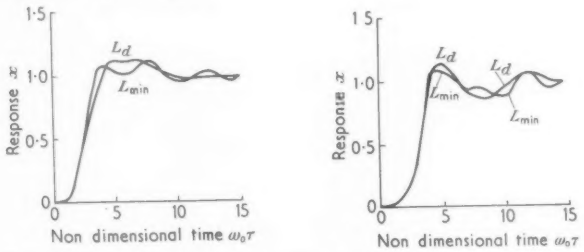

FIG. 2. Fourth and fifth order zero displacement error system

As θ increases, the roots of the characteristic equation vary, the damping of the lightly damped oscillation being increased while that of the other modes is either unchanged or slightly decreased. We note that since q_{n-1} increases as θ increases the 'total' damping of the system will increase. For a particular value of θ the characteristic equation has at least three (usually four) roots with equal negative real parts. For such a system L is denoted by L_d. The values of the normalized coefficients and the roots of the characteristic equation are given in Tables 4 and 5, obtained by the approximate procedure outlined above.

TABLE 4

Values of the normalized coefficients q_m for zero displacement error systems of order n with equal damping (L_d system)

n	q_0	q_1	q_2	q_3					
3	1	2·5	1·5	1	q_4				
4	1	2	3·38	1·38	1	q_5			
5	1	3	3	4·17	1·17	1	q_6		
6	1	3	6	4	5·07	1·07	1	q_7	
7	1	4	6	10	5	6·03	1·03	1	q_8
8	1	4	10	10	15	6	7·014	1·014	1

We see that, as the order of the system increases, the value of θ for equal damping decreases. Comparing Tables 3 and 5 we see that in passing from

$L_{\min}$ to L_d the damping of the least damped oscillation is increased about three times, the frequencies of the various modes being practically unchanged. Thus as shown in Fig. 2 the response of the system to a unit step disturbance is of a much smoother nature. The peak overshoot has increased slightly to 13 per cent for both systems.

TABLE 5

Roots of the characteristic equation for a zero displacement error L_d system of order n

n	*Roots*
3	$-0{\cdot}50,\ -0{\cdot}50 \pm 1{\cdot}32i$
4	$-0{\cdot}345 \pm 0{\cdot}53i,\ -0{\cdot}345 \pm 1{\cdot}54i$
5	$-0{\cdot}41,\ -0{\cdot}19 \pm 0{\cdot}90i,\ -0{\cdot}19 \pm 1{\cdot}70i$
6	$-0{\cdot}315 \pm 0{\cdot}347i,\ -0{\cdot}105 \pm 1{\cdot}17i$ $-0{\cdot}105 \pm 1{\cdot}77i$
7	$-0{\cdot}33,\ -0{\cdot}22 \pm 0{\cdot}70i,\ -0{\cdot}065 \pm 1{\cdot}36i$ $-0{\cdot}065 \pm 1{\cdot}83i$
8	$-0{\cdot}27 \pm 0{\cdot}283i,\ -0{\cdot}15 \pm 0{\cdot}91i$ $-0{\cdot}0425 \pm 1{\cdot}50i,\ -0{\cdot}0425 \pm 1{\cdot}86i$

Comparing the response curves of Fig. 2 with those based on the I.T.A.E. criterion (**2**) and on the Butterworth filters, (**5**) and (**6**), we see that the overshoot is greater, and the damping less, than with the I.T.A.E. systems. The overshoot is about the same as with the Butterworth filters, the damping is slightly less. The time for the error first to become zero (momentarily) is smaller than for either the I.T.A.E. systems or the Butterworth filters (for a given value of ω_0).

The advantage of the above determination over that of the I.T.A.E. method is that the coefficients given in Table 4 can be readily extended to systems of any order, being based on an analytical formula. The response curves of the systems L_d and $L_{\min}$ form a family of curves as the order of the system is increased. The justification of the use of the L criteria must depend on the final form of the response curves and upon the comparative ease with which the criteria can be calculated, especially when the approximate method is used. It is not surprising that the general shape of some of the response curves for L_d is not unlike that with the Butterworth filters. Other investigators have arrived at similar results (see the discussion of (**2**)).

REFERENCES

1. A. W. BABISTER, 'Response functions of linear systems with constant coefficients having one degree of freedom', *Quart. J. Mech. App. Math.* **10** (1957) 360.
2. D. GRAHAM and R. C. LATHROP, 'The synthesis of optimum transient response: criteria and standard forms', *Trans. A.I.E.E.* **72** (1953) 273.

3. A. HURWITZ, 'Über die Bedingungen, unter welchen eine Gleichung nur Würzeln mit negativen reelen Theilen besitzt', *Math. Ann.* **46** (1895) 273.
4. R. A. FRAZER and W. J. DUNCAN, 'On the criteria for the stability of small motions', *Proc. Roy. Soc.* A, **124** (1929) 642.
5. A. L. WHITELEY, 'Theory of servo systems, with particular reference to stabilization', *J. Inst. Elec. Engnrs.* **93** (1946) 353.
6. S. BUTTERWORTH, 'On the theory of filter amplifiers', *Wireless Engineer*, **7** (1930) 536.

CORRIGENDUM

'A SOURCE IN A ROTATING FLUID' *by* S. N. BARUA

In the paper mentioned above (*Quart. J. Mech. App. Math.* **8** (1955) 27) the sentence in which equation (11) appears should read as follows: Since $J_1(\alpha_n c/a)$ tends to $\alpha_n c/2a$ (instead of $\alpha_n c/a$) as c tends to zero, the expression for ϕ may be written as

$$\phi = \frac{W}{2\pi a^2}\left[x - a\sum \frac{1}{\alpha_n J_0^2(\alpha_n)} e^{-\alpha_n x/a} J_0(\alpha_n r/a)\right].$$

Consequently the equation (12) of the paper becomes

$$\left(\frac{a+d}{a}\right)^2 - \left(\frac{a+d}{a}\right)^{-2} - 4\log\left(\frac{a+d}{a}\right) = -0{\cdot}3918\left[2\sum \frac{e^{-\alpha_n x/a}}{J_0(\alpha_n)} + \left(\sum \frac{e^{-\alpha_n x/a}}{J_0(\alpha_n)}\right)^2\right],$$

and Table 1 becomes

x/a	$\sum \dfrac{e^{-\alpha_n x/a}}{J_0(\alpha_n)}$	d/a
0	$-1{\cdot}0$	0·68
$\frac{1}{2}$	$-0{\cdot}2845$	0·51
1	$-0{\cdot}5106 \times 10^{-1}$	0·28
2	$-0{\cdot}1191 \times 10^{-2}$	0·07

These results are illustrated in Fig. 1.

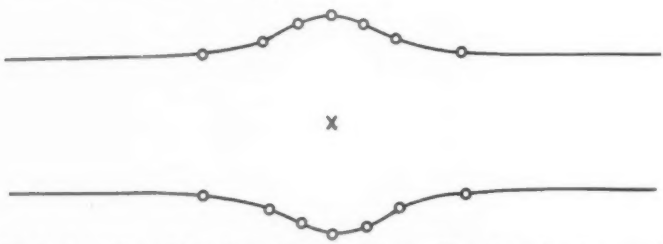

FIG. 1. A section of the discontinuity-surface. (The plotted points on the discontinuity-surface are the results of Table 1)

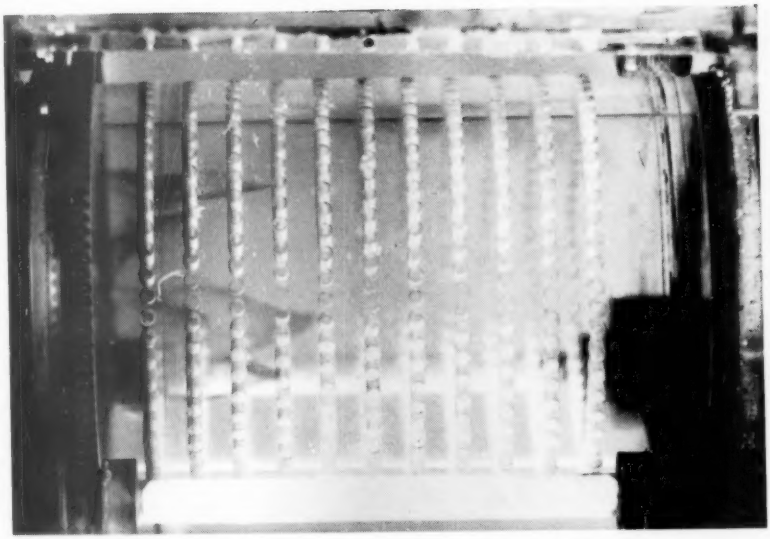

FIG. 6. Arrangement D; three streams springing from face of bung

CORRIGENDUM

This figure was omitted from 'Experiments on the Slow Swirling Flows of a Viscous Liquid Through a Tube' by A. M. Binnie, Part 3 of Volume X

THE QUARTERLY JOURNAL OF MECHANICS AND APPLIED MATHEMATICS

VOLUME X PART 4 NOVEMBER 1957

CONTENTS

The Editorial Board gratefully acknowledge the support given by: Blackburn & General Aircraft Limited; Bristol Aeroplane Company; Courtaulds Scientific and Educational Trust Fund; English Electric Company; Hawker Siddeley Group Limited; Metropolitan-Vickers Electrical Company Limited; The Shell Petroleum Co. Limited; Vickers-Armstrongs (Aircraft) Limited.
